13

The Pennsylvania State University
APPLIED RESEARCH LABORATORY
P.O. Box 30
State College, PA 16804

A TWO-SCALE SOLUTION OF THE FORCED RAYLEIGH-PLESSET EQUATION GOVERNING THE DYNAMICS OF CAVITATION BUBBLE VAPOROUS GROWTH

by

B. W. Lathrop
B. R. Parkin

Technical Report No. TR 91-002
February 1991

Supported by:
Office of Naval Research

L.R. Hettche, Director
Applied Research Laboratory

Approved for public release; distribution unlimited

REPORT DOCUMENTATION PAGE

Form Approved
OMB No. 0704-0188

1. AGENCY USE ONLY (Leave blank)	2. REPORT DATE	3. REPORT TYPE AND DATES COVERED

4. TITLE AND SUBTITLE
A TWO-SCALE SOLUTION OF THE FORCED RAYLEIGH-PLESSET EQUATION GOVERNING THE DYNAMICS OF CAVITATION BUBBLE VAPOROUS GROWTH

5. FUNDING NUMBERS

6. AUTHOR(S)
B. W. Lathrop and B. R. Parkin

7. PERFORMING ORGANIZATION NAME(S) AND ADDRESS(ES)
Applied Research Laboratory
Penn State University
P. O. Box 30
State College, PA 16804

8. PERFORMING ORGANIZATION REPORT NUMBER
TR- 91-002

9. SPONSORING/MONITORING AGENCY NAME(S) AND ADDRESS(ES)
Office of Naval Research
800 N. Quincy Street
Arlington, VA 22217-5000

10. SPONSORING/MONITORING AGENCY REPORT NUMBER
N00014-88-K-0404

11. SUPPLEMENTARY NOTES

12a. DISTRIBUTION/AVAILABILITY STATEMENT
Unlimited

12b. DISTRIBUTION CODE

13. ABSTRACT (Maximum 200 words)

A two-scale analysis of the forced Rayleigh-Plesset equation of cavitation bubble dynamics is performed. The problem of cavitation inception as it relates to bubble dynamics involves vaporous cavitation nucleus growth as it is influenced by the pressure distribution on a submerged body. This brings into prominence two widely varying time scales. The "laboratory time" is characterized by the bubble's travel over the body, while the "bubble time" is characterized by the very high natural frequency oscillations of the individual bubble. The laboratory time is expected to be much longer than the bubble time; thus they can be related by a very small parameter, ϵ.

Using these two time scales, a perturbation expansion is performed on the forced Rayleigh-Plesset equation and its initial conditions up to the third order in ϵ. The resulting zero and first-order equations are solved, subject to these solutions being independent of the laboratory time. In this case the integrability condition for each step is thereby identically satisfied.

14. SUBJECT TERMS
Rayleigh-Plesset equation, cavitation, bubble dynamics

15. NUMBER OF PAGES

16. PRICE CODE

17. SECURITY CLASSIFICATION OF REPORT	18. SECURITY CLASSIFICATION OF THIS PAGE	19. SECURITY CLASSIFICATION OF ABSTRACT	20. LIMITATION OF ABSTRACT
UNCLASSIFIED	UNCLASSIFIED	UNCLASSIFIED	UNLIMITED

The zero-order equation is an autonomous nonlinear second-order differential equation. An approximate closed-form, small oscillation solution is found and a numerical solution is found for oscillations of all amplitudes. Both forms of the solution are found to be periodic and a function of bubble time only.

The first-order equation is a nonhomogeneous linear second-order differential equation with periodic coefficients. Its homogeneous form is of the class of Hill's equations, and can be treated using Floquet theory. The complementary solution in normal or Floquet form is found numerically. Variation of parameters is used to find the particular integral. Again, the constants for the first-order solution are independent of the laboratory time and only the bubble time appears explicitly in the complementary function. The laboratory time enters the solution via the particular integral because the forcing function depends on the laboratory time.

The dynamic stability of these solutions was investigated. It was found that the present solutions are unstable and they are not suitable for inception calculations. Further study of the method of solution determined that a more general solution than the present one might be found which will still satisfy the integrability conditions at each step. Some basic zero-order equations have been formulated which may permit such a numerical solution to be found. No algorithm for the solution of these equations has been developed.

This report is a revision of the first author's thesis in Aerospace Engineering, which was submitted in partial fulfillment of the requirements for the Master of Science, December 1990.

ABSTRACT

A two-scale analysis of the forced Rayleigh-Plesset equation of cavitation bubble dynamics is performed. The problem of cavitation inception as it relates to bubble dynamics involves vaporous cavitation nucleus growth as it is influenced by the pressure distribution on a submerged body. This brings into prominence two widely varying time scales. The "laboratory time" is characterized by the bubble's travel over the body, while the "bubble time" is characterized by the very high natural frequency oscillations of the individual bubble. The laboratory time is expected to be much longer than the bubble time; thus they can be related by a very small parameter, ε.

Using these two time scales, a perturbation expansion is performed on the forced Rayleigh-Plesset equation and its initial conditions up to the third order in ε. The resulting zero and first-order equations are solved, subject to these solutions being independent of the laboratory time. In this case the integrability condition for each step is thereby identically satisfied.

The zero-order equation is an autonomous nonlinear second-order differential equation. An approximate closed-form, small oscillation solution is found and a numerical solution is found for oscillations of all amplitudes. Both forms of the solution are found to be periodic and a function of bubble time only.

The first-order equation is a nonhomogeneous linear second-order differential equation with periodic coefficients. Its homogeneous form is of the class of Hill's equations, and can be treated using Floquet theory. The complementary solution in normal or Floquet form is found numerically. Variation of parameters is used to find the particular integral. Again, the constants for the first-order solution are independent of the laboratory time and only the bubble time appears explicitly in the complementary function.The laboratory time enters the solution via the particular integral because the forcing function depends on the laboratory time.

The dynamic stability of these solutions was investigated. It was found that the present solutions are unstable and they are not suitable for inception calculations. Further study of the method of solution determined that a more general solution than the present one might be found which will still satisfy the integrability conditions at each step. Some basic zero-order equations have been formulated which may permit such a numerical solution to be found. No algorithm for the solution of these equations has been developed.

This report is a revision of the first author's thesis in Aerospace Engineering, which was submitted in partial fulfillment of the requirements for the degree of Master of Science, December 1990.

TABLE OF CONTENTS

Page

LIST OF FIGURES

Figures Page

NOMENCLATURE

Symbol	Definition	Where Defined
t	Real Time	
$t_S = \frac{t V_0}{D}$	Dimensionless Laboratory Time	Eq. 2.1
$\tau = t\sqrt{\frac{2\sigma}{\rho R_0^3}}$	Dimensionless Bubble Time	Eq. 2.2
$\varepsilon = \frac{V_0}{D}\sqrt{\frac{\rho R_0^3}{2\sigma}}$	Small Perturbation Parameter	Eq. 2.4
$C_p = \frac{p - p_0}{\frac{1}{2}\rho V_0^2}$	Pressure Coefficient	Eq. 2.6
$K = \frac{p_0 - p_v}{\frac{1}{2}\rho V_0^2}$	Cavitation Number	Eq. 2.7
p_v	Vapor Pressure of the Liquid	Eq. 2.5
$F(\varepsilon,\tau)$	Forcing Function	Eq. 2.9
$s = \frac{2S}{D}$	Dimensionless Along Arc Length Body	Eq. 2.10
S	Dimensional Arc Length Along Body	
D	Characteristic Body Length	
V_0	Free Stream Velocity	
ρ	Fluid Density	
σ	Fluid Surface Tension	
R_0	Free Stream Nucleus Radius	Eq. 2.20
p_a	Partial Pressure of Air	Eq. 2.19
$r = \frac{R}{R_0}$	Dimensionless Bubble Radius	Eq. 2.20

Symbol	Definition	Where Defined
$W_r = \frac{\rho R_0 V_0^2}{\sigma}$	Radial Weber Number	Eq. 2.26
p_0	Free Stream Static Pressure	
$q = \frac{1}{4} K W_r$		Eq. 2.32
$u(t) = \frac{r(t)}{\sqrt{1 + q}}$	Normalized Bubble Radius	Eq. 2.38
β	Henry's Law Constant	Eq. 2.69
$\gamma = \frac{p_a R_0}{2\sigma}$	Air Content Parameter	Eq. 2.72
$u_v = \sqrt{\frac{\gamma}{1+q}}$	Vortex Point Affix	Eq. 3.8
u_m	Maximum Normalized Radius	Eq. 3.14
I	Half-Period Integral	Eq. 3.15
T	Period of Zero-Order Solution	
$x = \frac{\tau}{T}$	Normalized Dimensionless Bubble Time	Eq. 3.17
$\lambda = 2I$	Period Parameter	Eq. 3.20
$a = \frac{1}{2}(u_m - 1)$		Eq. 3.23
$b = \dot{u}_m$		Eq. 3.24
$c = \frac{1}{2}(u_m + 1)$		Eq. 3.25
$z = u_0^{3/2} u$		Eq. 4.10

Symbol	Definition	Where Defined
$p(x) = \frac{\lambda^2}{2u_0^2}\left[\frac{5u_v^2}{u_0^2} - 1\right]$		Eq. 4.12
δ^*, ε^*	Mathieu Stability Coefficients	Eq. 4.13
λ_1, λ_2	Eigenvalues of the Fundamental Matrix	Eq. 4.41
v_1, v_2	Normal or Floquet Solutions	Eq. 4.51
α	First-Order Solution Stability Parameter	Eq. 4.34
Δ	Wronskian of Fundamental Solution Set	Eq. 4.35
γ_1, γ_2	Characteristic Floquet Exponent	Eq. 4.49
ϕ_1, ϕ_2	Periodic Part of Floquet Solution	Eq. 4.62
C	First-Order Initial Growth Rate	Eq. 4.83

CHAPTER 1

INTRODUCTION

1.1 Background

In a flow about a submerged body, the fluid is known to contain very small nuclei containing air and water vapor. These nuclei translate downstream at some velocity close to that of the free stream. Some of these will come in contact with the body and enter its boundary layer. Submerged bodies, such as circular cylinders, hydrofoils or hemispherical headforms, have pressure distributions that vary along their arc lengths. At some point on the body the local static pressure of the liquid will equal that of the liquid vapor pressure after which there will be a region in which the static pressure is less than vapor pressure. It is in this region that the nuclei can experience vaporous bubble growth. Therefore the critical point at which the static pressure equals the vapor pressure separates two possible regions of bubble behavior along the body.

If the nucleus enters the boundary layer of the body upstream of this critical point, it will travel along the body and act as a flaccid bubble. In this upstream region the bubble will grow, mainly due to internal gas pressure changes caused by the changing liquid static pressure, until it sees a local static equal to vapor pressure. After this point on the body the local static pressure is less than the vapor pressure within the bubble and the conditions are favorable for vaporous bubble growth. If the nucleus either enters the boundary layer of the body in this region or is conveyed from the flaccid bubble region into the favorable region, it will grow vaporously to a maximum radius and then collapse as the local static pressure rises.

If there is no separation on the body the bubble will continue to collapse rapidly and violently. For sufficiently low Reynolds numbers, however, some bodies will have laminar separation regions. If the separation bubble is short, it seems possible that collapse may not occur, and the bubble will come to rest within the laminar separation bubble where

it can grow by gas diffusion [1], [13]. This diffusive growth continues until the bubble diameter reaches the height of the separation zone. Then the bubble interacts with the free shear layer and is translated downstream. If the flow reattaches, the turbulent shear in this region breaks the bubble into froth, creating a narrow ring of visible cavitation. The point at which this cavitation becomes visible is called cavitation inception. This type is known as bubble-ring cavitation, which is a form of attached cavitation controlled primarily by laminar boundary layer separation.

The governing equation which describes isothermal cavitation vapor bubble growth or collapse is the Rayleigh-Plesset equation [16]. It describes the growth of a spherical bubble in the region of a body where the local static pressure is less than the liquid vapor pressure. It also applies at least in the initial stages of collapse when the static pressure rises down stream of the minimum pressure point on the body. An examination of this equation may provide direct insight into the hydrodynamically forced growth of the nuclei leading to cavitation inception. From this knowledge it is hoped that a relationship between the parameters of the flow and submerged body with respect to critical flow conditions for cavitation onset might be found.

1.2 Previous Investigations

The governing Rayleigh-Plesset equation[1] describing isothermal vaporous growth and collapse of a spherical bubble of radius, R, as a function of time, t, in a perfect fluid, is written as

$$R\frac{d^2R}{dt^2} + \frac{3}{2}\left(\frac{dR}{dt}\right)^2 = \frac{\gamma}{R^3} - \frac{1}{R} + F(t) \ . \qquad (1.1)$$

Equation (1.1) assumes that the static pressure is responsible for driving the bubble growth, and is contained in the time dependent forcing pressure , F(t).

[1]See Appendix D for more dedails.

that the forcing function pulse acting on a nucleus is characterized by two widely varying time scales. One dimensionless scale, called "laboratory time," t_s, is governed by the time it takes for the growing nucleus to move through the low pressure region in the boundary layer which promotes vaporous growth. The other dimensionless time scale, called "bubble time," τ, is associated with the very high natural frequency of the very small nuclei and depends on the period of natural vibration of the a typical microbubble. This guarantees a very rapid response of the bubble to external pressure changes. For every period of "slow" laboratory time there are many periods of the "fast" bubble time. Therefore, the two time scales can be related by a very small parameter, ε, which is simply the ratio of t_s to τ.

Using this idea, Baker expanded the forced Rayleigh-Plesset equation and its initial conditions in orders of the small parameter ε. He then found an approximate solution to the zero-order equation in terms of elliptic integrals and functions. Although this analysis was quite complex and involved some approximations, it compared well with a strict numerical solution of the zero-order equation. Also, it set up a basis for the analysis of the first-order equation of the expansion which can be combined with the zero-order findings to approximate better the total solution.

1.3 Objective of this Investigation

The main objective of this investigation is to find a solution of the forced Rayleigh-Plesset equation (1.1). In general this can be solved numerically using standard computer algorithms which do not consider the aforementioned time scales. Use of this type of numerical approach makes it extremely difficult to isolate any critical flow parameters or conditions between them which can lead to cavitation inception.

This investigation extends Baker's method of solution [2]. It involves a two-scale perturbation expansion based on the small parameter ε, which relates the two time scales present in the problem, t_s and τ. Application of this two-scale procedure produces a series

of linear or nonlinear partial differential equations for the various powers in ε. This type of mathematical technique is well known [11] and it is hoped that it will work well with the very nonlinear equation (1.1).

The first part of the present investigation considers the forcing function. This comes from the pressure distribution across a particular body. Baker used a hemispherical head-form so that the pressure distribution may be correlated with much experimental data. This analysis will attempt to use a circular cylinder as the governing body, in part to see if the analysis is valid for different cases. Supercritical flow over a circular cylinder exhibits a pressure distribution showing a laminar bubble just upstream of the turbulent separation [3], [4]. Thus, experimental pressure data for a circular cylinder will be used to derive a forcing function for the problem.

Next, the two-scale dynamical equations will be derived. Although Baker's solution of the zero-order equation gave some new approximations for the time of growth in terms of the radius, it can not be inverted explicitly to give the radius as a function of time. An inversion is needed in order to obtain the first-order solution. Thus, in the present analysis, we will rely on numerical methods, supplementing them with small oscillation analysis which leads to periodic solutions requiring no inversion. Baker also assumed that the zero-order solution was independent of the laboratory time, t_s. This investigation will also attempt to verify this fact or at least to see what further research is needed if conditions can be found which show that other zero-order solutions may be possible.

Lastly, the first-order equation is analyzed for the case of periodic zero-order solutions and a numerical first-order solution is obtained using the Floquet theory. First the complementary function is found and its dynamic and numerical stability is examined. Then the Particular integral is found using variation of parameters. The entire process is translated into Fortran and a numerical example of the complete solution is given.

CHAPTER 2

BACKGROUND AND FORMULATION

2.1 Development of the Time Scales

As mentioned from the outset, this problem involves two time scales. The first of these is associated with the time it takes for the growing nucleus to move through the low pressure region on the submerged body, and the second is associated with the very high frequency response time of the nucleus to external pressure changes.

It is desirable to have the two time scales in dimensionless form. By first defining a characteristic laboratory time, D/V_0, one can define the dimensionless laboratory time as

$$t_s = \frac{t V_0}{D} , \tag{2.1}$$

where t is real time, D is the characteristic diameter or other length of the body and V_0 is the free stream velocity. Now we define a characteristic time, $\sqrt{\rho R_0^3/2\sigma}$, involving only the physical properties of the bubble and liquid. This characteristic time enables one to define a dimensionless bubble time as

$$\tau = t\sqrt{\frac{2\sigma}{\rho R_0^3}} , \tag{2.2}$$

where ρ is the liquid density and σ is the liquid surface tension. Introduction of a small parameter ε as the ratio of the characteristic bubble time to the characteristic laboratory time yields:

$$\varepsilon = \frac{\sqrt{\rho R_0^3/2\sigma}}{D/V_0} = \frac{V_0}{D}\sqrt{\frac{\rho R_0^3}{2\sigma}} . \tag{2.3}$$

It should also be noted that such a definition also gives the ratio ε in terms of the nondimensional terms defined above, i.e.,

$$\varepsilon = t_s/\tau. \tag{2.4}$$

A relative comparison of the "slow" laboratory time scale and the "fast" bubble time scale shows that the ratio, τ/t_s , can have a magnitude of about 10^3 or less. This says that τ is of very short duration compared to the time scale t_s, hence there are many periods of τ for one period of t_s. It follows from equation (2.3) that ε should be a small number, often of the order of 10^{-3} . These are the same two time scales used by Baker [2] in his work. As he states, the fast bubble time characterizes the high frequency oscillations of the individual bubbles, whereas the slow laboratory time characterizes the forcing function across the governing body.

2.2 The Forcing Function

In a discussion of the translation of a bubble over a submerged body, what must be brought to light is the driving force which creates the environment for subsequent vaporous bubble growth and the start of collapse. Discussion has been made of the fact that for vaporous growth to occur there must be a region on the body where the static pressure of the flow is less than the vapor pressure of the liquid. This region starts on the body at a critical point where the static pressure equals that of the vapor pressure of the liquid. Downstream of this critical point in the growth region, the pressure is characterized by

$$p_v > p \geq p_{min} \ , \tag{2.5}$$

where p_v is the vapor pressure of the liquid and p_{min} is the minimum static pressure on the body.

Defining a pressure coefficient as a function of arc length along the body and the cavitation number respectively as

$$C_p(s) = \frac{p(s) - p_0}{\frac{1}{2}\rho V_0^2} \tag{2.6}$$

and

$$K = \frac{p_0 - p_v}{\frac{1}{2}\rho V_0^2} , \tag{2.7}$$

one can write the relationship in equation (2.5) as

$$K > -C_p(s) \geq -(C_p)_{min} . \tag{2.8}$$

Here, p_0 is the free stream static pressure. Equation (2.8) suggests that, depending on the value of K, the negative of the pressure coefficient can be used to measure the pressure force on the bubble that causes vaporous growth. If $C_p = -K$, the pressure force would be zero. Thus a positive forcing function which acts on a typical bubble can be defined as the negative difference in these two quantities or

$$F(\varepsilon\tau) = -C_p(s) - K = -[C_p(s) + K] . \tag{2.9}$$

It should be noted in this particular case that the region of vaporous growth and collapse extends along the arc of the body only as far as the separation point of the laminar region. Once the bubble enters the separation region, it is assumed that the process of vaporous growth ends and any growth that continues is due to gas diffusion from the liquid into the bubble. Figure 2.1 shows a schematic of the pressure distribution across a hemispherical headform borrowed from Baker [2]. It gives an example of the different states a bubble might see if it traveled across the entire body including the flaccid region, the dividing point where $C_p(s) = -K$, the vaporous growth region and the laminar separation point.

The forcing function is written as $F = F(t_s) = F(\varepsilon\tau)$ due to the fact that it acts over the low pressure or vaporous growth region of the body which is characterized by the laboratory time scale. As an aside, intuition says that the forcing function depends on a parameter that contains ε, and it is shown later that this is the case. Since the pressure coefficient is given as a function of arc length on the body, one must convert from the arc length to the laboratory time.

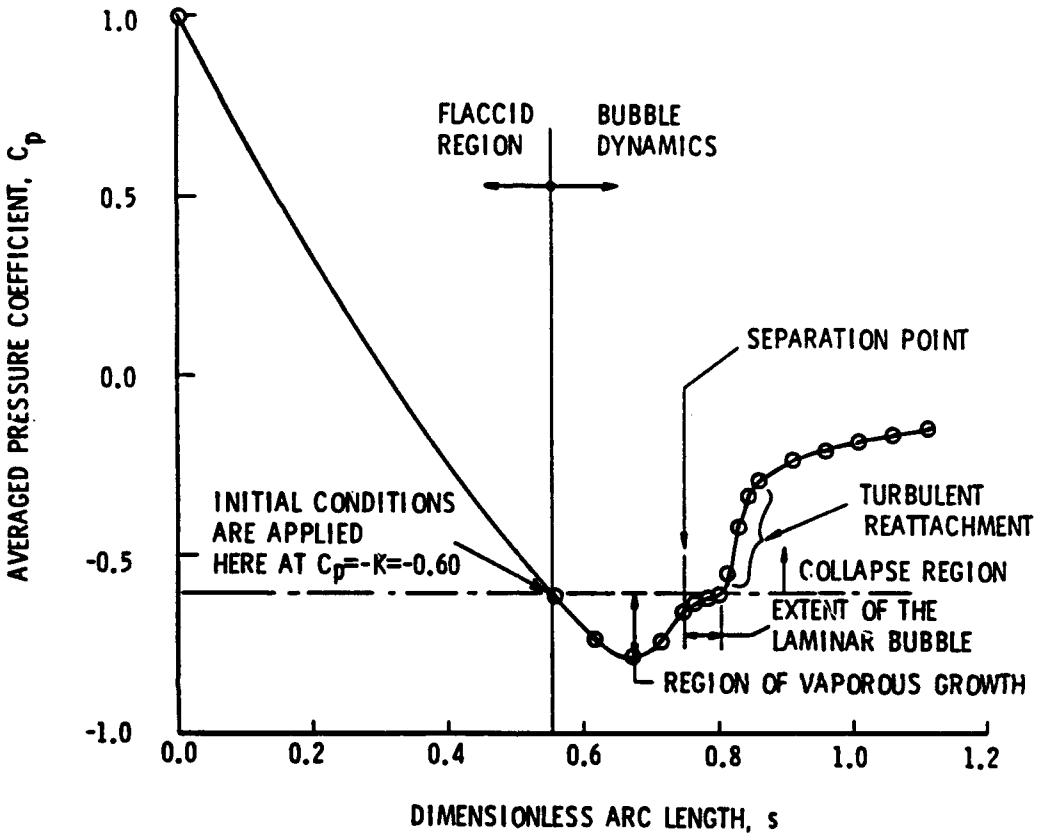

Figure 2.1 Schematic Diagram of the States as Seen by a Bubble Traveling Along a Hemispherical Headform, after Baker [2].

First, a dimensionless arc length is defined as

$$s = \frac{2S}{D} \tag{2.10}$$

where S is the dimensional arc length of the body. Assuming the boundary layer to be a vortex sheet, one can approximate its overall translational velocity as being one half of the local flow speed at the edge of the boundary layer, or

$$v(s) = \frac{V_0}{2}\sqrt{1 - C_p(s)} \ , \tag{2.11}$$

which then equals the convective speed of a typical bubble in the boundary layer. In terms of the body length this convective speed is

$$v(s) = \frac{dS}{dt} = \frac{dS}{ds}\frac{ds}{dt} \ . \tag{2.12}$$

Substituting the derivative of S from (2.10) and v(s) from equation (2.11) into equation (2.12) and solving for ds/dt one has

$$\frac{ds}{dt} = \frac{V_0}{D}\sqrt{1 - C_p(s)} \ . \tag{2.13}$$

Recalling equation (2.2) which relates the bubble time with real time, one can differentiate that equation to get

$$d\tau = \sqrt{\frac{2\sigma}{\rho R_0^3}}\, dt \ . \tag{2.14}$$

Substituting equation (2.4) for ε and (2.13) into equation (2.14) and integrating over s, one finds that an equation relating the dimensionless arc length to the laboratory time is

$$t_s = \varepsilon\tau = \int_{s_1}^{s_i} \frac{d\zeta}{\sqrt{1 - C_p(\zeta)}}, \quad i = 1, 2, \ldots . n \ . \tag{2.15}$$

In this case the suffix i corresponds to each pressure coefficient vs. its arc length datum point, s_i. This is the same transformation used by Baker [2].

What is now needed is the pressure coefficient data that are appropriate to any particular problem. The data must be either given as a function of arc length along the body or be readily convertible to such. We shall ask that the particular body from which the data are taken contain the necessary laminar separation region although its presence or absence will not preclude vaporous bubble growth. Baker used experimental C_p values given for a hemispherical headform. He determined that for cavitation numbers ranging from K = 0.6 to K = 0.7, the laminar separation points corresponded to positions of s = 0.813 and s = 0.731, respectively. He obtained very good results using these data.

In order to check the range of flow parameters, such as the cavitation number, this analysis will attempt to use data from a body containing a lower $(C_p)_{min}$, and thus be compatible with higher values of K. A circular cylinder was chosen because even at critical Reynolds numbers it exhibits laminar separation, and there exist some inception data [3] for this body although the inception is usually defined by the first appearance of cavitation bubbles within vortex cores in the separated shear layer . Reference [3] reports observations of cavitation in the laminar bubble. The pressure distribution used in this analysis comes from an NACA Technical Note by Gowen and Perkins [4]. Their graphical data showed a $C_p{}'_{min}$ of about - 2.6 for critical Reynolds numbers and at very low Mach numbers. The tabulated values used are given in appendix B, table B.1, and the smoothed data as a function of arc length interpolated from the table are shown in figure 2.2. Although the original values were simply read off of a graph, the fact that they exhibit the proper trend is more important than their accuracy since this analysis is somewhat qualitative.

The location of the laminar separation point is needed for the circular cylinder if one is to know when the analysis is no longer valid. Applying Thwaites' method and using a computer code given by Moran [5], we verified that in water at a free stream velocity of V_0 = 40 ft/s, a circular cylinder exhibits laminar separation. Using this code, and comparing its results with the best estimates from Schlichting [6] and Goldstein [7], we

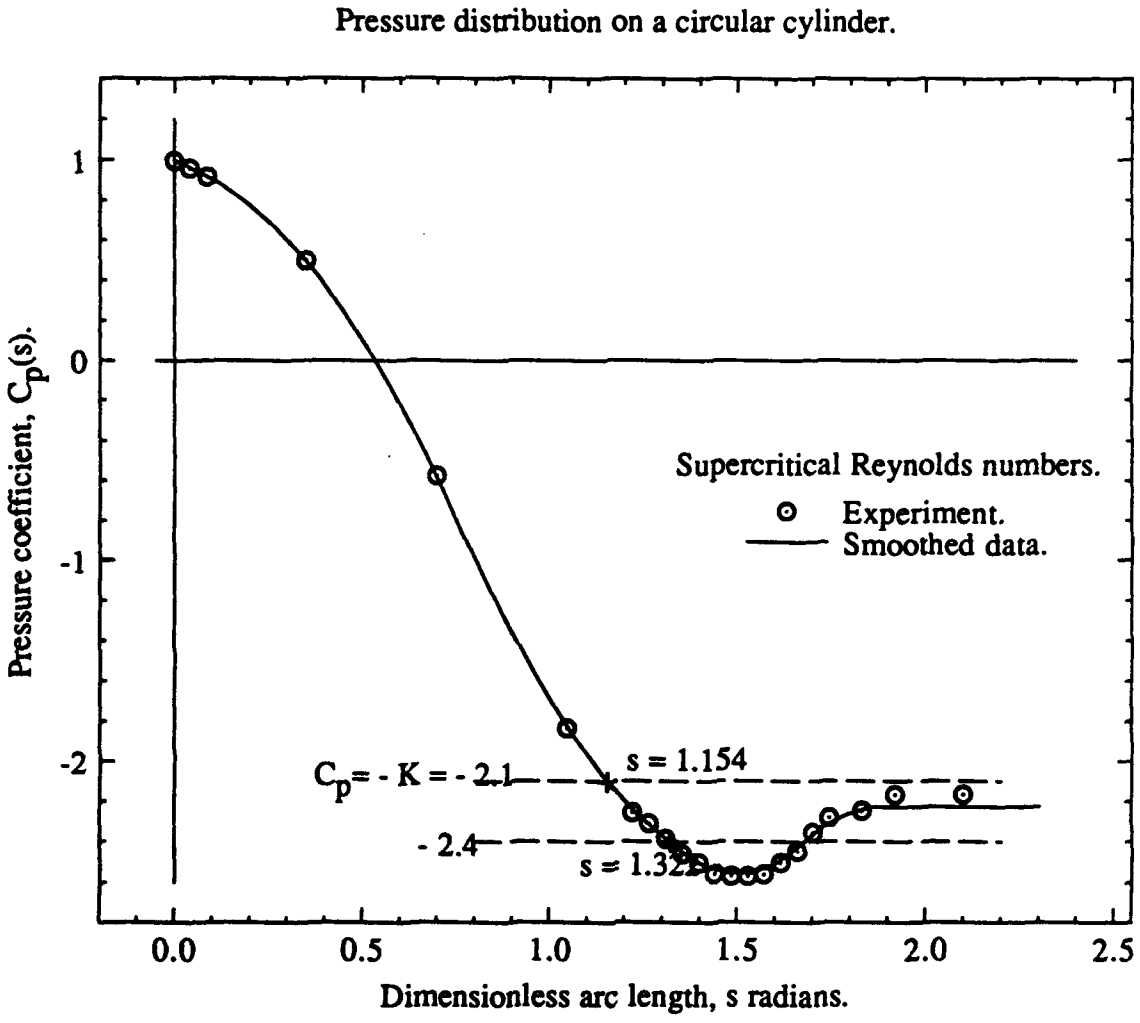

Figure 2.2 Experimental and Smooth Pressure Coefficient Data Versus Dimensionless Arc Length on a Circular Cylinder at Supercritical Reynolds Numbers

found separation to occur at approximately 110 degrees from the forward stagnation point or at a dimensionless arc length of s = 1.919. Knowing this, one finds a range of cavitation numbers that will allow favorable bubble growth and collapse to be from K = 2.1 to K = 2.4.

A Fortran code to determine the forcing function as a function of the laboratory time was developed and is contained in the complete code given in appendix A. It begins by curve fitting the given C_p vs s data using a cubic interpolation scheme, in order to produce evenly spaced values so that the integral in equation (2.15) can be evaluated using Simpson's rule. This calculation correlates the arc length (radians) with the dimensionless laboratory time. Care must be used when evaluating the integral at the stagnation point because of the square root singularity involved. A parabolic approximation is used over the first three points, including the singularity, to take care of this problem. The corresponding value of the forcing function is found by applying the chosen cavitation number to equation (2.9) for the interpolated C_p values. This step yields the forcing function as a function of laboratory time.

To give us a feel for a likely laboratory-time durations , figure 2.3 shows the pressure coefficient as a function of t_s as calculated from equation (2.15). Figure 2.4 is a schematic diagram of a typical forcing function showing its vaporous growth and collapse regions. The beginning of the positive growth region is located at the intersection of the horizontal line at $C_p = -K$ and and it is taken to be the origin of forcing function coordinates. Since this is the critical point where vaporous growth begins and the start of the region over which this investigation takes place, this is the point defined to be where the two time scales are equal to zero. It is convenient then to shift the coordinate axes to this point and have it be the origin. Depending on the value of K chosen, this shift will occur along a vector as shown in figure 2.4. The computer code developed also finds this new origin and so it automatically shifts the time axis so that it begins at zero. Figure 2.5 below

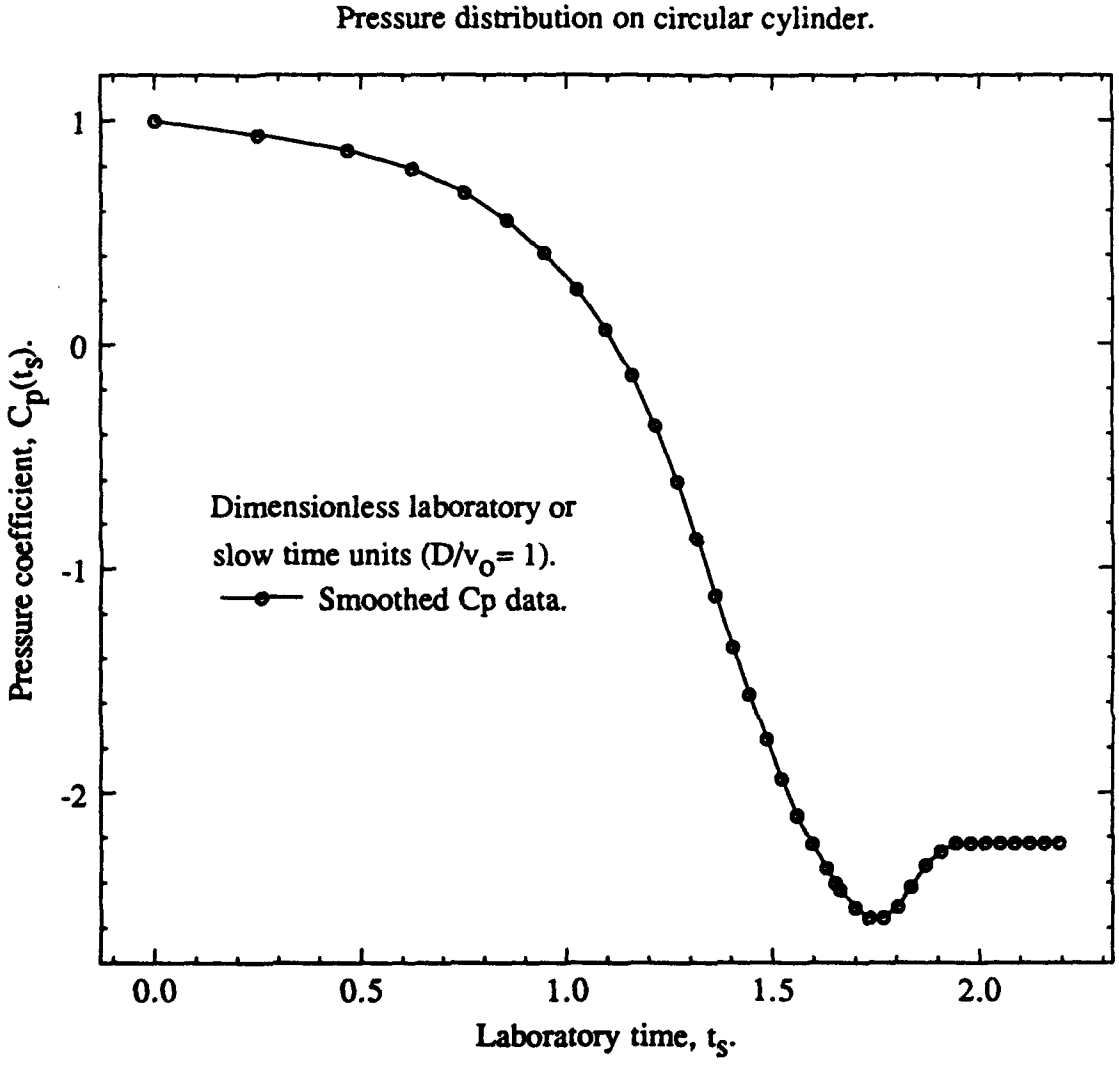

Figure 2.3 Pressure Distribution on a Circular Cylinder as a Function of the Labortatory Time.

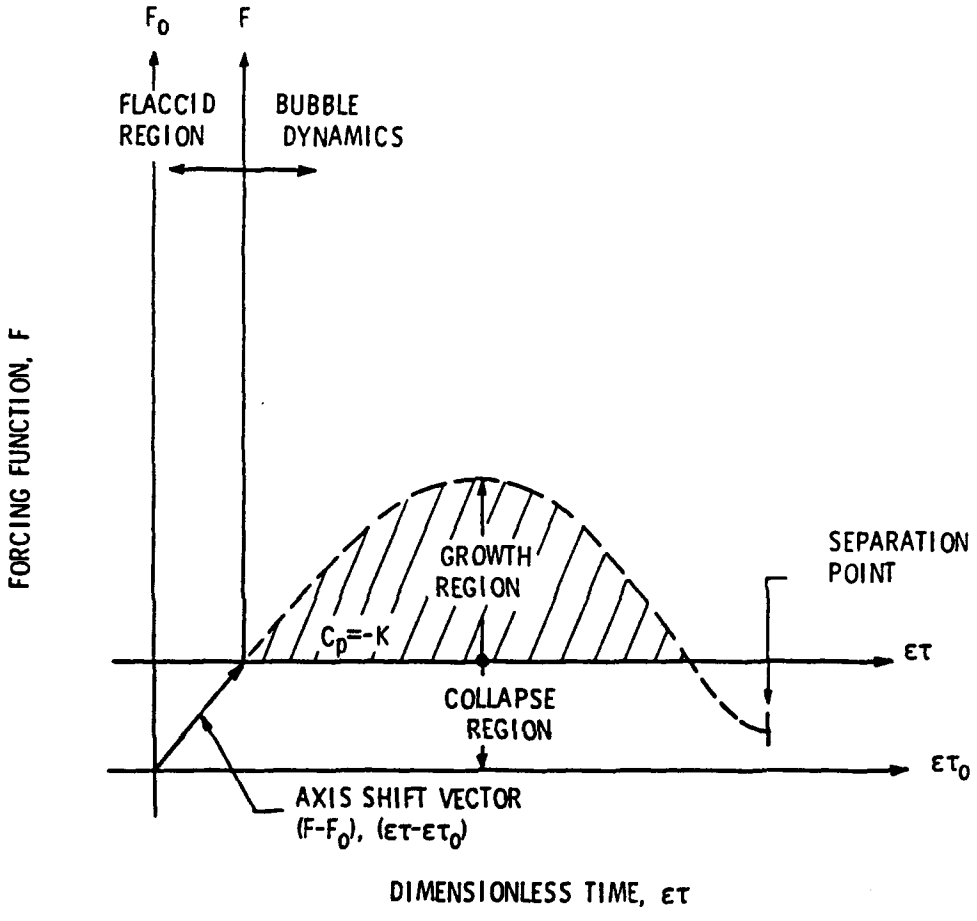

Figure 2.4 Schematic Diagram of a Typical Forcing Function Showing Regions of Vaporous Growth and Collapse.

Forcing function for two cavitation numbers.

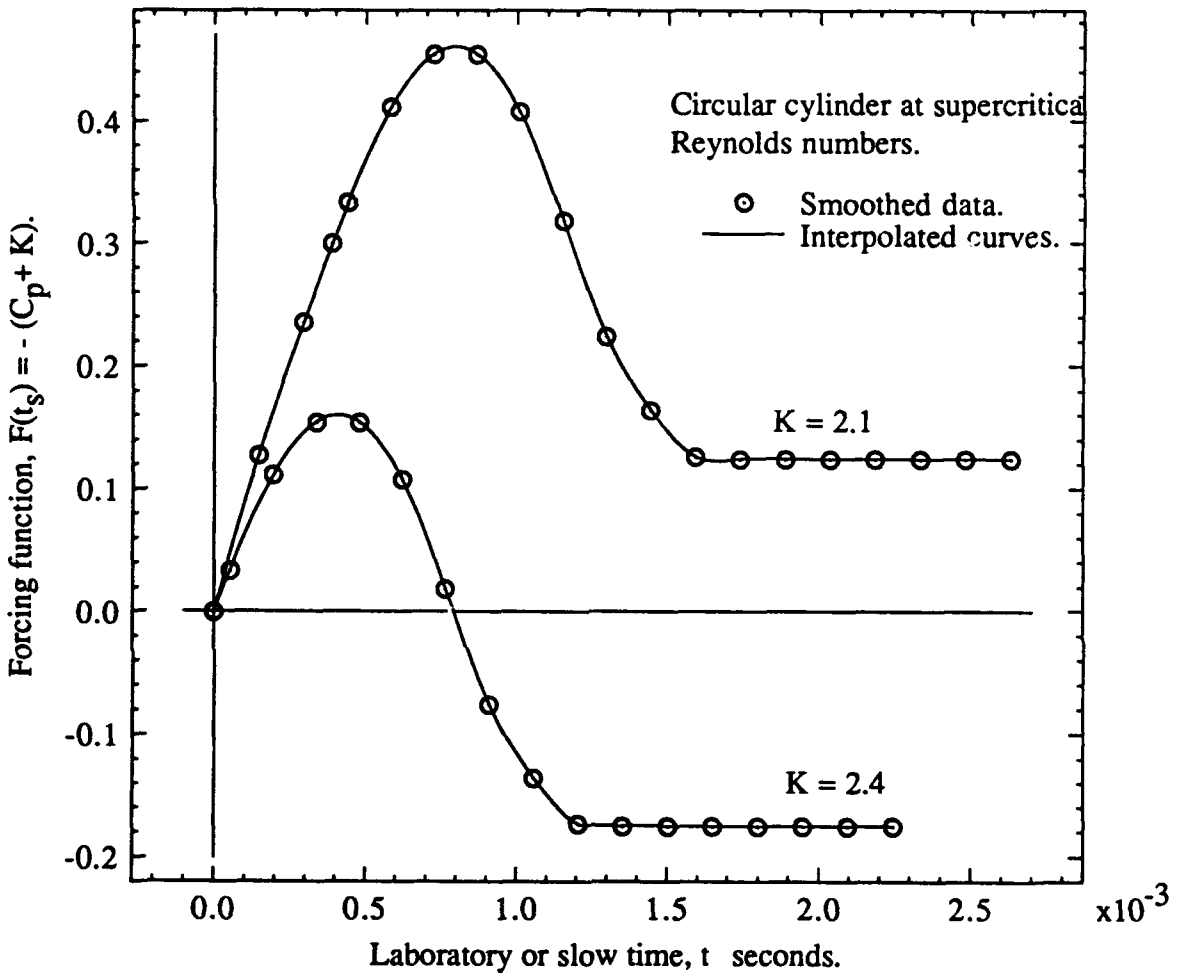

Figure 2.5 Forcing Function for a Circular Cylinder as a Function of Shifted Actual Time for Cavitation Numbers, K= 2.1 and K = 2.4.

shows the shifted forcing function for a circular cylinder at values of K = 2.1 and K = 2.4 as a function of the actual time. The actual time can be divided by the ratio of D/V_0 in order to get F in terms of the laboratory time, which is then used as an input to the bubble-dynamic analysis.

2.3 Flaccid Bubble Analysis

As described by Baker [2], the bubble grows as a flaccid balloon before it reaches the point where $C_p = -K$. It experiences successive states of isothermal equilibrium as its size changes from the time it reaches a point near the stagnation point on a submerged body, and it travels within the boundary layer before it reaches the region favorable to vaporous growth. The bubble experiences no vaporous growth during this first phase of its motion on the body. As sketched here, suchbubbles originate from free-stream micro-bubbles of some radius r at the free-stream static pressure p_0. The term, $2\sigma/r$, gives the pressure jump across the bubble surface. The internal pressure is the sum of vapour and air pressures as shown.

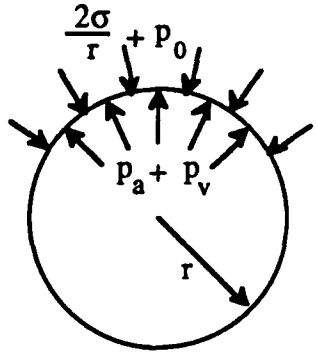

A Free-Stream Nucleus.

The flaccid bubble kinematics relates the bubble's radial motion to its movement along the dimensionless arc length, s, of the headform. Depending on the size of the submerged body, this length is the dimensional arc length of the headform, S, divided by some characteristic body length, D. The rate of change of pressure experienced by the bubble is therefore,

$$\frac{dC_p}{dt} = \frac{dC_p}{ds}\frac{ds}{dt} \cdot \qquad (2.16)$$

This form is sought because the experimental pressure distribution is given in terms of s.

The kinematics of the previous section, as embodied in equation (2.13), provides an expression for ds/dt. Substituting equation (2.13) into equation (2.16), one gets the rate of change of pressure experienced by a nucleus as it travels across a body to be

$$\frac{dC_p}{dt} = \frac{V_0}{D}\sqrt{1 - C_p}\,\frac{dC_p}{ds} \quad . \tag{2.17}$$

This is all the kinematics that are needed. Next we use Boyle's law for an isothermal flaccid bubble and the force (pressure) balance across the bubble wall. Then we combine these three results to achieve expressions for the bubble's flaccid growth characteristics.

The bubble contains both air and water vapor. Therefore inside the bubble the total pressure is

$$p_i = p_a + p_v \quad . \tag{2.18}$$

Only the air obeys Boyle's law, which requires that

$$p_a R^3(t) = p_{a_0} R_0^3 \quad , \tag{2.19}$$

where p_{a_0} = partial pressure of air inside the free stream nucleus at $R = R_0$. A dimensionless bubble radius is now defined using the free stream nucleus radius, R_0, such that

$$r(t) = R(t)/R_0 \quad . \tag{2.20}$$

It is noted that p_{a_0} is a constant, and in the free stream when $r = 1$, $p_a = p_{a_0}$. Now if p(t) is the static pressure outside the bubble and σ is the surface tension, on the bubble wall the pressure forces are in balance and

$$p_i = \frac{2\sigma}{R(t)} + p(s) \quad . \tag{2.21}$$

So for a bubble in the free stream, as in the illustrative sketch above,

$$p_{a_0} + p_v = \frac{2\sigma}{R_0} + p_0 \quad , \tag{2.22}$$

and for a bubble inside the boundary layer

$$p_a + p_v = \frac{2\sigma}{R(t)} + p(s) \ . \tag{2.23}$$

Solving (2.22) and (2.23) for p_a and p_{a_0} respectively and substituting them into Boyle's law, equation (2.19), one finds the result,

$$\left[\frac{2\sigma}{R(t)} + p(s) - p_v\right]R^3(t) = \left[\frac{2\sigma}{R_0} + p_0 - p_v\right]R_0^3 \ . \tag{2.24}$$

By substituting (2.6) and (2.7) for the various pressure differences into (2.24) and using the nondimensional bubble radius, one finds that

$$\left[\frac{2\sigma}{R_0 r(t)} + \frac{1}{2}\rho V_0^2(C_p + K)\right]r^3(t) = \frac{2\sigma}{R_0} + \frac{1}{2}\rho V_0^2 K \ . \tag{2.25}$$

Multiplying through by $R_0/2\sigma$ and defining a radial Weber number as

$$W_r = \frac{\rho R_0 V_0^2}{\sigma} \ , \tag{2.26}$$

one obtains a cubic equation for the dimensionless flaccid bubble radius in the form

$$\frac{1}{4}W_r\left[C_p(t) + K\right]r^3(t) + r^2(t) - \left[1 + \frac{1}{4}K W_r\right] = 0 \ . \tag{2.27}$$

This equation can be solved exactly and its derivative taken to obtain expressions for the flaccid bubble radius and growth rate as functions of real time, t. Because of the fact that the Rayleigh-Plesset equation governs the growth of the bubble after the point of vaporous growth, this expression and its derivative can be used to form initial conditions at the critical point where vaporous growth begins.

In the special case when $C_p = 0$, equation (2.27) can be factored as follows:

$$\left[\frac{K W_r}{4}(r^2 + r + 1) + r + 1\right](r - 1) = 0.$$

The only root of physical interest is $r = 1$, as should be the case for a nucleus in the free stream. Another special case occurs when $C_p = -K$. Then the cubic term is lost. and we find that the two remaining roots are

$$r = \pm\sqrt{1 + \frac{K W_r}{4}}$$

The positive root is a useful physical quantity in the dynamical solution of Chapter 3. We note here that it pertains to those values of Cp and K which mark the origin of coordinates in figures 2.4 and 2.5. That is, for any value of $K \leq -C_p|_{min}$, vaporous growth first becomes possible; and from equation (2.20), it gives the ratio of microbubble size at that initial condition to a typical free-stream nucleus size.

2.3.1 Formulation of the Flaccid Bubble Radius, r(t)

The cubic flaccid bubble equation can be solved exactly. Because of the fact that the non-dimensional bubble radius is very close to unity, one can easily find a solution using a simple perturbation of the form

$$r = 1 - x \,, \tag{2.28}$$

where $0 < x << 1$. Substituting this into (2.27) and neglecting terms of order x^3 and higher, one sees that a quadratic equation for x remains and it is

$$(3A + 1)x^2 - (3A + 2)x + \frac{1}{4}C_p W_r = 0 \,, \tag{2.29}$$

where $A = \frac{1}{4}(C_p + K) W_r$. The two roots of x are found to be

$$x = \frac{1}{2}\frac{(3A + 2)}{(3A + 1)}\left[1 \pm \sqrt{1 - C_p W_r \frac{(3A + 1)}{(3A + 2)^2}}\right] \tag{2.30}$$

The proper root must be decided upon for this particular case. Consider the case in which $C_p \rightarrow -K$; then $A \rightarrow 0$. Due to the conditions imposed upon x by equation (2.28), the negative root must be chosen to satisfy $0 < x << 1$. The value of x is therefore

$$\lim_{A \rightarrow 0} x = 1 - \sqrt{1 + \frac{1}{4}K W_r} \,. \tag{2.31}$$

For ease of writing a new variable is introduced, namely:

$$q = \frac{1}{4} K W_r . \tag{2.32}$$

In the limit as $C_p = -K$, equation (2.31) gives $x = 0$ corresponding to a nucleus of $r = 1$ as it is in the free stream. The same result is found if one applies this condition to the cubic flaccid bubble equation. Setting $C_p = -K = 0$ in equation (2.27), we find

$$r^2 - 1 = 0 , \tag{2.33}$$

which has a root at $r = 1$. For $C_p = -K \neq 0$ and neglecting the cubic term as before, the equation for r is written as

$$r^2 - 1 - q = 0. \tag{2.34}$$

Equation (2.34) yields the same result as one gets by substituting (2.31) into (2.28), nameley:

$$r = \sqrt{1 + q} . \tag{2.35}$$

Substitution of (2.30) into (2.28), with the expression for A in mind, yields

$$r(t) = 1 - \frac{1}{2}\frac{(3A + 2)}{(3A + 1)} \left[1 \pm \sqrt{1 - C_p W_r \frac{(3A + 1)}{(3A + 2)^2}} \right] . \tag{2.36}$$

This then is the flaccid bubble radius as a function of actual time, in terms of the flow parameters C_p, K, and W_r. It is valid only in the region from the stagnation point up to the initial point of vaporous growth. This is similar to the form derived by Baker [2], and as was shown by him, shows very good agreement with experimental results of nucleus measurements in this region.

2.3.2 Calculation of the Initial Radius, r(0)

For the vaporous growth phase the initial point at which the dimensionless laboratory time and the dimensionless bubble time are measured is the point on the body where $C_p = -K$. Since vaporous growth is preceded by the flaccid bubble region, the initial conditions for vaporous growth from the flaccid bubble equations should be evaluated at

the point on the body surface where this C_p value is found. Recalling that equation (2.35) was derived at the point where $C_p = -K$ and if $t = t_0$ at this point, it can be written as

$$r(t_0) = \sqrt{1 + q} \quad . \tag{2.37}$$

This then is the initial bubble radius at $t = t_0$ and $t_s = \tau = 0$, corresponding to the point on the body where $C_p = -K$. Using this result one can define the dimensionless parameter for any real time as

$$u(t) = \frac{r(t)}{\sqrt{1 + q}} \quad , \tag{2.38}$$

which is called the *normalized bubble radius*. Initially when $t = t_0$,

$$u(t_0) = 1. \tag{2.39}$$

This normalized bubble radius can be applied to all further equations involving t and its derivatives. Since its initial value is unity, it makes the scaling of the solutions much easier to handle. Therefore the normalized bubble radius will be employed in those results which form the basic ingredients for subsequent analyses of bubble dynamics.

2.3.3 Formulation of the Flaccid Bubble Growth Rate, $\dot{r}(t)$

Another important characteristic of the flaccid bubble problem is the bubble growth rate. The flaccid bubble growth rate is defined as the first derivative of the flaccid bubble radius with respect to real time, t. This rate is found by differentiating the cubic flaccid bubble equation. Thus from (2.27)

$$\frac{3}{4} W_r \left[C_p(t) + K\right] r(t) \frac{dr}{dt} + \frac{1}{4} r^2(t) W_r \frac{dC_p}{dt} + 2\frac{dr}{dt} = 0 \quad . \tag{2.40}$$

Substituting for $\frac{dC_p}{dt}$ from (2.17) and solving for $\frac{dr}{dt}$, one finds the flaccid bubble growth rate to be

$$\frac{dr}{dt} = \frac{\frac{1}{8} r^2(t) W_r \frac{v_0}{D} \sqrt{1 - C_p(t)} \left(-\frac{dC_p}{ds}\right)}{1 + \frac{3}{8} r(t) W_r \left[C_p(t) + K\right]} \quad . \tag{2.41}$$

This rate is a function of the flaccid bubble radius, the flow parameters - C_p, K, W_r, the free stream velocity, v_0, and also some body parameters. Particular to the body is the characteristic diameter, D, and its pressure coefficient curve. This curve leads to the forcing function on to a given body that ultimately stimulates the bubble nucleus vaporous growth. This again is similar to the result achieved by Baker [2] and as he shows, it relates well to experimental results.

To normalize this result with the same parameter used in the flaccid bubble radius result, equation (2.38) and its derivative is applied to (2.41) resulting in

$$\frac{du}{dt} = \frac{\frac{1}{8}u^2(t)\,W_r\frac{v_0}{D}\sqrt{(1+q)(1 - C_p(t))}\left(-\frac{dC_p}{ds}\right)}{1 + \frac{3}{8}u(t)\,W_r\sqrt{1+q}\left[C_p(t) + K\right]} . \tag{2.42}$$

This is the normalized flaccid bubble growth rate. Its initial value when t = 0 will be discussed in a later section.

2.3.4 Calculation of the Initial Flaccid Bubble Growth Rate, $\dot{r}(0)$

The initial growth rate begins when $t = t_0$ and $t_s = \tau = 0$, and at the point on the body where $C_p = -K$. Using this relationship and substituting (2.37) into (2.41), one gets an expression for the initial bubble growth rate with respect to real time which is

$$\left.\frac{dr}{dt}\right|_{t=0} = \frac{1}{8}(1+q)\,W_r\frac{v_0}{D}\sqrt{1 + K}\left(-\frac{dC_p}{ds}\right)_{C_p = -K} . \tag{2.43}$$

It is desired to analyze the growth rate in terms of the dimensionless slow laboratory time, t_s. To express the initial growth rate in terms of this time scale , the derivative of the relationship

$$t_s = \frac{V_0}{D}t , \tag{2.44}$$

is substituted into (2.43), resulting in

$$\left.\frac{dr}{dt_s}\right|_{t_s=0} = \frac{1}{8}(1+q)\,W_r\sqrt{1 + K}\left(-\frac{dC_p}{ds}\right)_{C_p = -K} . \tag{2.45}$$

Relative to this time scale the initial bubble growth rate loses its explicit relationship to the characteristic body diameter and free stream velocity, although the square of the free stream velocity is contained in the Weber number.

Writing the initial bubble radius with respect to slow time in normalized form, one needs the derivative with respect to slow time of equation (2.38). Applying this to the result in equation (2.45), one sees that it becomes

$$\left.\frac{du}{dt_s}\right|_{t_s = 0} = \frac{1}{8} W_r \sqrt{(1 + q)(1 + K)} \left(- \frac{dC_p}{ds}\right)_{C_p = - K} . \qquad (2.46)$$

This is the normalized initial bubble growth rate with respect to the slow laboratory time. One gets the same result from evaluating equation (2.42) at $t_s = 0$ and converting it to the slow time scale via equation (2.44).

So far the two initial conditions and the forcing function have been found for the Rayleigh-Plesset equation in terms of the two dimensionless time scales involved in the perturbation expansion for the point when $C_p = - K$. These can now be used to help solve the expanded equations which will be derived from perturbation theory.

2.4 Formulation of the Dynamical Bubble Equations to Order ε^3

The pulse-forced Rayleigh-Plesset equation (1.1) written in terms of the dimensionless radius, r, with respect to real time, t, is

$$r\frac{d^2r}{dt^2} + \frac{3}{2}\left(\frac{dr}{dt}\right)^2 = \frac{\gamma}{r^3} - \frac{1}{r} + F(t) , \qquad (2.47)$$

where F(t) is some forcing function characteristic of the governing body and the flow properties[1]. As noted in section 1.2 above, this is the governing equation for vaporous growth and collapse of a spherical isothermal cavitation bubble. It is a second order ordinary differential equation requiring the two initial conditions given above in equations

[1] See Appendix D for the derivation of this dimensionless form of equation (1.1).

(2.37) and (2.45). To derive an appropriate solution to this equation we shall expand it in ascending powers of the small perturbation parameter ε.

The method of multiple scales is used because of the two widely varying time scales present in the problem. In the two-scale form [11], the small parameter ε allows the effect of the fast bubble time to be pulled into the slower laboratory time in a uniform fashion. The slow laboratory time scale, t_S, is the characteristic time for the bubble to pass along the low pressure region in the boundary layer of a particular body. This time scale characterizes the forcing function since it depends on the body. The fast bubble time scale, τ, is the characteristic time of the free stream nucleus oscillation period. This scale is very fast compared to the slow time scale, so the two are related according to,

$$t_S = \varepsilon\tau \ . \tag{2.48}$$

From these two time scales and the small perturbation parameter, the dynamical equation can be expanded to order ε^3.

We shall write the first and second derivative expansions in terms of the two time scales, because it is assumed that

$$r = r(t_s,\tau,\varepsilon). \tag{2.49}$$

Taking the derivative of r with respect to real time, using the chain rule and (2.48), one has

$$\frac{dr}{dt} = \frac{\partial r}{\partial t_s} + \frac{1}{\varepsilon}\frac{\partial r}{\partial \tau} \ , \tag{2.50}$$

and differentiating again, one gets

$$\frac{d^2r}{dt^2} = \frac{\partial^2 r}{\partial t_s^2} + \frac{2}{\varepsilon}\frac{\partial^2 r}{\partial t_s \partial \tau} + \frac{1}{\varepsilon^2}\frac{\partial^2 r}{\partial \tau^2} \ . \tag{2.51}$$

Next we applying the above first and second derivative expansions to a general perturbation expansion of r of the form

$$r = r_0 + r_1\varepsilon^1 + r_2\varepsilon^2 + r_3\varepsilon^3 + \dots \ , \tag{2.52}$$

which leads one to the completely expanded final forms. They are, up to order ε^3,

$$\frac{dr}{dt} = \frac{1}{\varepsilon}\frac{\partial r_0}{\partial \tau} + \left[\frac{\partial r_0}{\partial t_s} + \frac{\partial r_1}{\partial \tau}\right] + \varepsilon\left[\frac{\partial r_1}{\partial t_s} + \frac{\partial r_2}{\partial \tau}\right] + \varepsilon^2\left[\frac{\partial r_2}{\partial t_s} + \frac{\partial r_3}{\partial \tau}\right] \quad (2.53)$$

and

$$\frac{d^2r}{dt^2} = \frac{1}{\varepsilon^2}\left[\frac{\partial^2 r_0}{\partial t_s^2}\right] + \frac{1}{\varepsilon}\left[\frac{\partial^2 r_1}{\partial t_s^2} + 2\frac{\partial^2 r_0}{\partial t_s \partial \tau}\right] + \left[\frac{\partial^2 r_2}{\partial t_s^2} + 2\frac{\partial^2 r_1}{\partial t_s \partial \tau} + \frac{\partial^2 r_0}{\partial t_s^2}\right]$$

$$+ \varepsilon\left[\frac{\partial^2 r_3}{\partial t_s^2} + \frac{\partial^2 r_2}{\partial t_s \partial \tau} + \frac{\partial^2 r_1}{\partial t_s^2}\right] . \quad (2.54)$$

Determination of each term of equation (2.47) can be based on the general expansion for r and its derivatives (2.53) and (2.54). As was shown previously in section 2.2, the forcing function $F(\varepsilon t)$ is involved only in the first order of ε. This fact leads to the first order equation being the only nonautonomous expansion equation.

The two initial conditions, $r(t_0)$ and $dr(t_0)/dt$, must also be expanded by this method. This is accomplished by equating the flaccid bubble initial radius of (2.37) and the flaccid bubble initial growth rate of (2.45) to (2.52) and (2.53) respectively, and equating like powers of ε.

To unify the non-dimensional radius we introduce from equation (2.38), the substitution of

$$r = u\sqrt{1+q} \quad , \quad (2.55)$$

where $q = KW_r/4$, as before. This comes from the flaccid bubble radius and allows one to write the normalized isothermal Rayleigh-Plesset equation with initial conditions consistent with those used by Baker [2]. Once solved for their respective u_i's, the resulting set of differential equations and initial conditions can, using (2.55), be substituted into (2.52) in order to achieve a final perturbation solution for the non-dimensional bubble radius as a function of real time. The normalized differential equations and initial conditions up to order ε^3 are displayed below.

ε^0 Order Equation:

$$u_0\frac{\partial^2 u_0}{\partial \tau^2} + \frac{3}{2}\left(\frac{\partial u_0}{\partial \tau}\right)^2 = \frac{u_v^2}{u_0^3(1+q)^{3/2}} - \frac{1}{u_0(1+q)^{3/2}} \tag{2.56}$$

with initial conditions,

$$\left.\begin{aligned} u_0(0,0) &= 1 \\ \frac{\partial u_0(0,0)}{\partial \tau} &= 0 \end{aligned}\right\} . \tag{2.57}$$

ε^1 Order Equation:

$$\frac{\partial^2 u_1}{\partial \tau^2} + \frac{3}{u_0}\frac{\partial u_0}{\partial \tau}\left(\frac{\partial u_1}{\partial \tau}\right) + \frac{u_1}{u_0}\left[\frac{\partial^2 u_0}{\partial \tau^2} + \frac{1}{u_0^2(1+q)^{3/2}}\left(\frac{3u_v^2}{u_0^2} - 1\right)\right]$$

$$= -2\left[\frac{\partial^2 u_0}{\partial \tau\, dt_s} + \frac{3}{2}\frac{1}{u_0}\frac{\partial u_0}{\partial \tau}\frac{\partial u_0}{\partial t_s}\right] + \frac{F(\varepsilon, t_s)}{u_0(1+q)^{3/2}} , \tag{2.58}$$

with initial conditions,

$$\left.\begin{aligned} u_1(0,0) &= 0 \\ \frac{\partial u_1(0,0)}{\partial \tau} + \frac{\partial u_0(0,0)}{\partial t_s} &= \frac{1}{8}W_r\sqrt{(1+q)(1+K)}\left(-\frac{dC_p}{ds}\right)_{C_p = -K} \end{aligned}\right\} . \tag{2.59}$$

ε^2 Order Equation:

$$\frac{\partial^2 u_2}{\partial \tau^2} + \frac{3}{u_0}\frac{\partial u_0}{\partial \tau}\left(\frac{\partial u_2}{\partial \tau}\right) + \frac{u_2}{u_0}\left[\frac{\partial^2 u_0}{\partial \tau^2} + \frac{1}{u_0^2(1+q)^{3/2}}\left(\frac{3u_v^2}{u_0^2} - 1\right)\right]$$

$$= -\left[2\frac{\partial^2 u_1}{\partial \tau \partial t_s} + 2\frac{u_1}{u_0}\frac{\partial^2 u_0}{\partial \tau \partial t_s} + \frac{3}{u_0}\frac{\partial u_0}{\partial \tau}\left(\frac{\partial u_1}{\partial t_s}\right) + \frac{3}{u_0}\frac{\partial u_0}{\partial t_s}\left(\frac{\partial u_1}{\partial \tau}\right) + \frac{\partial^2 u_0}{\partial t_s^2}\right.$$

$$\left. + \frac{3}{2}\frac{1}{u_0}\left(\frac{\partial u_0}{\partial t_s}\right)^2\right] - \frac{u_1}{u_0}\frac{\partial^2 u_1}{\partial \tau^2} - \frac{3}{2}\frac{1}{u_0}\left(\frac{\partial u_1}{\partial \tau}\right)^2 + \frac{u_1^2}{u_0^4(1+q)^{3/2}}\left[\frac{6u_v^2}{u_0^2} - 1\right], \qquad (2.60)$$

with initial conditions,

$$\left.\begin{aligned} u_2(0,0) &= 0 \\ \frac{\partial u_2(0,0)}{\partial \tau} + \frac{\partial u_1(0,0)}{\partial t_s} &= 0 \end{aligned}\right\} \qquad (2.61)$$

ε^3 Order Equation:

$$\frac{\partial^2 u_3}{\partial \tau^2} + \frac{3}{u_0}\frac{\partial u_0}{\partial \tau}\left(\frac{\partial u_3}{\partial \tau}\right) + \frac{u_3}{u_0}\left[\frac{\partial^2 u_0}{\partial \tau^2} + \frac{1}{u_0^2(1+q)^{3/2}}\left(\frac{3u_v^2}{u_0^2} - 1\right)\right] =$$

$$-\left[2\frac{\partial^2 u_2}{\partial \tau \partial t_s} + 2\frac{u_2}{u_0}\frac{\partial^2 u_0}{\partial \tau \partial t_s} + \frac{3}{u_0}\frac{\partial u_0}{\partial \tau}\left(\frac{\partial u_2}{\partial t_s}\right) + \frac{3}{u_0}\frac{\partial u_0}{\partial t_s}\left(\frac{\partial u_2}{\partial \tau}\right) + 2\frac{u_1}{u_0}\frac{\partial^2 u_1}{\partial \tau \partial t_s}\right.$$

$$\left. + \frac{3}{u_0}\frac{\partial u_1}{\partial t_s}\left(\frac{\partial u_1}{\partial \tau}\right) + \frac{\partial^2 u_1}{\partial t_s^2} + \frac{u_1}{u_0}\frac{\partial^2 u_0}{\partial t_s^2} + \frac{3}{u_0}\frac{\partial u_0}{\partial t_s}\left(\frac{\partial u_1}{\partial t_s}\right)\right] + \frac{u_1}{u_0}\frac{\partial^2 u_2}{\partial \tau^2} + \frac{u_2}{u_0}\frac{\partial^2 u_1}{\partial \tau^2}$$

$$+ \frac{3}{u_0}\frac{\partial u_1}{\partial \tau}\left(\frac{\partial u_2}{\partial \tau}\right) + \frac{2u_2u_1}{u_0^4(1+q)^{3/2}}\left[\frac{6u_v^2}{u_0^2} - 1\right] - \frac{u_1^3}{u_0^5(1+q)^{3/2}}\left[\frac{10u_v^2}{u_0^2} + 1\right], \qquad (2.62)$$

with initial conditions

$$\left.\begin{aligned} u_3(0,0) &= 0 \\ \frac{\partial u_3(0,0)}{\partial \tau} + \frac{\partial u_2(0,0)}{\partial t_s} &= 0 \end{aligned}\right\} \qquad (2.63)$$

2.5 Estimates of Flow and Perturbation Parameter Ranges

In the previous sections many parameters have been defined. It is of prime concern in this investigation to achieve results which are directly related to the characteristics of the fluid flow and the governing body. As will be shown later all flow characteristics are combined into one parameter, a so called vortex point affix defined in the bubble radius versus radial velocity phase plane of the zero-order solution. This parameter, called u_v, is used throughout the analysis. The objective of this section is to determine ranges of the parameters that define the flow from typical values of obsevable flow quantities.

There are three basic dimensionless parameters that define the flow. These are the radial Weber number, W_r, the cavitation number, K, and the air content parameter, γ. The radial Weber number, as defined in equation (2.26), is based on the initial radius of the bubble nucleus in the free stream. For water, experiments have shown that typical nucleus radii vary in size over the range

$$5 < R_0 < 150 \quad \mu m\,, \qquad (2.64)$$

and the smaller the nucleii the greater their numbers. Along with the density and the surface tension for water at 70° F, the Weber number also contains the free stream velocity, V_0. Typical velocities obtainable in water tunnels vary in the range

$$0 < V_0 < 80 \quad ft/s\,. \qquad (2.65)$$

From these ranges, we find the range estimate for the radial Weber number for water to be

$$0 < W_r < 1215\,. \qquad (2.66)$$

The cavitation number, as defined in equation (2.7), depends on the difference in free stream static pressure and vapor pressure as well as the speed of the flow. Previously, in his forced bubble growth analysis, Baker [2] used a small range of cavitation number values typical of a hemispherical headform. But since cavitation numbers can reach as high as 2 or 3 for certain conditions, for this estimate we use an expanded range that could include a variety of models. This range varies from

$$0.1 < K < 3.0 \ . \tag{2.67}$$

The Weber and cavitation numbers are both contained in the parameter q, as defined in equation (2.32). Using the ranges for these in equations (2.66) and (2.67), we find the range of q to be approximately

$$0 < q < 911 \ . \tag{2.68}$$

The air content parameter depends on the size of the initial nucleus radius and the partial pressure of the gas at the liquid-gas interface, p_a. This partial pressure is found using Henry's Law where

$$p_a = \beta\alpha \ . \tag{2.69}$$

Henry's Law constant, β, is in general a function of pressure and temperature. But for pressures well above atmospheric it is nearly independent of pressure, but it still depends on the temperature. At a temperature of 70° F, Henry's Law constant is

$$\beta = 0.99 \ \frac{\text{psia}}{\text{ppm}} \ , \tag{2.70}$$

where "ppm" refers to molal parts per million. The amount of any dissolved gas, α, in water tunnel tests typically varies within the range

$$3 < \alpha < 15 \ \ \text{ppm} \ . \tag{2.71}$$

The air content parameter is defined as the ratio of the saturation air pressure to the pressure due to surface tension, namely:

$$\gamma = \frac{p_a R_0}{2\sigma} = \frac{\beta\alpha R_0}{2\sigma} \quad . \tag{2.72}$$

Substituting the range of variables from (2.64), (2.70) and (2.71) into (2.72), one finds the range for the dimensionless air content parameter to be approximately

$$1 < \gamma < 105 \quad . \tag{2.73}$$

The relationship between the slow laboratory time, t_s, and the fast bubble time, t, is given by the small perturbation parameter, ε. It can be expressed as

$$\varepsilon = \frac{R_0}{D} W_r^2, \tag{2.74}$$

which directly combines the key flow parameters in the Weber number and the characteristic body diameter, D, into the single parameter, ε. Figure 2.6 below, shows the dimensionless relationships between the perturbation parameter, ε, the body, the nucleus sizes and the measurable flow, and fluid properties in accordance with equation (2.74).

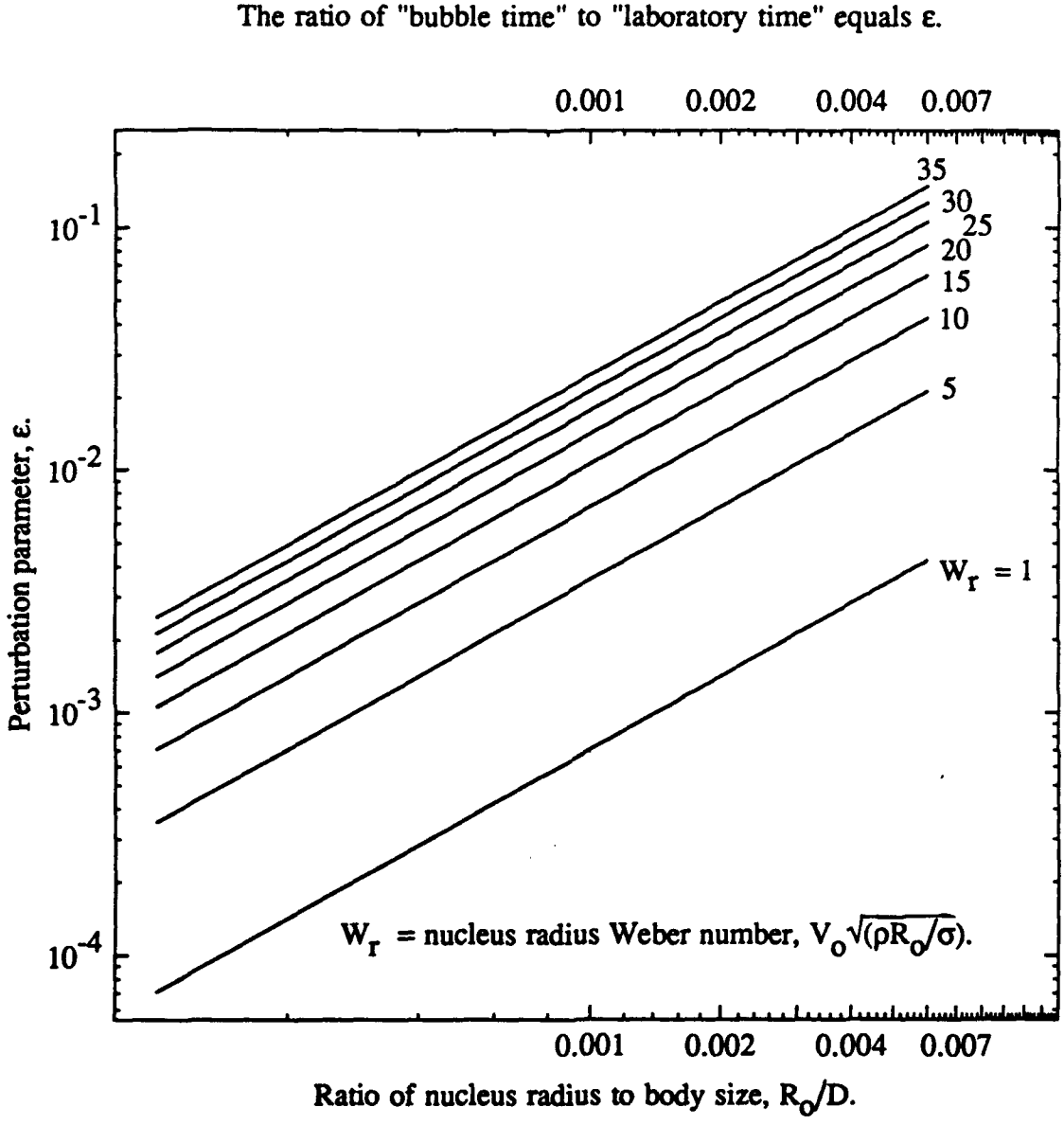

Figure 2.6 Values of Perturbation Parameter, ε, for Ranges of Radial Weber Number and Nucleus Size to Characteristic Body Length.

CHAPTER 3

THE ZERO-ORDER SOLUTION

3.1 The First Integral

From the previous development the zero-order form of the Rayleigh-Plesset differential equation in terms of the normalized dimensionless bubble radius $u_0(\tau)$ is

$$u_0 \frac{\partial^2 u_0}{\partial \tau^2} + \frac{3}{2}\left(\frac{\partial u_0}{\partial \tau}\right)^2 = \frac{\gamma}{u_0^3 (1+q)^{5/2}} - \frac{1}{u_0 (1+q)^{3/2}} \tag{3.1}$$

with the initial conditions

$$u_0(0) = 1 \tag{3.2}$$

$$\left.\frac{\partial u_0}{\partial \tau}\right|_{\tau = 0} = 0 \ . \tag{3.3}$$

It is assumed at this point that the zero-order equation is independent of the slow laboratory time, t_s, and therefore can be written as an ordinary differential equation in terms of the fast bubble time, τ. The reasons for this independence are addressed in section 3.5 below.

An important fact about this zero-order equation is that it is autonomous and therefore its first integral is easily found. By letting

$$v = \frac{du_0}{d\tau} \ , \tag{3.4}$$

one can write (3.1) as two coupled first order equations, namely equation (3.4) and

$$\frac{d(u_0^3 v^2)}{du_0} = \frac{2\gamma}{u_0 (1+q)^{5/2}} - \frac{2u_0}{(1+q)^{3/2}} \ . \tag{3.5}$$

In anticipation of the discussion in section 3.5 we integrate both sides of equation (3.5) partially with respect to τ in order to obtain a first integral, one finds it to be

$$u_0^3 v^2 = \frac{2\gamma}{(1+q)^{5/2}} \ln(u_0) - \frac{u_0^2}{(1+q)^{3/2}} + \left[A(t_s) + \frac{1}{(1+q)^{3/2}}\right] , \tag{3.6}$$

where the quantity $\left[A(t_s) + \frac{1}{(1+q)^{3/2}} \right]$ is the constant of integration which must satisfy the initial condition of equation (3.2). To also satisfy the condition in (3.3) at $t_s = \tau = 0$, however, A(0) must equal zero, which leaves

$$u_0^3 v^2 = \frac{1}{(1+q)^{3/2}} \left[\frac{2\gamma}{(1+q)} \ln(u_0) - u_0^2 + 1 \right] . \qquad (3.7)$$

Further arguments that A = constant = 0 and that the zero-order equation can be independent of t_s will be shown in section 3.5.

The left hand side of this first integral is proportional to the kinetic energy of the cavitation bubble motion, whereas the right hand side is proportional to the potential energy, - V, of the bubble. Thus equation (3.7) can be plotted in a potential energy versus u_0 plot and in a phase plane of $\dot{u}_0$ versus u_0 as shown in Figure 3.1 and the nature of its phase-plane trajectories analyzed.

3.2 Phase-Plane Analysis

Had the quantity A not been zero in equation (3.6), suggesting a step-forced zeroth order equation, the plot of the potential function and its corresponding phase plane trajectories would lead to the well-known solution of the autonomous equation arrived at by Baker [2] and others before him. The phase plane then includes both vortex and saddle points, and a separatrix which separates closed periodic trajectories from ones that grow without bound.

Under the assumption that A is equal to zero, equation (3.7) can be plotted in the phase plane and its trajectories analyzed. Figure 3.1 shows schematically the results of this analysis for a typical value of the dissolved air content parameter, $\gamma = 1.4$, after Baker [2]. The saddle point vanishes and all trajectories originate from the point at $u_0 = 1, v = 0$. In figure (3.1) the expression (1 + Q) is simply an approximate form of the exact expression for $\sqrt{1+q}$ used in this analysis. Baker assumed that q was a small number less than one which is not necessarily the case in this investigation. Despite this difference, figure 3.1

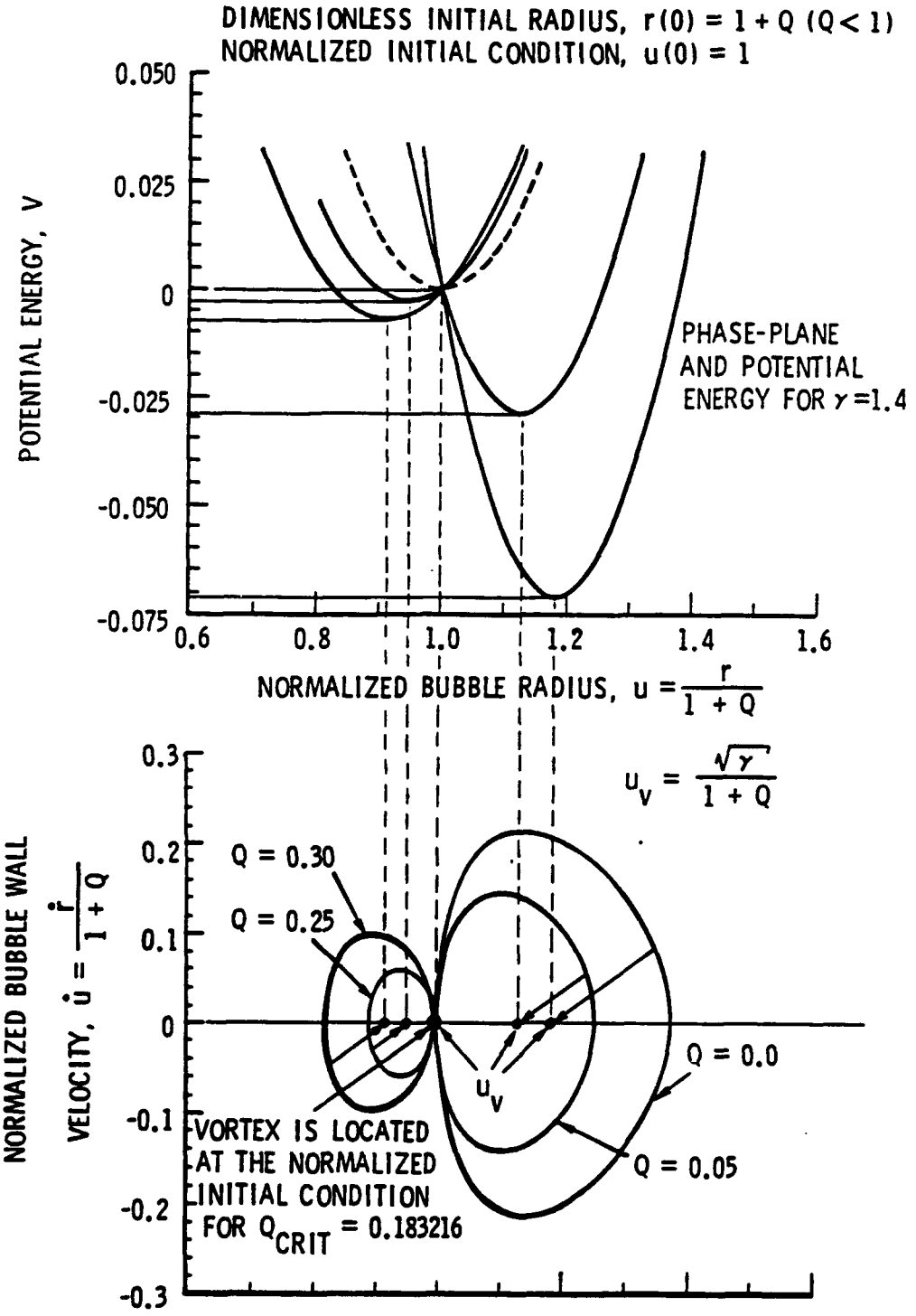

Figure 3.1 Schematic Diagram of the Phase Plane and Level Lines of Potential Energy Plot for the Zero-Order Analysis, after Baker [1].

shows the same qualitative phase plane relationships as found here. It is seen that the location of the minimum potential energy point for a given value of q corresponds to the vortex point in the phase plane about which the trajectories are focused. These vortex points move from left to right as the value of q decreases to zero. Free oscillations of the bubble will then have amplitudes determined by distance of the minimum energy level below zero because the system being conservative, the initial energy is the total available and it is set by the initial conditions to be at zero. The trajectories on the right represent oscillations of expansion with significant vaporous growth accompanied by a reduction in the partial air pressure in the bubble. Those on the left are compressive oscillations in which the air contained in the bubble supplies the restoring pressure as before and the mass of vapor in the bubble is reduced.

The dotted curve in the upper potential energy plot corresponds to the case where the trajectory and the vortex are isolated at the origin in the phase plane. The motion in this critical case is null except in the possible event of a momentary random disturbance which would excite free oscillations of the bubble. Trajectories for this case would be centered about the vortex point at $u_0(0) = 1$, $v(0) = 0$. The oscillation amplitude would depend on the intensity of the momentary pulse. It would supply an initial increment of energy to the bubble causing the initial energy level in figure 3.1 to move from zero, as required by the present initial conditions, to some higher energy level. These trajectories are not shown in figure 3.1 because a random disturbance for that particular case is not contemplated. We require the initial conditions, $u_0(0) = 1$, $v(0) = 0$, to be satisfied strictly. Nevertheless the natural frequency of these vibrations is of interest and these are discussed for small oscillations in the section 3.41 below.

The importance of this critical case is that it separates the bubble motion into the distinct types, oscillations of compression and expansion. Trajectories to the right of the critical point represent larger amplitude oscillations involving vaporous growth and a small amount of air induced motion. Since this investigation considers primarily the vaporous

growth region, the trajectories to the right of the critical point will be emphasized, although as will be found later there can be some flow conditions under which those on the left can play a role.

The location of the vortex points corresponding to the minimum of the potential energy curves is found by setting the first derivative of equation (3.7) equal to zero and solving for u_0, resulting in the affix of the vortex point being defined analytically by

$$u_v = \sqrt{\frac{\gamma}{1 + q}} \ . \tag{3.8}$$

Then for any air content, at the critical point where $u_v = 1$, a critical value of q can be defined as

$$q_{crit} = \gamma - 1 \ . \tag{3.9}$$

If $q_{crit} = 0$, then $\gamma = 1$ which sets a minimum value for the dissolved air content parameter for positive q values. Since q depends on the cavitation number and the Weber number, a limiting value of $q = 0$ corresponds to $K = 0$ or $v_0 = 0$. This result is equivalent to that achieved by Baker [2], except in this case the value of q is not necessarily less than one. Therefore, the denominator of equation (3.8) cannot be approximated using the binomial expansion as stated before.

3.2.1 Measurable Flow Parameters and the Value of u_v

The analytic expression for the vortex point affix, u_v, in equation (3.8) contains all three of the dimensionless flow parameters described in section 2.5, namely: γ, W_r, and K, but it does not include the body size, D, because it applies only to the bubble. By using u_v and the small perturbation parameter, ε which does not include the air content parameter, γ, or the cavitation number, K, but all flow variables and headform sizes can be contained in ε and u_v. Therefore it is useful to complement the relationships of figure 2.6 with another illustration that includes the remaining physical variables. We shall consider cases of $u_v \geq 1$ only.

The range of cavitation numbers is constrained by likely values of $C_p|_{min}$ for various submerged bodies. Thus if a particular vortex point is desired, various combinations of flow variables and headform sizes can be used to arrive at this number. Using the critical values of q and the air content parameter arrived at above, along with the ranges of values for the Weber Number and cavitation number from section 2.5, one sees that values of u_v vary in the range from

$$1 \leq u_v \leq 10 \ . \tag{3.10}$$

A relationship for these parameters is shown in figure 3.2. The plot parameter, z, in the figure is used to relate the two scales and is given by

$$z = \frac{1}{\sqrt{1 + q}} = \frac{u_v}{\sqrt{\gamma}} \ . \tag{3.11}$$

To use the graph, a cavitation number is chosen and traced horizontally to the appropriate Weber number. This point corresponds to a certain value of z directly below it. Finding the vertical intersection of this value of z with the chosen air content, γ, one can then move horizontally to the scale on the right in order to find the affix of the vortex point . Finally, since the radial Weber number is known one only needs to know the ratio R_0/D from figure 2.6 in order to find the proper value of ϵ for the hydrodynamic configuration. And since u_v is now known, values of u_{max} and λ follow from figures 3.3 and 3.4 below.

3.3 The Period of the Zero-Order Solution

The phase plane analysis shows that the first integral yields closed trajectories. Therefore both the zero-order radius and growth rate are periodic with respect to τ. By separating the differential $d\tau$ from u_0 and its differential in equation (3.7), one has

$$\int_0^T d\xi \ = \ (1+q)^{3/4} \int_1^{u_0} \sqrt{\frac{\zeta^3}{2u_v^2 \ln(\zeta) \ - \ \zeta^2 \ + \ 1}} \ d\zeta \ . \tag{3.12}$$

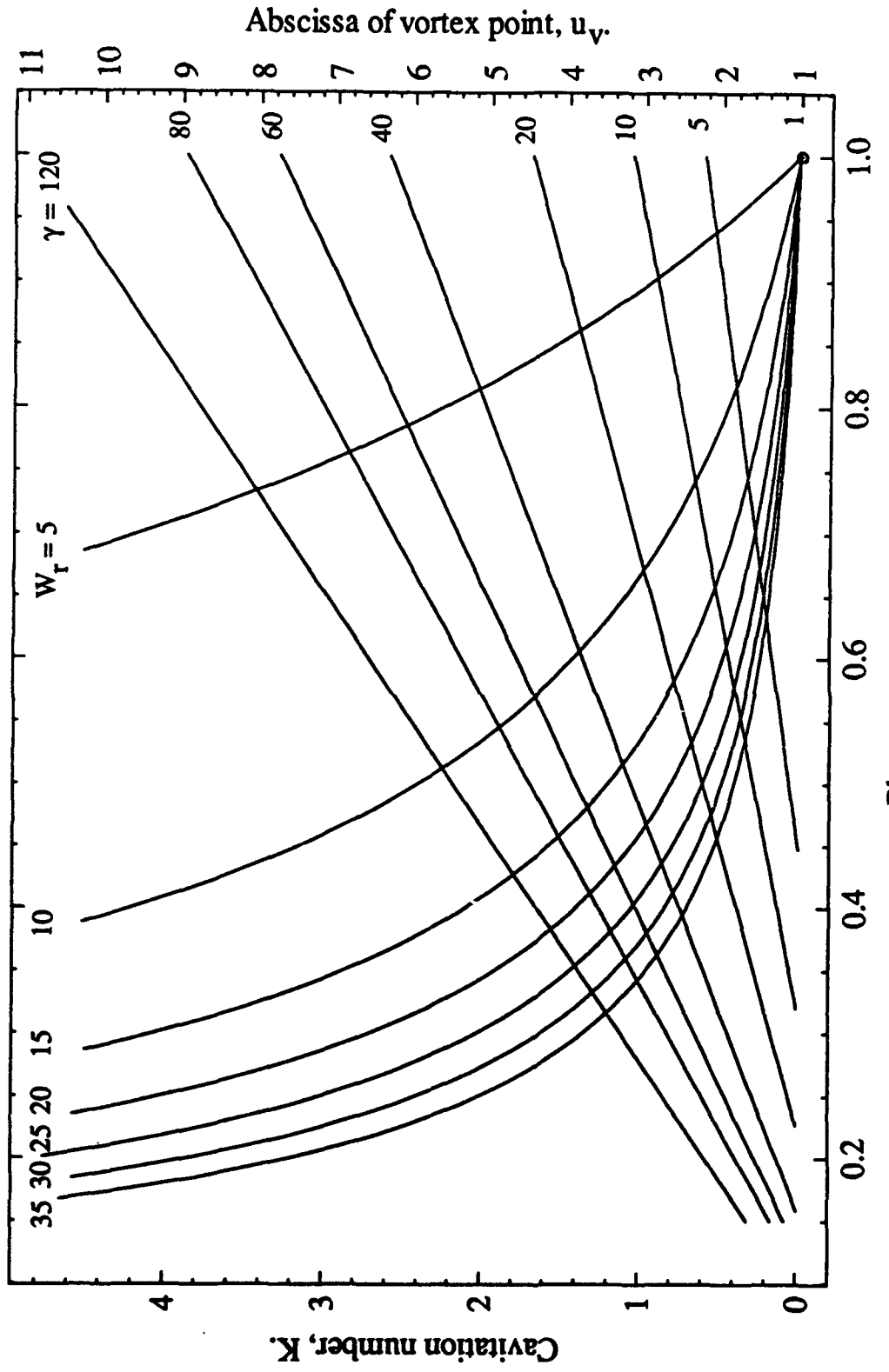

Figure 3.2 Affix of Vortex Point for Likely Ranges of Cavitation Number, Weber Number and Air Content Parameter.

Because the solution is periodic this integral can be evaluated over half a period, say T/2, and its evaluation takes the form,

$$\frac{T}{2} = (1+q)^{3/4} \int_1^{u_m} \sqrt{\frac{u_0^3}{2u_v^2 \ln(u_0) - u_0^2 + 1}}\, du_0 , \qquad (3.13)$$

where the upper limit on the right hand integral, $u_m(u_v)$, is the maximum normalized radius the oscillating bubble will reach.

The bubble grows from it's normalized value of unity to this maximum value and then returns to unity. The maximum u_m occurs at exactly half the period of oscillation and corresponds to half way around a trajectory in the phase plane plane. The value of u_m as a function of u_v is obtained from solving equation (3.7) for $u_o > 1$ under the condition that $v = 0$, thus

$$2u_v^2 \ln(u_m) - u_m^2 + 1 = 0 . \qquad (3.14)$$

We see by inspection when $u_0 = u_m = 1$ for any u_v, that equation (3.14) is satisfied. On the other hand if $u_v = 1$ then $u_m = 1$ is the physically acceptable root of equation (3.14). Therefore at the initial point where $u_0(0) = 1$ there will be no bubble motion if $u_v = 1$, as discused in section 3.2 above. Although a closed form of the required solution for $u_m(u_v)$ is unobtainable, equation (3.14) can easily be solved for its inverse, $u_v(u_m)$. But here we have used the numerical methods of regula falsi or bisection in order to get the desired results. Figure 3.3 shows u_m as a function of u_v and includes a nonlinear least squares curve fit over the range of u_v values. The curve fit matches the calculated data very well but it was not used in the numerical calculations in order to secure the greatest accuracy in subsequent numerical work in which values of u_v must be prescribed.

Defining the integral of equation (3.13) in terms of a prescribed u_v from

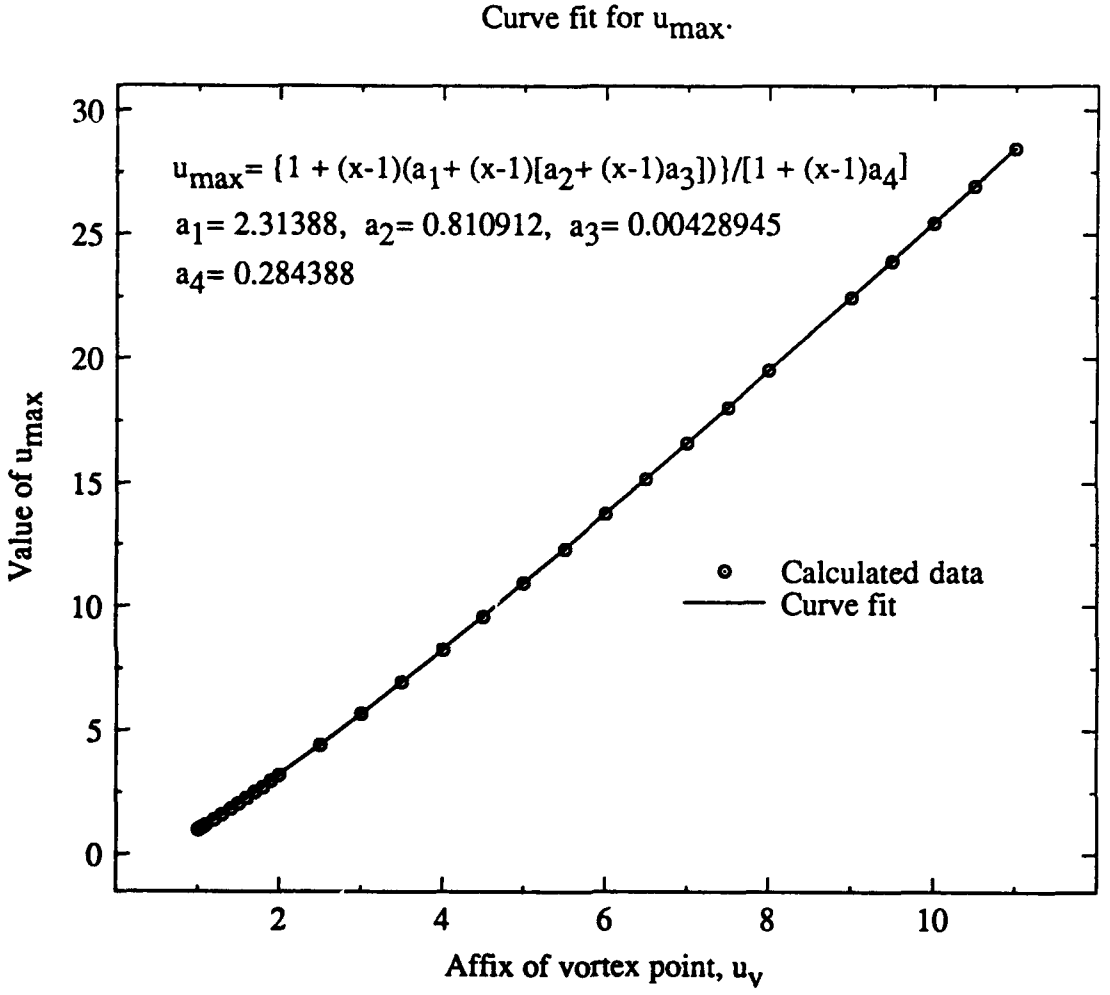

Figure 3.3 Maximum Normalized Zero-Order Bubble Radius for a Range of u_v.

equation (3.14) and excluding the constant term in front of the integral, we write the *half-period integral* as

$$I(u_v) = \int_1^{u_m} \sqrt{\frac{\zeta^3}{2u_v^2 \ln(\zeta) - \zeta^2 + 1}}\, d\zeta \ . \qquad (3.15)$$

Since the half-period integral is now known, we can write the oscillation period of the solution $u_0(u_v,\tau)$ to be

$$T(u_v) = 2(1+q)^{3/4} I(u_v) \ . \qquad (3.16)$$

The period is a function of both u_v and the flow parameters contained in the quantity q.

By using this period the non-dimensional bubble time, τ, can also be normalized. This is done by defining the normalized dimensionless bubble time, x, as

$$x = \frac{\tau}{T} \ . \qquad (3.17)$$

When $\tau = 0$, $x = 0$ and after one period when $\tau = T$, $x = 1$. This also allows the value of u_m to occur at $x = 1/2$.

3.4 Zero-Order Equation Solution

From the first integral of equation, (3.7) and the normalized bubble time from equation (3.17), the exact first integral of the zero-order equation now looks like

$$\frac{du_0}{dx} = \frac{T}{(1+q)^{3/4}} \sqrt{\frac{2u_v^2 \ln(u_0) - u_0^2 + 1}{u_0^3}} \ . \qquad (3.18)$$

If one separates variables in equation (3.18) the problem of finding the inverse solution, $x(u_v,u_0)$, is reduced to the quadrature,

$$\int_0^x d\xi = \frac{1}{\lambda} \int_1^{u_0} \sqrt{\frac{\zeta^3}{2u_v^2 \ln(\zeta) - \zeta^2 + 1}}\, d\zeta \ , \qquad (3.19)$$

where the *period parameter*, λ, is a constant for a given value of u_v and is related to the period by

$$\lambda(u_v) = \frac{T(u_v)}{(1+q)^{3/4}} = 2I(u_v) \ . \qquad (3.20)$$

These results make the zero-order solution a one-parameter family, $u_0(x,u_v)$, which is convenient for further analysis. It is noted that the other major components involved in this equation also have been derived with this dependent parameter, such as $u_m(u_v)$ and $\lambda(u_v)$. Figure 3.4 shows a graph of the period parameter over the range of u_v along with a least squares curve fit of the function. Next we shall adopt the notation of equation (3.20) and use it in equation (3.18) in order that it will have the same notation as equation (3.19) :

$$\frac{du_0}{dx} = \lambda(u_v) \sqrt{\frac{2u_v^2 \ln(u_0) - u_0^2 + 1}{u_0^3}} \ . \qquad (3.18\,a)$$

Equations (3.4) and (3.18*a*) have been used in order to calculate a number of phase plane trajectories for the range, $0.50 \le u_V \le 1.50$, enabling us to see how the trajectories change as the value of u_V passes through unity. These trajectories are shown in figure 3.5 below.

A solution to equation (3.19) would yield $x = x(u_0)$. By approximating the logarithmic air content parameter with a cubic polynomial, Baker [2] found an approximate solution for $x(u_0)$ in terms of elliptic integrals and functions. Of more general use is the inverse of this function, or $u_0 = u_0(x)$. We shall proceed numerically because Baker's solution holds for a rather small range of u_v and it can not be inverted.

3.4.1 Zero-Order Small Oscillation Study

From the phase plane plot of $\dot{u}_0$ vs u_0 it is seen that for a given value of u_v that the

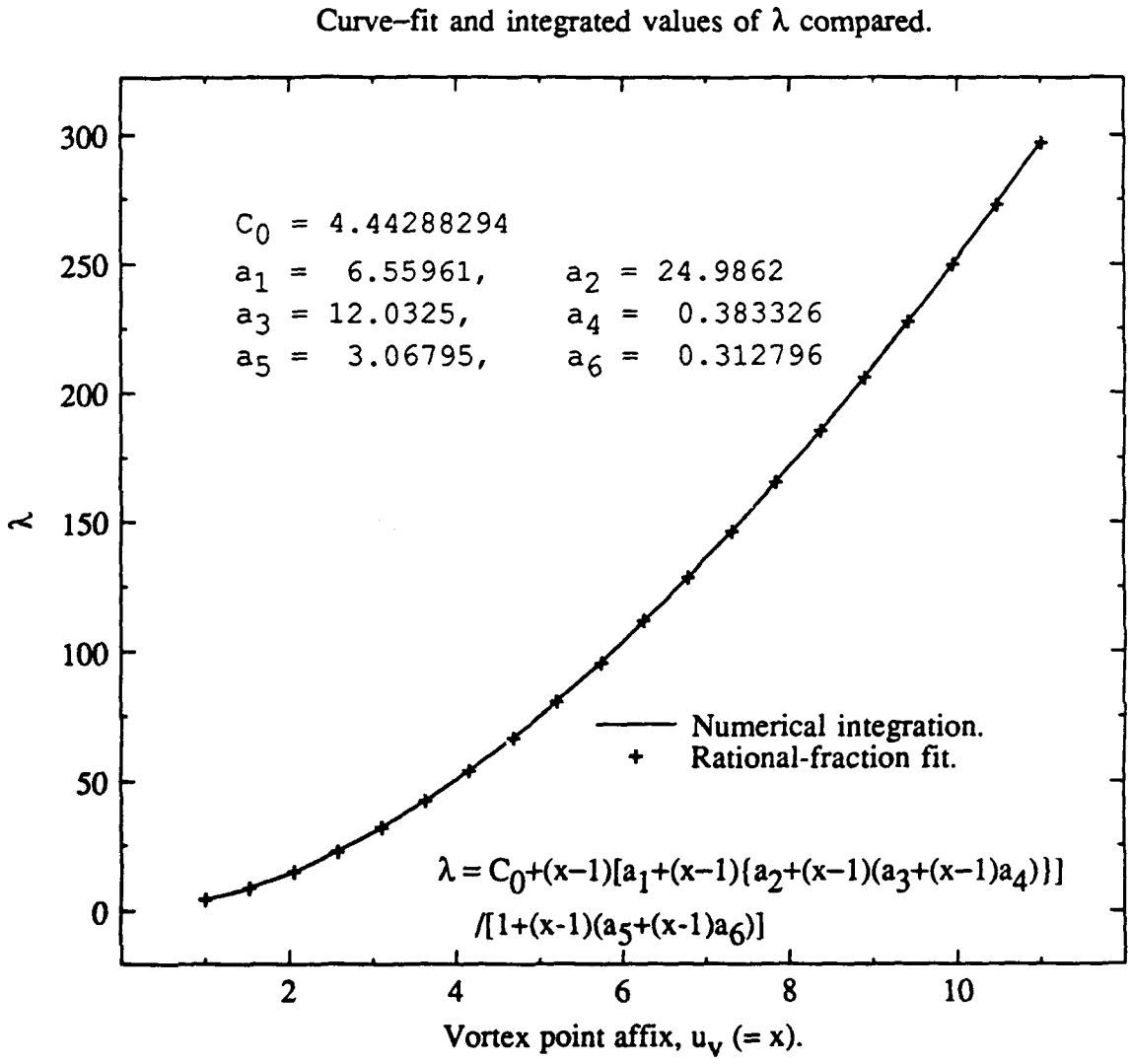

Figure 3.4 Values of the Period Parameter, λ, for a Range of u_v Values.

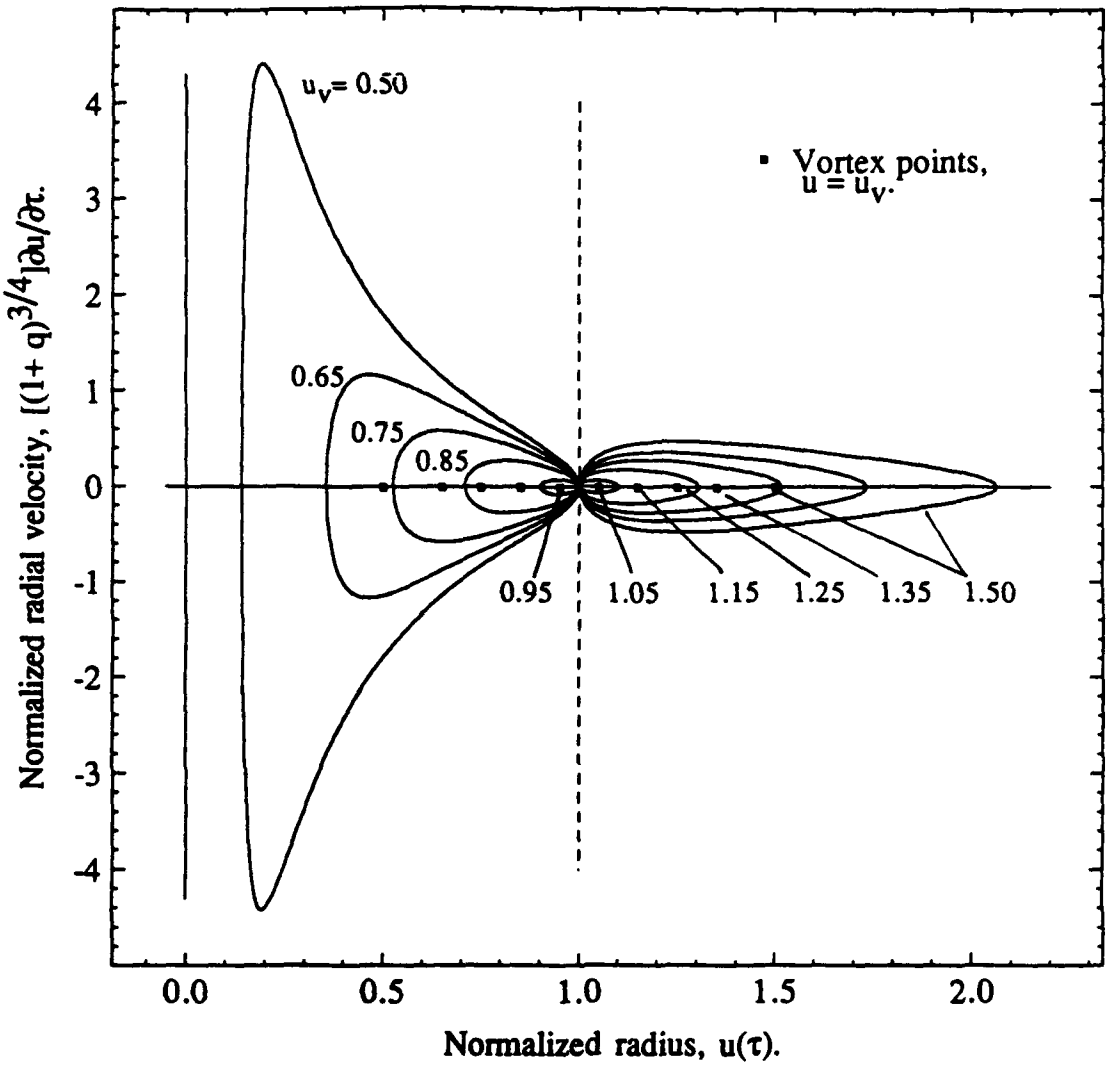

Figure 3.5 Phase Plane Trajectories Calculated for Several u_v Values in the Range $0.5 \leq u_v \leq 1.5$.

curves are closed and nearly elliptical, especially for small values of u_v near 1.0. Consequently, an ad hoc small-oscillation form or the zero-order solution was sought for the case when

$$u_v = 1 + \delta, \tag{3.21}$$

where $\delta << 1$. For this case an approximate form of the first integral was sought using the equation for an ellipse. To most closely approximate the form of the first integral the ellipse was chosen to be centered at c, one -half the distance between the two points, 1 and u_m, on the u_0 axis. The length of the vertical.axis is determined by the requirement that the period of oscillation must also agree with the correct result. The use of these conditions leads to an equation for an ellipse of the form

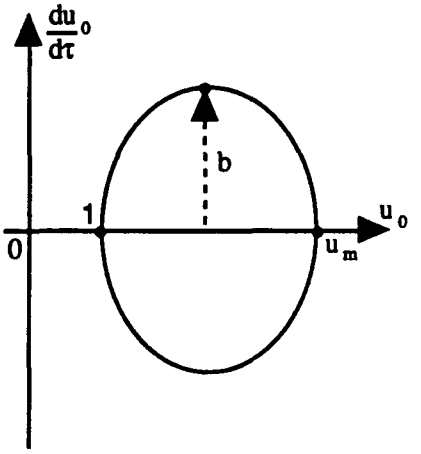

$$\frac{\dot{u}_0^2}{b^2} + \left(\frac{u_0 - c}{a}\right)^2 = 1 , \tag{3.22}$$

where

$$a = \frac{1}{2}(u_m - 1) , \tag{3.23}$$

$$b = (\dot{u}_0)_{max} , \tag{3.24}$$

and

$$c = \frac{1}{2}(u_m + 1) . \tag{3.25}$$

The coefficients a, b and c are all functions of u_v since $u_m = u_m(u_v)$ and b comes from the first integral equation which is also a function of u_v. The quantity b equals the maximum value of $\dot{u}_0$, which must be arrived at numerically. But as will be shown below, the approximate solution can be written independently of the parameter b.

Solving equation (3.22) for $\dot{u}_0 = \frac{du_0}{d\tau}$ and separating the solution into two integrals, we find

$$\frac{b}{a}\int_0^{\tau} d\zeta = \int_1^{\xi} \frac{d\eta}{\sqrt{1 - \eta^2}}, \tag{3.26}$$

where

$$\xi = \frac{u_0 - c}{a} . \tag{3.27}$$

Integrating this equation over the limits and solving for u_0, one gets a solution of the form,

$$u_0(\tau) = c - a\cos\left(\frac{b}{a}\tau\right) . \tag{3.28}$$

This is an oscillatory function of bubble time with a period determined by one circuit around a phase plane trajectory as defined by the u_v value. Evidently u0 will have its maximum value when

$$u_0(T/2) = c + a. \tag{3.29}$$

This will certainly be true if $\frac{b}{a}\tau = \pi$, and since $\tau = \frac{T}{2}$, we have

$$\frac{b}{a} = \frac{2\pi}{T} . \tag{3.30}$$

When this result is used in equation (3.28) and the normalized bubble time from equation (3.17) is applied, the small oscillation approximate solution becomes

$$u_0(u_v,x) = c - a\cos(2\pi x) . \tag{3.31}$$

Equations (3.23) and (3.25) show that c and a depend on $u_m(u_v)$, and so equation (3.31) depends on u_v , as well as the normalized bubble time, x. As with the exact solution, the approximate solution has no explicit dependence on the parameter b. Equation (3.31) is designed to have the correct nonlinear amplitude and period as determined by u_v, however.

Moreover, when $x = 0$ equation (3.31) yields $u_0(u_v,0) = 1$. Differentiating (3.31) with respect to x and evaluating it at $x = 0$ one has $\left.\frac{du_0}{dx}\right|_{x=0} = 0$. Thus equation (3.31) satisfies the initial conditions.

Next we need to find the variation of u_m with u_v, when $\delta \equiv .u_v - 1 << 1$ from equation (3.21). Knowing that u_m also doesn't vary greatly from unity for small oscillations, we can be approximate it by

$$u_m = 1 + y_m \ , \tag{3.32}$$

where $y_m << 1$, but y_m is slightly larger than δ. First one substitutes equation (3.32) into equation (3.14) and expands the logarithmic term to $O(y_m^3)$ in order to obtain a quadratic equation in y_m.which can be solved for $y_m(u_v)$. Then equation (3.21) can replace u_v in this solution in order to expand it to $O(\delta^2)$. Thus one gets the rather accurate expansion,

$$u_m = 1 + 2\delta + \tfrac{1}{3}\delta^2 \ . \tag{3.33}$$

Substituting this result into c and a for u_m in order to get a small oscillation expansion for $u_0(x; u_v)$ we see that it looks like

$$u_0 = 1 + \delta(\ + \frac{\delta}{6})(1 - \cos 2\pi x) \ . \tag{3.34}$$

It is seen that as $\delta \rightarrow 0$, both u_0, and $u_m \rightarrow 1$ which agrees with the initial condition.

In order to get an independent evaluation we now find a limiting small-oscillation form of the period parameter, λ, as given in detail in Appendix C. Here we only outline the analysis. To this end we may generalize equation (3.32) by writing $u_0 = 1 + \zeta$ so that when $\zeta = y_m$, $u_0 = u_m$, but generally $0 \le \zeta \le y_m$ because $1 < u_0 \le u_m$. Then the dummy of integration in equation (3.15) is replaced by u_0 and the denominator inside the radical of equation (3.15) can be expanded to $O(\zeta^3)$ and expressed in factored form using the three roots of the approximating cubic at the three ζ values of $0, \le y_m, \le b_0$. The period integral then becomes

$$I(u_v) = \int_0^{y_m} \sqrt{\frac{(1+\zeta)^3}{\frac{2}{3}u_v^2 \zeta (y_m - \zeta)(b_0 - \zeta)}}\, d\zeta \,. \tag{3.35}$$

Additional expansions of the integrand, as explained in Appendix C, and term-by-term integrations of the result give the respective components of I in terms of y_m. The sum of these components gives the rough estimate,

$$I = \frac{\pi}{u_v\sqrt{2}}\left(1 + \frac{1}{3}y_m + \frac{1}{4}y_m^2\right). \tag{3.36}$$

Because of equation (3.35), equation (3.36) contains the limiting value, $b_0 = 3$ as $y_m \to 0$ and $u_v \to 1$. Equation (3.36) shows that as $u_v \to 1$, $I = \frac{\pi}{\sqrt{2}}$, exactly. But since b_0 and y_m depend on $u_v = 1 + \delta$, one can replace the estimate of (3.36) as an expansion of the half-period integral in powers of δ by consistent use of expansions of the formulas of appendix C for y_m and b_0. But we prefer to use the expansion of equation (3.33). This expansion can be used to expand the quantities y_m and b_0, keeping terms up to order δ^2, in order to obtain a small oscillation form of the half-period integral, replacing equation (3.36). Multiplying the result by a factor of 2, the small oscillation form of the period parameter is

$$\lambda = \pi\sqrt{2}\left(1 + \frac{3}{2}\delta + \frac{77}{48}\delta^2\right). \tag{3.37}$$

As $\delta \to 0$, the value of $\lambda \to \pi\sqrt{2}$ which sets the value of λ for $u_v = 1$. As explained in section 3.2, this value of l is the period parameter for free oscillations which are expanding in one part of the cycle and are compressive during the other part. It is also noted in appendix C that equation (3.35) is a complete elliptic integral of the third kind, from which the limiting value of $\frac{\pi}{\sqrt{2}}$ has been found in order to check the limit from equation (3.36).

These small oscillation results are useful for similar studies of the first-order equation. A comparison the small oscillation results with numerical calculations shows that the small oscillation equations are very accurately valid for the range of u_v from unity up to 1.03.

3.4.2 Numerical Solution

Since there is no closed form solution for $u_0(x)$, an integral such as the one in equation (3.19) is generally evaluated numerically. For this task we have used Simpson's rule for incremental steps of u_0. The integrand on the right side of equation (3.19) contains integrable singularities at $u_0 = 1$ and u_m, and their presence must be accounted for in the numerical work.

This integrand from the right side of equation (3.19), labeled F, is

$$F = \sqrt{\frac{u_0^3}{2u_v^2 \ln(u_0) - u_0^2 + 1}} \quad . \tag{3.38}$$

The denominator of F has roots, as seen from equation (3.14), at $u_0 = 1$ and $u_0 = u_m$. By using a small perturbation analysis about these points approximate formulas can be derived to avoid discontinuities.

This is done by first perturbing u_0 about the point $u_0(0) = 1$, so we let

$$u_0 = 1 + \delta, \tag{3.39}$$

where $\delta << 1$. Substituting this into (3.38) and using a series expansion for small parameters, one finds a general first order approximation for F about the point corresponding to $x = 0$ to be

$$F|_{x=0} = \frac{A}{\sqrt{\delta}} + B\sqrt{\delta} \tag{3.40}$$

where A and B are arbitrary constants. To determine the two constants (3.40) is evaluated at two incremental steps in x. Letting h represent an incremental step, one finds that the two equations are

$$\left.\begin{aligned} A + Bh &= \sqrt{h}F_1 \\ A + 2Bh &= \sqrt{2h}F_2 \end{aligned}\right\} \tag{3.41}$$

Here F_1 and F_2 are equation (3.38) evaluated at x equal h and 2h respectively. When these two equations for A and B are solved, a so called "start" value for equation (3.38) integrated over 2h is

$$\text{start} = \frac{2\sqrt{2}}{3\lambda(u_v)} h (4F_1 - \sqrt{2}F_2) \ . \tag{3.42}$$

The constant $\lambda(u_v)$ is needed to make the 'start' value consistent with equation (3.19). This is labelled a 'start' value since it is used at the beginning of the integration when $x = 0$.

The other singularity occurs at the point where $u_0(\frac{1}{2}) = u_m$. Applying the same method for

$$u_0 = u_m - \delta \ , \tag{3.43}$$

one finds that the first order approximation of equation (3.38) reduces to

$$F|_{x=\frac{1}{2}} = A\sqrt{\delta} + B\delta^{3/2} \ . \tag{3.44}$$

Solving for the A and B as before yields a so called "stop" value for equation (3.38) over 2h of

$$\text{stop} = \frac{4}{15\lambda(u_v)} h (4\sqrt{2}F_1 - F_2) \ . \tag{3.45}$$

Here F_1 and F_2 are equation (3.38) evaluated at x equal $\frac{1}{2}$ - h and $\frac{1}{2}$ - 2h, respectively. This is labelled a "stop" value since it is used at the end of the first half period of the solution when $x = \frac{1}{2}$.

The fact that the zero-order solution is periodic allows the "start" value to be used over the first two steps of the integration nearest $x = 0$ and also over the last two steps at the end nearest $x = 1$. Similarly, the "stop" value can be used over the two steps just preceding and just following $x = \frac{1}{2}$. Periodicity also warrants integration only up to the $x = \frac{1}{2}$ point since the values of the solution between one-half and one will correspond to the reverse of those between one and one-half.

The numerical calculation of the zero-order solution involves first finding a value of u_m for a given value of u_v using equation (3.14). Simpson's rule is then employed over the range of steps between the first two and last two for $0 < x < \frac{1}{2}$. The curve over this interval is well behaved and resembles a versine curve, as exemplified in the small oscillation analysis. Then the start and stop values are added to the result. These values are then used in a cubic interpolation scheme to produce evenly spaced values of u_0 over the whole range of x from 0 to 1. A Fortran source code for these calculations is given in appendix A.

The numerical solution for u_0 and its derivative versus x for various values of u_v are shown in figure 3.6. It is seen that the curves resemble versine curves, insuring a smooth transition to the small oscillation result. To get a better picture of the zero-order solution's periodicity, figure 3.7 shows u_0 and its derivative over two periods in x for a single value of $u_v = 1.05$ where they have nearly trigonometric shapes. These results pertain to the case in which $u_v > 1$. In order to compare such solutions with solutions when $u_v < 1$, figure 3.8 shows calculated results for $u_v = 1.5$, 1.0 and 0.5. These curves appear to show a 180° phase shift as u_v passes through unity. The cause of this can be seen in the phase plane of figure 3.5 in which trajectories on the right of $u_0 = 1$ are traced in the counter clockwise sense as x increases, starting on the upper part of a loop. Trajectories to the left start on the lower branch of a loop and also proceed in the counter clockwise direction with increasing x. The elongated shape of the trajectory for $u_v = 1.5$, showing rather modest values of $\dot{u}$ especially on its right, insures that in figure (3.8) the central part of the solution near x = 1/2 will be relatively gently rounded compared to its behavior in the neighborhood of $u_0 = 1$. In this latter region figure 3.5 shows larger velocities which increase rapidly from zero near $u_0 = 1$. Therefore in figure 3.8 the solution is relatively steep near x = 0 and 1. On the trajectory for $u_v = 0.5$ of figure 3.5 the larger and rapidly changing velocities are found near its left extremity. Consequently, figure 3.8 shows sharp minima at x = 0.5 and 1.5, but gentle rounding near its maxima at x = 0 and x = 1.

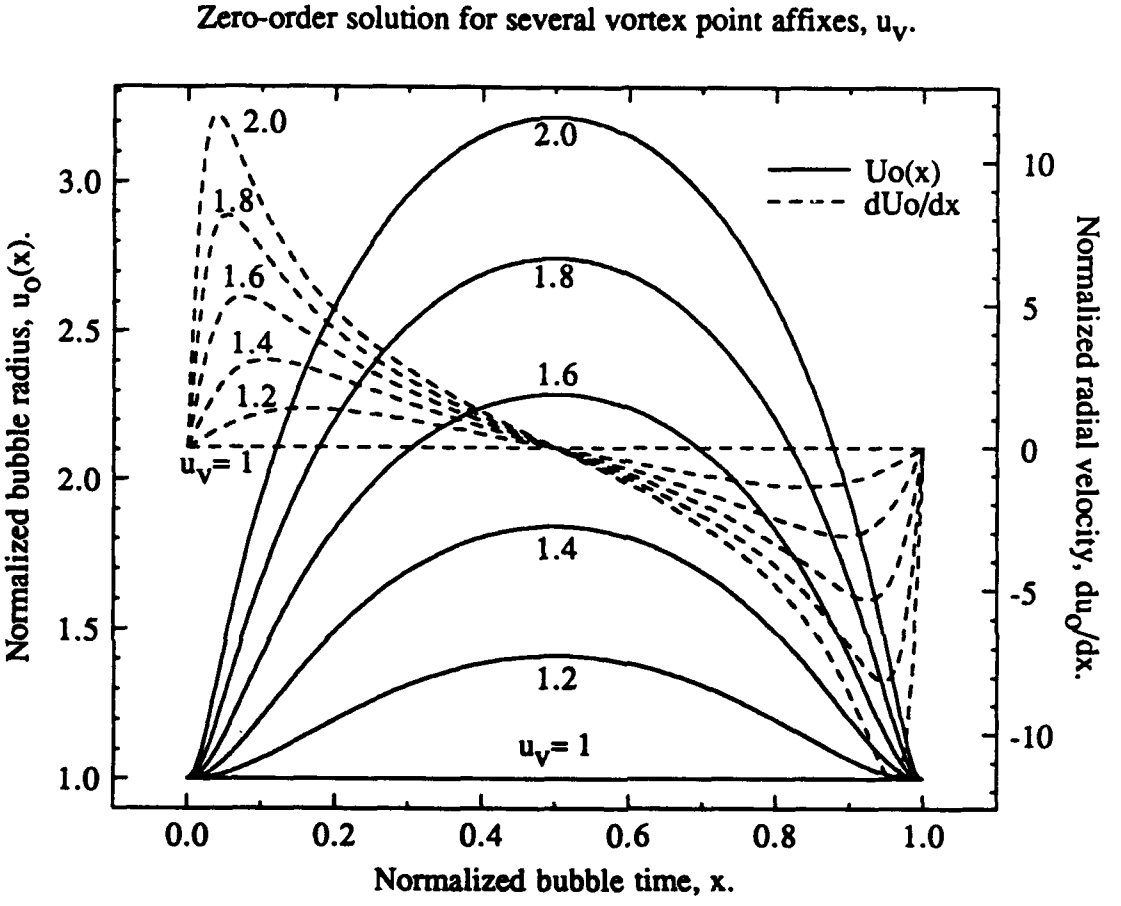

Figure 3.6 Numerical Zero-Order Solution as a Function of Normalized Bubble Time for Several Values of u_v.

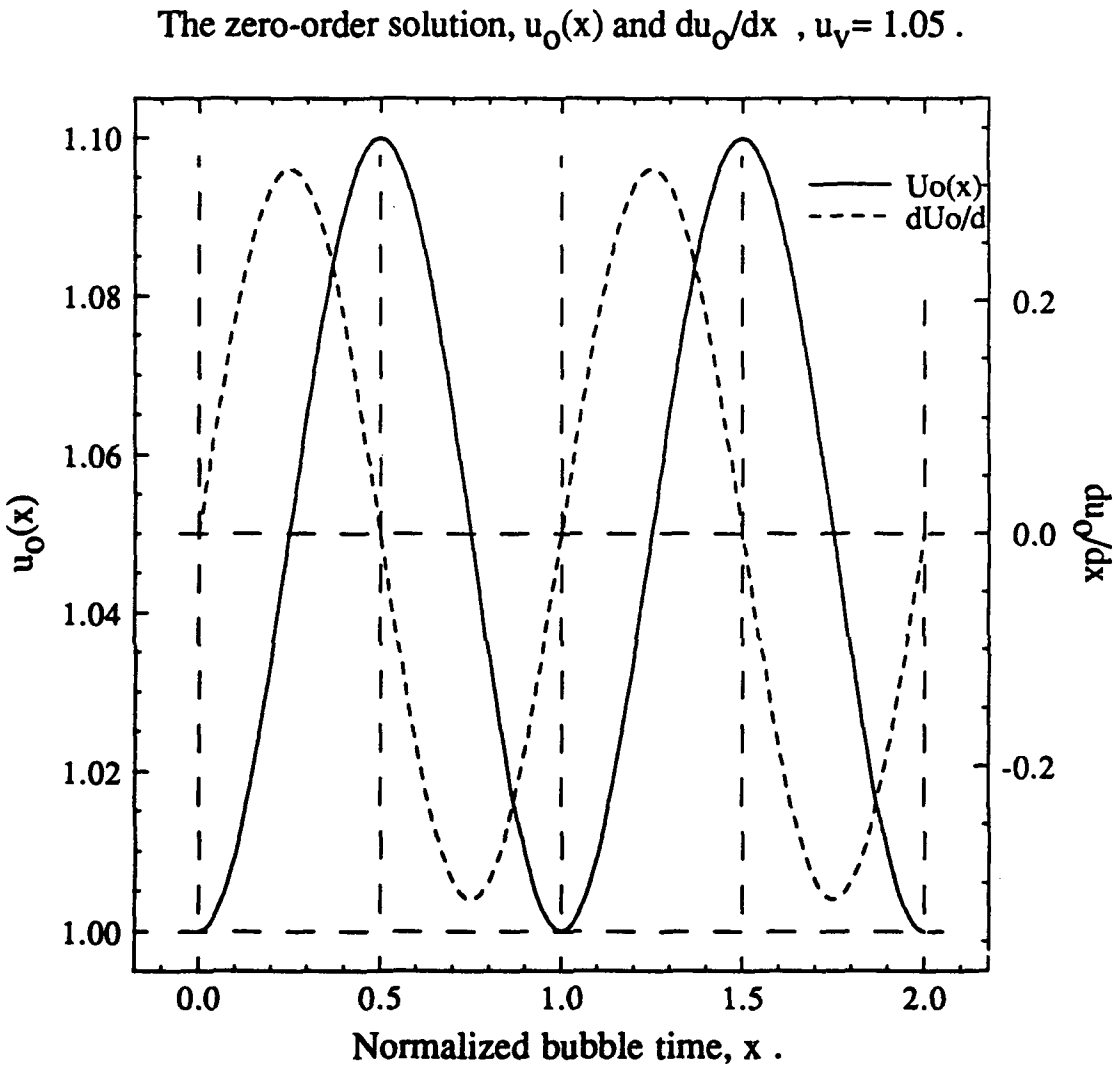

Figure 3.7 Numerical Zero-Order Solution Over Two Periods in Normalized Bubble Time for a Value of $u_v = 1.05$

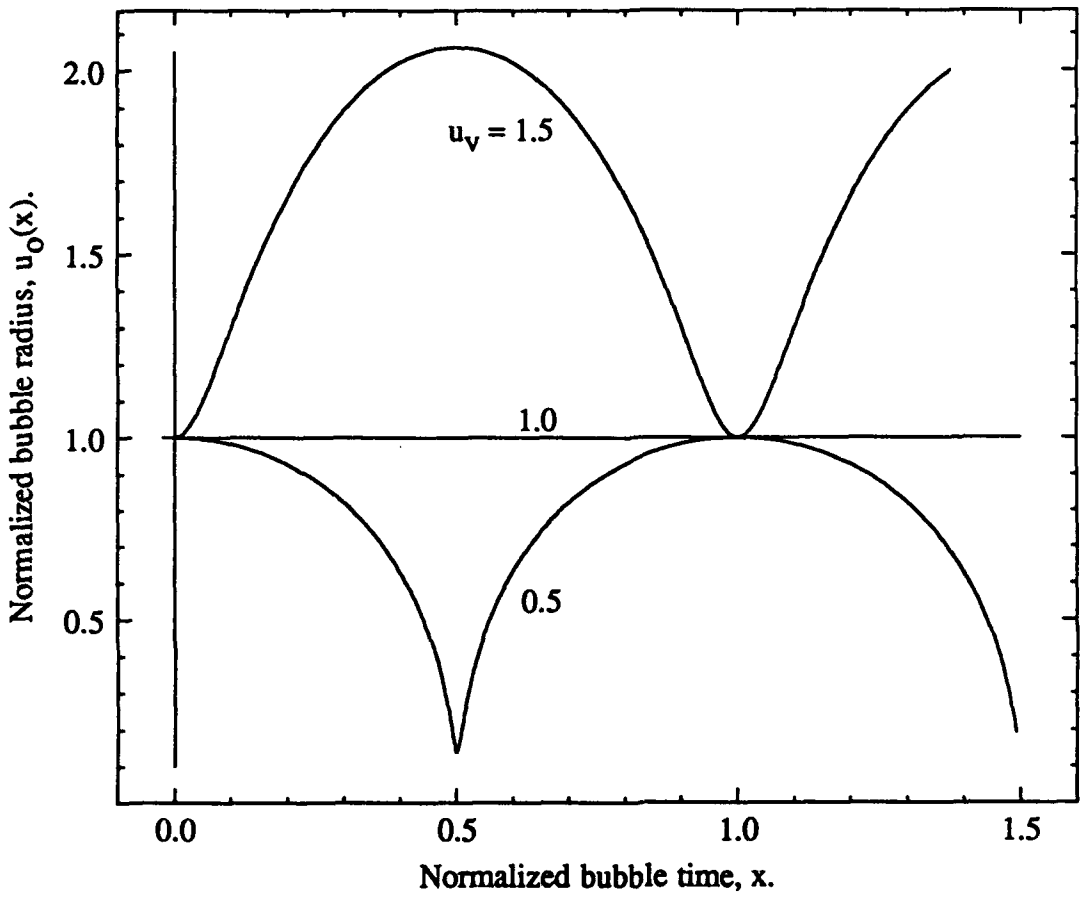

Figure 3.8 Calculated Oscillations of Expansion, $u_v > 1$, Compared with Compressive Oscillations, $u_v < 1$.

3.4.3 Approximate Solution Using Fourier Series

It is seen that the small oscillation approximate solution resembles the first two terms of an even function expressed in a Fourier cosine series. This encouraged the development of a compatible approximate solution for the zero-order solution using Fourier series expansions.

Considering the fact that the zero-order solution is periodic and also an even function as displayed by the numerical results, it seems fitting that the data from the numerical solution over one period could easily be fitted to a truncated Fourier cosine series in which the a_n vary continuously with u_v. Then by doing this for a large number of u_v values, curve fits for the needed $a_n(u_v)$ terms can be found using a least squares method. The array of equations for the appropriate number of Fourier cosine terms represents essentially a closed form approximate u_0 solution as a function of x for a given value of u_v. The advantages of having such a solution are found in the relative speed and ease of computation, along with the fact that many of the complications associated with numerical methods are avoided.

The first thing is to determine the number of terms to include in the truncated series. Initially 100 a_n coefficients were calculated by recursion [14] for a number of u_v values. The same was done for 50 a_n coefficients and the results compared to the corresponding numerical data. It was seen that a truncation to 50 coefficients loses very little accuracy compared to the numerical results.

Adopting a 50 coefficients truncation for the Fourier series at numerous values of u_v over the range from 1 to 10, 50 separate curve fits were then applied to the a_n's over their corresponding range of u_v. This is to say that only the lower numbered terms were used for smaller values of u_v, and as u_v increased so did the number of terms. It was found that all except a_0 were effectively handled if they were represented by a rational fraction in terms of u_v. A quartic polynomial seemed most appropriate for a_0. Each curve fit was determined using a least squares method. Then given a value of u_v the appropriate

number and value of a_n's can be determined and each multiplied by it's cosine of its frequency and summed up over a period in x from 0 to 1, yielding a truncated series zero-order solution.

The convenience of curve fitting does cost some accuracy. It was found that in summing up the cosine terms the required value of $u_0(0,u_v) = 1$ was missed by various small amounts depending on the value of u_v. To insure that this initial condition is satisfied by the approximation, the error, $\Delta(u_v)$, between the Fourier solution and the initial condition at $x = 0$ is calculated and added to the total sums for all x in [0,1].

Examples of the results obtained for several values of u_v are shown and are compared with numerical results for the same values in figure 3.9. This method yields reasonably good approximations to the zero-order solution and retains the main features which are dependent on u_v. But when this method was used to represent u_0 in the first-order analysis, the accumulated errors were excessive. Thus to retain accuracy, only numerical methods were used in the following first-order analysis.

3.5 Time Scale Dependence

Throughout this analysis the zero-order equation has been assumed to be independent of the laboratory time, t_s. The object of this section is to investigate this assumption by using the coupled time scale terms of the first-order equation. If there is a possibility that there may be a dependence upon t_s we must uncover it. Beginning from the elliptical small oscillation result for u_0, a generalized 2-scale analysis is applied such that $u_0 = u_0(t_s,\tau; u_v)$.

3.5.1 Small Oscillations

One begins the argument by returning to equation (3.22) and differentiating the whole equation partially with respect to τ. This leaves the right side of the equality equal to zero. Integrating this again leaves a constant of integration which is at most a function of t_s, such that

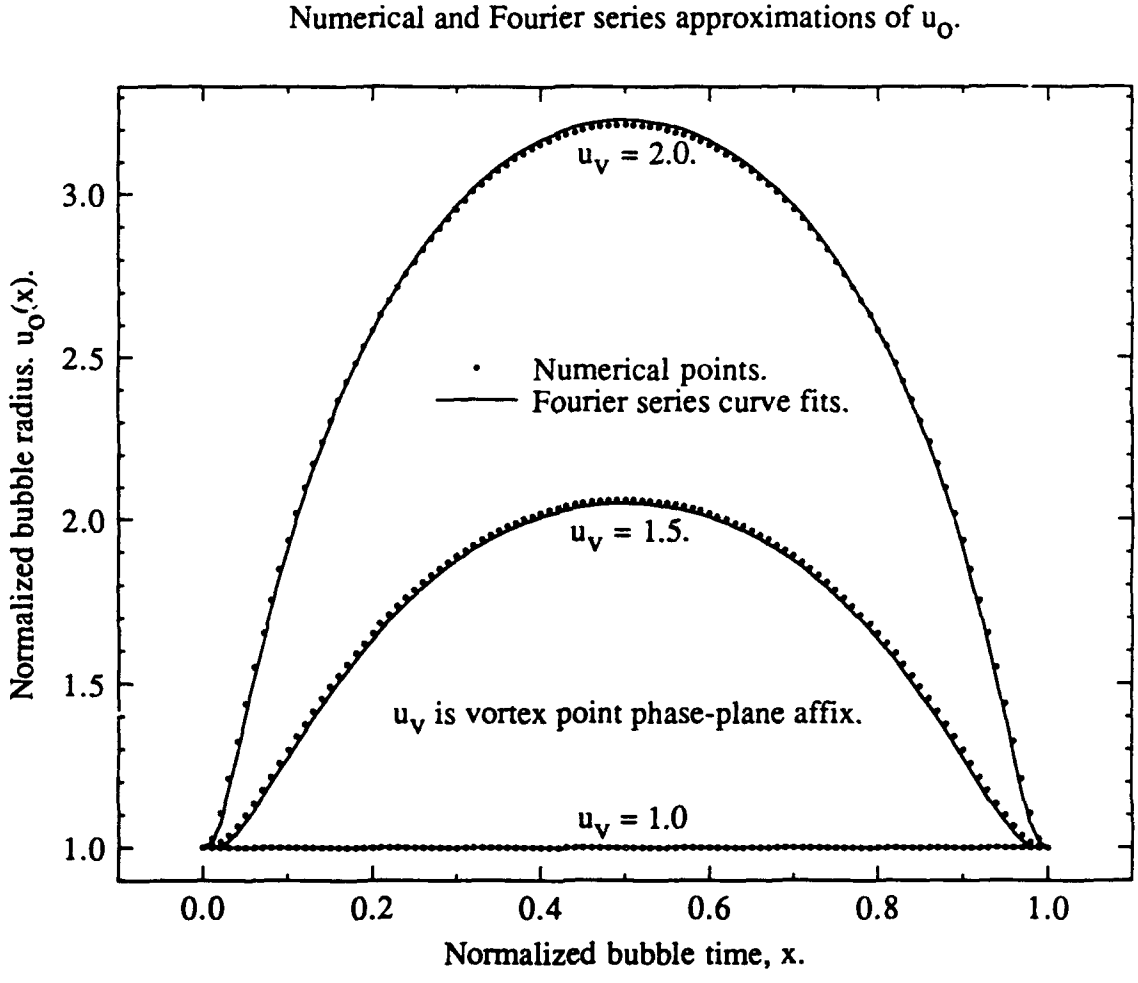

Figure 3.9 Comparison of Numerical Zero-Order Solutions with 50-Term Truncated Fourier Series Approximations for Several u_v Values.

$$\frac{\dot{u}_0^2}{b^2} + \left(\frac{u_0 - c}{a}\right)^2 = 1 + A(t_s) , \tag{3.46}$$

where $A(0) = 0$ to hold with the initial conditions. Separating this into two integrals as in the previous analysis and integrating, one finds the bubble time plus another constant of integration depending on the laboratory time, such that

$$\frac{b}{a}\tau = \sin^{-1}\xi + B(t_s) + \frac{\pi}{2} , \tag{3.47}$$

where $B(0) = 0$ from the initial conditions and now

$$\xi = \frac{u_0 - c}{a\sqrt{1 + A(t_s)}} . \tag{3.48}$$

Substituting for ξ and solving for u_0, one finds the 2-scale representation as

$$u_0(t_s,\tau; u_v) = c - a\sqrt{1 + A(t_s)}\left[\cos\left(\frac{b}{a}\tau - B(t_s)\right)\right] . \tag{3.49}$$

In order to suppress secular terms in the zero-order solution the coupled time scale terms in the first-order expansion equation must be set equal to zero. To ensure this, they are set equal to zero here and evaluated using the generalized 2-scale equation (3.49) for u_0.

The coupled time scale terms from the first-order expansion equation set to zero are

$$2u_0 \frac{\partial^2 u_0}{\partial t_s \partial \tau} + 3\frac{\partial u_0}{\partial t_s}\frac{\partial u_0}{\partial \tau} = 0 . \tag{3.50}$$

Substituting equation (3.49) and its partial derivatives into equation (3.50), we find that

$$\begin{aligned} &\frac{bc}{\sqrt{1 + A}}\left[\frac{dA}{dt_s}\sin\left(\frac{b}{a}\tau - B\right) - 2(1 + A)\frac{dB}{dt_s}\cos\left(\frac{b}{a}\tau - B\right)\right] \\ &\quad - \frac{5}{2}ab\frac{dA}{dt_s}\sin\left(\frac{b}{a}\tau - B\right)\cos\left(\frac{b}{a}\tau - B\right) \\ &- ab(1 + A)\frac{dB}{dt_s}\left[3\sin^2\left(\frac{b}{a}\tau - B\right) - 2\cos^2\left(\frac{b}{a}\tau - B\right)\right] = 0 . \end{aligned} \tag{3.51}$$

Expanding the arguments using trigonometric identities and factoring out terms involving the bubble time, τ, we can write the above equation as

$$\frac{b\,c}{\sqrt{1 + A}}\left\{\left[\frac{dA}{dt_s}\cos B - 2(1 + A)\frac{dB}{dt_s}\sin B\right]\sin\frac{b}{a}\tau \right.$$

$$\left. - \left[\frac{dA}{dt_s}\sin B - 2(1 + A)\frac{dB}{dt_s}\cos B\right]\cos\frac{b}{a}\tau\right\}$$

$$- \frac{5}{4}a\,b\left\{\left[\frac{dA}{dt_s}\cos 2B\right] - 2(1 + A)\frac{dB}{dt_s}\sin 2B\,\sin 2\frac{b}{a}\tau)\right.$$

$$\left. - \left[\frac{dA}{dt_s}\sin 2B - 2(1 + A)\frac{dB}{dt_s}\cos 2B\right]\cos 2\frac{b}{a}\tau\right\}$$

$$- \left[\frac{a\,b}{2}(1 + A)\frac{dB}{dt_s}\right] = 0\,. \qquad (3.52)$$

The trivial solution to this equation is $dA/dt_s = dB/dt_s = 0$. If a more general solution exists, it must exist for all time τ and t_s. Since the constants in front of the major brackets are not equal to zero and the periodic terms involving the bubble time are linearly independent functions and not all are equal to zero at the same time, the only way to satisfy the equality is to equate each square bracketed term to zero. This leads to five independent equations all of which are equal to zero.

The first two square bracketed expressions lead to two equations which can be solved for the two unknowns, A and B. Looking at the first of the square bracketed expressions, we see that it can be written as

$$\frac{1}{(1 + A)}\frac{dA}{dt_s} - 2\frac{dB}{dt_s}\frac{\sin B}{\cos B} = 0\,. \qquad (3.53)$$

An integration of (3.53) with respect to laboratory time yields

$$\ln(1 + A) + \ln(\cos^2 B) = C\,, \qquad (3.54)$$

where C is an integrating constant. Evaluating this for the initial values of A and B, one sees that $C = 0$. Solving this equation for A in terms of B, one has

$$A = \frac{\sin^2 B}{\cos^2 B} \ . \tag{3.55}$$

Its derivative with respect to laboratory time is then

$$\frac{dA}{dt_s} = 2\frac{dB}{dt_s}\frac{\sin B}{\cos^3 B} \ . \tag{3.56}$$

These two expressions can now be substituted into the second square bracketed expression from equation (3.53) to obtain an equation solely in terms of B. It is

$$2\frac{dB}{dt_s}\left[\frac{\sin^2 B}{\cos^3 B} + \frac{\sin B}{\cos^2 B}\right] = 0 \ . \tag{3.57}$$

This equation is satisfied if either $dB/dt_s = 0$, or the part in brackets is equal to zero. Equating the bracketed term to zero we get

$$\tan B = -1 \ , \tag{3.58}$$

which leads to

$$B = (3+4n)\frac{\pi}{4} \quad \text{and} \quad -(1+4n)\frac{\pi}{4}, \qquad n = 0, 1, 2, 3, \ldots \tag{3.59}$$

But these values of B violate the initial condition which requires that $B(0) = 0$. Therefore, the only solution to equation (3.57) for all t_s is

$$\frac{dB}{dt_s} = 0 \ , \tag{3.60}$$

or, from the initial value,

$$B(t_s) = 0 \ . \tag{3.61}$$

Substituting this back into equation (3.55) one gets the constant value of A for all t_s to be

$$A(t_s) = 0 \ , \tag{3.62}$$

which satisfies the initial value.

It now must be determined whether the other three expressions derived from equation (3.52) hold for the same values of A and B. Applying the previous procedure on

the third and fourth square bracketed expressions from (3.52), first find the expression for A to be

$$A = \frac{1 - \cos 2B}{\cos 2B} \ . \tag{3.63}$$

Substituting this and its derivative into the fourth expression we get for B

$$2 \frac{dB}{dt_s} \sec^2 2B = 0 \ . \tag{3.64}$$

This equation says that since secant squared never equals zero for any B, again $dB/dt_s = 0$, and

$$B(t_s) = 0 \ . \tag{3.65}$$

Putting this back into equation (3.63) one again gets the result

$$A(t_s) = 0 \ . \tag{3.66}$$

It is also recognized that the fifth bracketed expression from equation (3.52) is also satisfied for both these conditions. Applying these results to equation (3.49) one gets the same expression derived earlier which was independent of the laboratory time, t_s. Evidently in the small oscillation case, the zero-order solution is indeed independent of the laboratory time, t_s. It now remains is to determine whether or not this is the case for the formal zero-order equation over the full range of the parameter, u_v.

3.5.2 The Integrability Condition: Basic Structure and Most General Solution

The integrability condition is usually satisfied by substitution of an explicit zero order solution, $u_0(\tau,t_s)$ in order to find the dependence of u_0 upon t_s. In the present case this can be done only for values of u_v very near 1 where the small oscillation solution applies. As preparation for the determination the form of u_0 with respect to t_s for all values of u_v we now consider the properties of u_0 that follow from the partial differential equation itself, namely:

$$2 u_0 \frac{\partial^2 u_0}{\partial \tau \partial t_s} + 3 \frac{\partial u_0}{\partial \tau} \frac{\partial u_0}{\partial t_s} = 0 \ . \tag{3.50}$$

If u_0 should happen to be independent of t_s this integrability condition is certainly satisfied. But are there also forms of $u_0(t,t_s)$ depending on t_s as well as τ which satisfy the integrability condition ? That is the question to be answered and some knowledge about the basic properties of the partial differential equation and the forms of the integrability functions that will satisfy it may be helpful.

This partial differential equation is a hyperbolic quasilinear equation in normal form with characteristic directions on the lines τ= constant and t_s = constant. In order to see this we let $p = \frac{\partial u_0}{\partial \tau}$, $q = \frac{\partial u_0}{\partial t_s}$, $r = \frac{\partial^2 u_0}{\partial \tau^2}$, $s = \frac{\partial^2 u_0}{\partial \tau \partial t_s}$ and $w = \frac{\partial^2 u_0}{\partial t_s^2}$.

Then the two equations,

$$dp = r\,d\tau + s\,dt_s \tag{3.67}$$

and

$$dq = s\,d\tau + w\,dt_s, \tag{3.68}$$

result directly from the chain rule applied to the formulas for p and q. The partial differential equation can now be expressed as

$$s + \frac{3}{2u_0}\,p\,q = 0\,. \tag{3.69}$$

Suppose next that one has a curve Γ in the t,t_s plane along which u_0 and its normal derivative, $\frac{du_0}{dn}$, are prescribed. This is the same as saying that u_0 , p and q as well as dp and dq are known along Γ. Consequently, along Γ we have three equations in three unknowns:

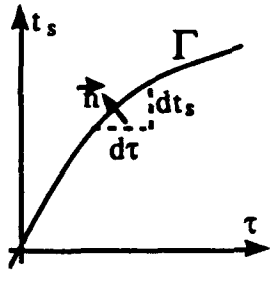

$$0 + r\,dt + s\,dt = dp\,, \tag{3.70}$$

$$0 + s\,dt + w\,dt = dq\,, \tag{3.71}$$

$$0 + s \quad + 0 = -\frac{3}{2u_0}\,pq\,. \tag{3.72}$$

These equations enable us to determine the derivatives r, s and w everywhere along Γ, provided that Δ, the determinant of these equations, never vanishes along Γ. When this is true Γ is called an ordinary curve and it is possible to find derivatives of u_0 of all orders along Γ and one can therefore expand u_0 as a Taylor series about every point on Γ in order to determine the solution on a strip in the τ,t_s plane. The width of this strip is determined by the radius of convergence of the series at every point along Γ. Characteristic directions at any point on Γ are defined as those directions for which Δ vanishes. In such a situation the derivatives of u_0 can not be found and the computation of the solution as described above can not be carried out. In the present case if any point on Γ is tangent to such a direction we must have

$$\Delta = \begin{vmatrix} d\tau & dt_s & 0 \\ 0 & d\tau & dt_s \\ 0 & 1 & 0 \end{vmatrix} = d\tau\, dt_s = 0, \tag{3.73}$$

and the solution can not be continued as indicated above. Clearly, all lines τ = constant and t_s = constant must be characteristic lines as stated at the outset.

When Γ is an ordinary curve one can use Cramer's rule in order to find the values of r, s, and w at any point on Γ. Thus we have for the present problem the solution,

$$(\Delta)\ s = \begin{vmatrix} d\tau & dp & 0 \\ 0 & dq & dt_s \\ 0 & -\frac{3}{2u_0}pq & 0 \end{vmatrix}. \tag{3.74}$$

On a characteristic, since $\Delta = 0$, the best that we can hope for is that solution for s will be simply indeterminate on Γ. Such will be the case if we also insist that

$$\begin{vmatrix} d\tau & dp & 0 \\ 0 & dq & dt_s \\ 0 & -\frac{3}{2u_0}pq & 0 \end{vmatrix} = d\tau\, dt_s\, \frac{3}{2u_0}pq = 0 \qquad (3.75)$$

along the characteristics. This characteristic relationship provides the key for the determination of the dependence of u_0 upon the laboratory time t_s. In order to see how, we recall that all derivatives in the zero–order partial differential equation determining u_0 are taken with respect to τ. Therefore solution u_0 is reduced to a quadrature by means of two partial integrations with respect to τ and its only dependence on t_s is found in the constants of integration $A(t_s)$ and $B(t_s)$. But in terms of the integrability condition from the first order perturbation equation, a partial integration over τ implies that $dt_s = 0$. But

$$du_0 = \frac{\partial u_0}{\partial \tau} d\tau + \frac{\partial u_0}{\partial t_s} dt_s = p\, d\tau + q\, dt_s.$$

Therefore we have

$$q\, dt_s = du_0 - p\, d\tau .$$

Therefore the characteristic relationship,

$$d\tau\, dt_s\, \frac{3}{2u_0}pq = 0,$$

becomes

$$d\tau \frac{3}{2u_0} p(du_0 - p\, d\tau) = 0.$$

But the factor $d\tau \frac{3}{2u_0} p$ is certainly not generally zero. Therefore the condition $(du_0 - p\, d\tau) = 0$ suggests that u_0 is independent of t_s in general.

The fact that the integrability condition of Equation (3.50) has a rather symmetric form and has a cross second derivative for its highest order term suggests that one might find a general form for $u_0(\tau,t_s)$ which is analogous to d'Alembert's well known solution for the wave equation. In order to exploit this symmetry we can let $v = \frac{\partial u_0}{\partial \tau}$ as before.

Then the integrability condition is

$$\frac{2}{v}\frac{\partial v}{\partial t_s} + \frac{3}{u_0}\frac{\partial u_0}{\partial t_s} = 0 . \tag{3.76}$$

Evidently this equation can be rewritten as $\frac{\partial}{\partial t_s} \ln (v\, u^{3/2}) = 0$, from which one finds that $u_0^{3/2}\frac{\partial u_0}{\partial \tau} = f(\tau)$. A second partial integration with respect to τ leads to

$$u_0^{5/2} = \int \frac{5}{2} f(\tau)\, d\tau + h(t_s) = g(\tau) + h(t_s).$$

Consequently, the integrability condition will be satisfied by any functions $g(\tau)$ and $h(t_s)$ in an equation of the general form,

$$u_0(\tau,t_s) = [g(\tau) + h(t_s)]^{2/5}. \tag{3.77}$$

That this result is the most general form of the *integrability function* can be verified directly by differentiation to show that

$$2u_0 \frac{\partial^2 u_0}{\partial \tau \partial t_s} = -\frac{6}{25}[g(\tau) + h(t_s)]^{-6/5} \text{ and that } 3\frac{\partial u_0}{\partial \tau}\frac{\partial u_0}{\partial t_s} = \frac{6}{25}[g(\tau) + h(t_s)]^{-6/5}.$$

As we have noted, equation (3.77) is expressed in characteristic coordinates. In order to exhibit a form which gives the solution on an ordinary curve, $\Gamma(\tau_1,t_1)$ as illustrated above, we need a transformation between the characteristic and Γ coordinates, $\tau = \phi(\tau_1,t_1)$ and $t_s = \psi(\tau_1,t_1)$. For example, suppose we take $\tau = (\tau_1 + t_1)/\sqrt{2}$ and $t_s = (\tau_1 - t_1)/\sqrt{2}$, corresponding to Γ being a line at 45° with respect to the horizontal and upon which $t_1 = 0$. Then one can write

$$u_0(\tau_1,t_1) = [g_1(\tau_1 + t_1) + h_1(\tau_1 - t_1)]^{2/5},$$

where the suffixes on g_1 and h_1 denote that the Γ coordinates have been rescaled in order to cause $u_0(\tau_1,t_1)$ to resemble more closely the classical d'Alembert solution. This formal resemblance must not be allowed to obscure the fact that physically, the proper coordinates are τ and t_s and that the question of whether or not the zero–order solution depends on t_s as well as τ is uppermost in our minds.

Two successive partial integrations of Equation (3.1) with respect to τ have given the quadrature,

$$\tau + b(t_s) = (1+q)^{3/4} \int_1^{u_0} \frac{\xi^{3\backslash 2}\, d\xi}{\sqrt{2u_v^2 \ln \xi - \xi^2 + 1 + a(t_s)}} \qquad (3.78)$$

which is certainly not of the general form required by the integrability function. Equation (3.78) can be brought into an acceptable form if $a(t_s) = b(t_s) = 0$. This choice satisfies the initial conditions and we may then write the solution symbolically as $u_0(t_s,\tau) = G(\tau)$, where it is supposed that the integral can be evaluated and inverted (numerically if need be.) More generally one could suppose, because of the small oscillation result discussed above, that this inversion might have a form such as,

$$u_0(\tau,t_s) = A(t_s)\, F[\tau + B(t_s)].$$

The general form of Equation (3.77), appears to preclude this possibility, however; and this conclusion is reinforced by the direct use of this tentative form of u_0 in the integrability condition, equation (3.50).

3.5.3 A Direct Approach to the General Solution

Since the inverse form, $\tau[u_v;\, u_0,\, a(t_s), b(t_s)]$, has been reduced to the quadrature of equation (3.78), one can use the Leibnitz rule in order to test further the finding obtained thus far in the hope that if there is a dependence on t_s , it might at least be found numerically. We shall start our direct approach using the closed–form result, $v = \partial u_0/\partial\tau$, which we shall now write as

$$(1+q)^{3/2}\, v^2 = [2u_v^2 \ln u_0 - u_0^2 + 1 + a(t_s)]/u_0^3 \,. \qquad (3.79)$$

Therefore the mixed second derivative is found to be

$$\frac{\partial v}{\partial t_s} = \left\{ \frac{u_v^2 - u_0^2}{v\, u_0^4 (1+q)^{3/2}} - \frac{3v}{2u_0} \right\} \frac{\partial u_0}{\partial t_s} + \frac{1}{(1+q)^{3/2}} \frac{1}{2u_0^3 v} \frac{da}{dt_s},$$

so that the second–order term in the integrability condition is

$$2\, u_0 \frac{\partial^2 u_0}{\partial \tau\, \partial t_s} = \left[\frac{2(u_v^2 - u_0^2)}{v\, u_0^3 (1+q)^{3/2}} - 3v \right] \frac{\partial u_0}{\partial t_s} + \frac{1}{(1+q)^{3/2}} \frac{1}{u_0^2 v} \frac{da}{dt_s}. \qquad (3.80)$$

The second term in the integrability condition, involving the product of $\partial u_0/\partial \tau$ and $\partial u_0/\partial t_s$, can be written as $3v \frac{\partial u_0}{\partial t_s}$ which eliminates the term, $-3v \frac{\partial u_0}{\partial t_s}$, in the mixed second order derivative of equation (3.80) from the integrability condition. Consequently the integrability condition, when written as $2u_0 \frac{\partial v}{\partial t_s} + 3v \frac{\partial u_0}{\partial t_s} = 0$, becomes

$$\left[\frac{2(u_v^2 - u_0^2)}{v\, u_0^3 (1+q)^{3/2}} \right] \frac{\partial u_0}{\partial t_s} + \frac{1}{(1+q)^{3/2}} \frac{1}{u_0^2 v} \frac{da}{dt_s} = 0.$$

This result simplifies to

$$2(u_v^2 - u_0^2) \frac{\partial u_0}{\partial t_s} + u_0 \frac{da}{dt_s} = 0. \qquad (3.81)$$

The only factor depending on $b(t_s)$ results from the derivative, $\partial u_0/\partial t_s$. After applying Leibnitz's rule [12] to equation (3.78) and rearranging the result, one finds that

$$\frac{\partial u_0}{\partial t_s} = v \frac{db}{dt_s} + \frac{v}{2} (1+q)^{3\backslash 4} \frac{da}{dt_s} \int_1^{u_0} \left[\frac{\xi}{2u_v^2 \ln \xi - \xi^2 + 1 + a(t_s)} \right]^{3/2} d\xi, \text{ or that}$$

$$\frac{\partial u_0}{\partial t_s} = v \frac{db}{dt_s} + \frac{v}{2(1+q)^3} \frac{da}{dt_s} \int_1^{u_0} \frac{d\xi}{\xi^3 v^3}. \qquad (3.82)$$

Equation (3.82) can now be substituted into the integrability condition of (3.81) After separating the terms involving the derivatives of $a(t_s)$ and $b(t_s)$, Then one finds that

$$\left\{ u_0 + \frac{(u_v^2 - u_0^2)}{(1+q)^3} v \int_1^{u_0} \frac{d\xi}{[\xi v(\xi,a)]^3} \right\} \frac{da}{dt_s} + 2(u_v^2 - u_0^2) v \frac{db}{dt_s} = 0. \qquad (3.83)$$

The integrability condition of equation (3.83) is a single condition for the two unknown functions, $a(t_s)$ and $b(t_s)$. If a and b are truly independent arbitrary functions then they must vanish identically. Otherwise, equation (3.83) implies that a and b are interdependent .

Suppose therefore, that we were to consider a = a(b). The differential dt_s is then eliminated from Equation (3.83). If in general the differentials da and db are not zero simultaneously, equation (3.83) will be satisfied only if the coefficients of da and db vanish. Then we would have two equations for the unknowns $a(t_s)$ and u_0. If these equations were solved for values of the unknowns near their starting values, a = 0 and $u_0 = 1$. Then one would evaluate Equation (3.78) from 1 to u_0 and so calculate the sum, $t_s + b(t_s)$, with the help of the condition $t_s = \varepsilon\tau$. But he could not determine t_s or b without an added constraint which does not appear to exist for this formulation. Thus we see that if $a(t_s)$ and $b(t_s)$ are not independent functions of integration , the system of equations is not closed. Moreover even if the system were closed, these two equations do not vanish at the initial condition, where a(0) = v(0,0) = 0 and $u_0(0,0) = 1$. Then the requirement that the coefficients of da and db vanish for all t_s and τ is certainly not satisfied.

Suppose next, that one considers the differential equation (3.83) and the quadrature of Equation (3.78) as two of a governing system of equations. How might the system be closed? One possibility may be suggested by the behavior of the zero-order radial velocity, $\frac{du_0}{d\tau}$, which from the chain rule and the condition $dt_s = \varepsilon d\tau$, is

$$\frac{du_0}{d\tau} = \frac{\partial u_0}{\partial \tau} + \varepsilon \frac{\partial u_0}{\partial t_s} . \tag{3.84}$$

The two partial derivatives of u_0 in equation (3.84) are given by the square root of equation (3.79) and by equation (3.82), respectively. Equation (3.84) can be used to determine the maximum and minimum values of u_0. These values are given by the two roots of $\frac{du_0}{d\tau} = 0$, namely:

$$\frac{\sqrt{[2u_v^2 \ln u_0 - u_0^2 + 1 + a(t)]/u_0^3}}{(1+q)^{3/4}} + \varepsilon \left[v \frac{db}{dt_s} + \frac{v}{2(1+q)^3} \frac{da}{dt_s} \int_1^{u_0} \frac{d\xi}{\xi^3 v^3} \right] = 0. \tag{3.85}$$

If the roots of (3.85) can be found starting at the initial point, the value of u_{max}, say, permits one to assign a series of equally spaced points over the interval $[1,u_{max}]$. Let the first new value of u_0 be $1+h$, where h is the step size. Of course, u_{max} and u_{min} must be found at each step because the values of a and b will change with each computational step. Therefore it is possible that the size of each step should be found from integration of equation (3.84) and equation (3.85) should be reserved for the determination of u_{min} and u_{max}. We note in equation (3.85) that $a(t_s)$ and $b(t_s)$ are the unknowns. The same is true of equation (3.83). Equation (3.78) has a, b and τ as unknowns, provided that u_0 can be found from integrating equation (3.83). Then by making use of $t_s = \varepsilon\tau$, we see that the fundamental unknowns are a, b and τ at each step and there are three equations. Therefore, the system is closed; but it remains to design an algorithm for a step by step solution. All of this is conjectural. Therefore the present study is restricted to the case in which $a = b = 0$ and the integrability condition is indeed satisfied. This approach may be useful preparation for an attack on this generalized problem, should it be necessary. The present special formulation will reveal some aspects of the solution properties that must also be dealt with even in a generalized approach. This will be especially true in the neighborhood of of the initial point $\tau = t_s = 0$ because a and b will be very small in this neighborhood.

CHAPTER 4

FIRST-ORDER EQUATION ANALYSIS

4.1 Statement of Equation

The two-scale perturbation expansion in section 2.4.2 gives the first-order linear perturbation partial differential equation for $u_1(\tau,t_s)$ where u_1 is the first order normalized dimensionless bubble radius, u_1. The two dimensionless time scales are t_s, and τ and the first order equation was found to be,

$$\frac{\partial^2 u_1}{\partial \tau^2} + \frac{3}{u_0}\frac{\partial u_0}{\partial \tau}\left(\frac{\partial u_1}{\partial \tau}\right) + \frac{u_1}{u_0}\left[\frac{\partial^2 u_0}{\partial \tau^2} + \frac{1}{u_0^2(1+q)^{3/2}}\left(\frac{3u_v^2}{u_0^2} - 1\right)\right]$$

$$= -2\left[\frac{\partial^2 u_0}{\partial \tau\, \partial t_s} + \frac{3}{2}\frac{1}{u_0}\frac{\partial u_0}{\partial \tau}\frac{\partial u_0}{\partial t_s}\right] + \frac{F(t_s)}{u_0(1+q)^{3/2}}\,, \qquad (4.1)$$

with initial conditions of

$$u_1(0,0) = 0 \qquad (4.2)$$

and

$$\frac{\partial u_1(0,0)}{\partial \tau} + \frac{\partial u_0(0,0)}{\partial t_s} = \frac{1}{8}W_I\sqrt{(1+q)(1+K)}\left(-\frac{dC_p}{ds}\right)_{C_p=-K}. \qquad (4.3)$$

In equation (4.1), $F(t_s)$ is the pressure forcing function of section 2.2 and the term to the right of the equality in (4.3) is the flaccid bubble response, from section 2.3.4, to $F(t_s)$. The first-order equation depends on the zero-order equation and its derivatives as well the affix of the vortex point, u_v.

To write this equation in terms of the normalized bubble time, x, one applies equation (3.17) and its derivatives to equation (4.1). In section 3.5 we have taken the zero-order solution to be independent of the slow laboratory time, t_s, so that those terms containing derivatives of u_0 with respect to t_s must vanish. Moreover, the mixed derivative terms in the second-order equation of u_2 also vanish for the same reason. Thus, the first-

order equation may be considered to be independent of the laboratory time, t_s, and can be written as an ordinary differential equation depending only on the bubble time, τ. Applying this and the period parameter from equation (3.20), we can write a normalized form of the first-order equation as

$$\frac{d^2u_1}{dx^2} + \frac{3}{u_0}\frac{du_0}{dx}\left(\frac{du_1}{dx}\right) + \frac{u_1}{u_0}\left[\frac{d^2u_0}{dx^2} + \frac{1^2}{u_0^2}\left(\frac{3\,u_v^2}{u_0^2} - 1\right)\right] = \frac{\lambda^2 F(\epsilon,x)}{u_0}, \qquad (4.4)$$

with corresponding initial conditions of

$$u_1(0) = 0 \qquad (4.5)$$

and

$$\frac{du_1(0)}{dx} = \frac{1}{8}W_r(1+q)^{5/4}\sqrt{(1+K)}\left(-\frac{dC_p}{ds}\right)_{C_p=-K}. \qquad (4.6)$$

This leaves a single-degree-of-freedom system governed by a linear second-order nonhomogeneous ordinary differential equation. Due to the fact that the zero-order equation has periodic solutions, this ordinary differential equation has time dependent periodic coefficients that can produce parametric excitations in the system. This type of system is discussed by Nayfeh and Mook [7] among others, and as they suggest it can be solved using the Floquet theory for the homogeneous solution and variation of parameters for the particular solution [12].

4.2 Homogeneous Solution from the Floquet Method

4.2.1 Standard Form of the Equation

The linearity of equation (4.4) permits the forcing term to be set to zero, leaving a homogeneous equation involving only derivatives with respect to the normalized bubble time, x. The homogeneous part of Equation (4.4) can then be written as

$$\frac{d^2u}{dx^2} + p_1(x)\frac{du}{dx} + p_2(x)u = 0, \qquad (4.7)$$

where

$$p_1(x) = \frac{3}{u_0}\frac{du_0}{dx}, \tag{4.8}$$

and

$$p_2(x) = \frac{1}{u_0}\left[\frac{d^2u_0}{dx^2} + \frac{\lambda^2}{u_0^2}\left(\frac{3u_v^2}{u_0^2} - 1\right)\right]. \tag{4.9}$$

For ease of writing and to avoid confusion in later analysis, the first-order subscript is dropped for the homogeneous form of the equation. Because they depend on u_0, both coefficients, $p_i(x)$, are periodic functions in x with a normalized period of unity.

Equation (4.7) can be expressed in standard form by eliminating the first derivative term. Using the transformation

$$u = \frac{z}{u_0^{3/2}} \tag{4.10}$$

and its derivatives, one can write equation (4.7) in the standard form,

$$\frac{d^2z}{dx^2} + p(x)z = 0\ , \tag{4.11}$$

where

$$p(x) = \frac{\lambda^2}{2u_0^2}\left[\frac{5u_v^2}{u_0^2} - 1\right]. \tag{4.12}$$

The parameter p(x) is also a periodic function, dependent on the zero-order solution and u_v. Figure 4.1 shows the form of p(x) for various values of u_v. It is seen that as the value of u_v increases, portions of the function p(x) become increasingly steeper and steeper. This phenomenon causes equation (4.11) to become increasingly stiff with rising u_v values, and some care must be taken if this equation is to be evaluated numerically.

This standardized form of the first-order equation in (4.11) is among the class known as Hill's equations, and can have stable or unstable solutions depending on the value of u_v in p(x). For the special case when p(x) has the form

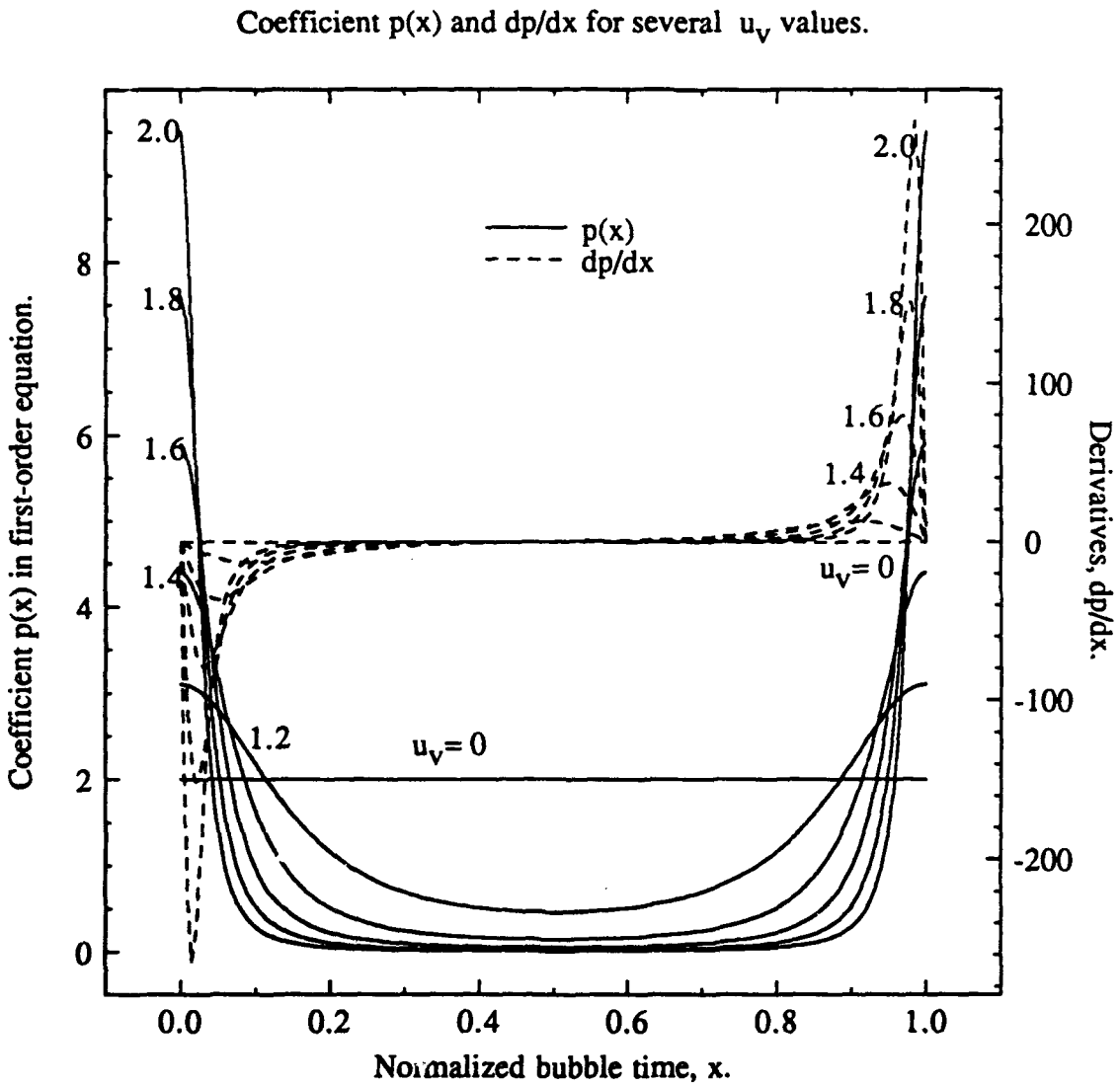

Figure 4.1 The Periodic Coefficient, p(x), and its Derivative from the Standard Form of the First Order Equation for Several Values of u_v.

$$p(x) = d^* + 2e^*\cos(2x) \ , \tag{4.13}$$

where d* and e* are stability parameters, equation (4.11) reduces to a form of Mathieu's equation dealing with the problem of vibrations of an elliptic membrane. With the homogeneous first-order equation in this standard form its stability and its solution are well known and are given by Abramowitz and Stegun [9] among others.

4.2.2 Small Oscillation Stability Analysis

As discussed in Nayfeh and Mook [8], the stability of equations (4.7) and (4.11) is the same. So the stability of one will be the same as that of the other. Using the small oscillation results from the zero-order solution for the case

$$u_v = 1 + \delta \ , \tag{4.14}$$

where $\delta << 1$, a small oscillation form of the standard equation can be obtained. Substituting the small oscillation expressions for u_0 and l from equations (3.34) and (3.37) into equation (4.11) and keeping terms to the second order in δ, one finds a small oscillation form of the homogeneous first-order equation to be

$$\frac{d^2z}{dx^2} + 4\pi^2\left[1+\delta\frac{11}{2}\cos(2\pi x) + \delta^2\left(\frac{61}{6} - \frac{55}{12}\cos(2\pi x) + \frac{69}{8}\cos(4\pi x)\right)\right] z = 0. \tag{4.15}$$

Equation (4.15) can be recognized as a Hill's equation.By letting $\theta = \pi x$ and ruling out terms containing 4θ; one can write this equation to the second-order in δ, except for the neglected 4θ term, as

$$\frac{d^2z}{d\theta^2} + 4\left[1 + \delta^2\frac{61}{6} + \delta\left(\frac{11}{2} - d\frac{55}{12}\right)\cos(2\theta)\right] z = 0 \ . \tag{4.16}$$

This is a standard Mathieu equation with the form of the coefficients as described in equation (4.13). The term $\delta^2\frac{69}{8}\cos(4\pi x)$ from equation (4.15) was left out of the expression in (4.16) in order to produce the proper form for a Mathieu equation. This

omission seems acceptable since similar results to the present analysis were obtained while only keeping terms up to the first order in δ.

Comparing the coefficient in equation (4.16) to the Mathieu form in equation (4.13), we find that the stability parameters are

$$\delta^* = 4\left(1 + \delta^2 \frac{61}{6}\right) \tag{4.17}$$

and

$$\varepsilon^* = \delta\left(11 - \delta \frac{55}{6}\right) . \tag{4.18}$$

Therefore both δ^* and ε^* are functions of δ.

The stability of the Mathieu equation can be visualized by plotting δ^* against ε^*. In the δ^*,ε^* plane. for the present case there are two curves of neutral stability [9] given by,

$$\delta^* = 4 - \frac{1}{12}(\varepsilon^*)^2 + \frac{5}{13824}(\varepsilon^*)^4 + \ldots \tag{4.19}$$

and

$$\delta^* = 4 + \frac{5}{12}(\varepsilon^*)^2 - \frac{763}{13821}(\varepsilon^*)^4 + \ldots \quad . \tag{4.20}$$

In the region between these two curves the solution to the Mathieu equation is unstable, while outside these curves the solution is stable. Remembering that

$$\delta = u_v - 1 , \tag{4.21}$$

one can plot equations (4.17) and (4.18) as in figure 4.2 for various small values of u_v. Note that two such curves are plotted in figure 4.2 . One curve is shown as a continuous curve with circled points showing various u_v values in the interval [1,1.013]. The second curve is shown as a sequence of small black squares and this curve covers the u_v interval [1, 0.987] . Included in this figure are the neutral stability curves from equations (4.19) and (4.20).

As $\delta \rightarrow 0$ and $u_v \rightarrow 1$, the Mathieu equation in question yields neutral stability parameters of $\delta^* \rightarrow 4$ as $\varepsilon^* \rightarrow 0$. Similarly, both neutral stability curves also approach a

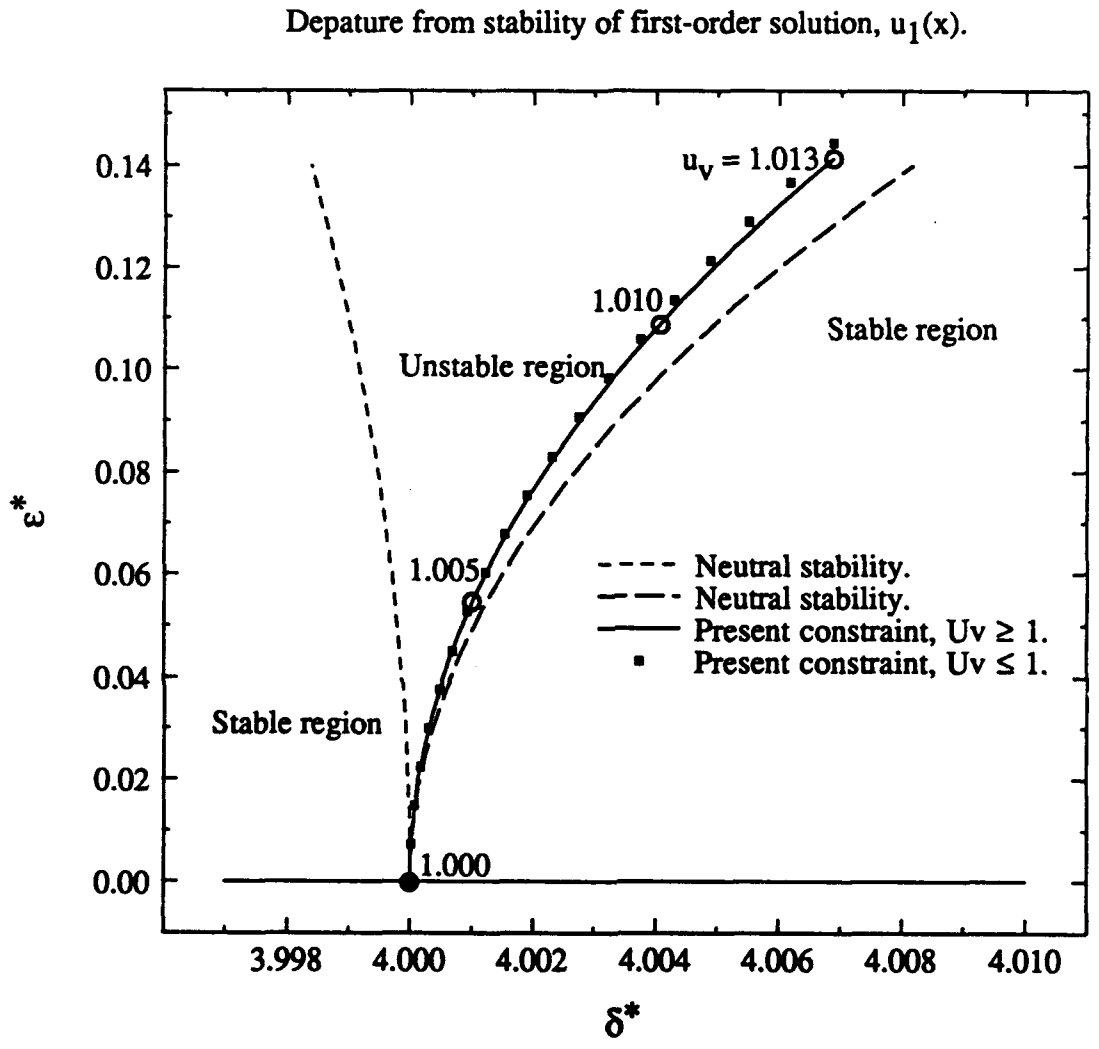

Figure 4.2 The Stability Region of the First-Order Differential Equation for Small Oscillations.

value of $\delta^* \rightarrow 4$ when $\varepsilon^* \rightarrow 0$. This shows that the homogeneous part of the first-order solution departs from a point of neutral stability at $u_v = 1$, continuing into an unstable region as u_v increases or decreases. When $u_v = 1$, the period parameter assumes the value $\lambda = \pi\sqrt{2}$ and the Mathieu equation in (4.11) becomes the equation of a harmonic oscillator which is indeed neutrally stable. It appears from figure 4.2 that the small oscillation solution curves continue to stay in the unstable region for all higher values of u_v, although the small oscillation approximation will break down as the value of u_v increases or decreases too far outside of the range [0.98, 1.03].

4.2.3 Floquet Method

The homogeneous first-order equation describes the behavior of a system governed by a linear ordinary differential equation with periodic coefficients. The functional behavior of single-degree-of-freedom systems can be characterized using the Floquet theory. This theory determines general properties of the solutions from systems governed by equations of the form (4.7), without actually solving them. These properties can then be used to determine numerical approximations to the solutions. These approximations have factors that are periodic, allowing them to be used over many cycles, whereas other numerical solution techniques tend to accumulate excessive errors when used over an extended range. The nonperiodic factors are exponentials which also permit accurate numerical evaluation. The following development is given by Nayfeh and Mook [8], and applied to the equation at hand.

Since equation (4.7) is a second-order linear homogeneous equation, it has two linearly independent solutions $u_1(x)$ and $u_2(x)$. Here the subscripts refer to the two independent solutions to the first-order homogeneous equation and not to the first or second-order equations of the two scale expansion. Functions such as u_1 and u_2 are usually referred to as a fundamental set of solutions because every solution is a linear combination of these two solutions, and because they satisfy the fundamental initial conditions of

$$\left.\begin{array}{llll} u_1(0) = 1 & \dot{u}_1(0) = 0 \\ u_2(0) = 0 & \dot{u}_2(0) = 1 \end{array}\right\} . \tag{4.22}$$

Since the zero-order solution is periodic, equations (4.8) and (4.9) are also periodic and

$$p_i(x) = p_i(x + T) , \tag{4.23}$$

where T is the period and in the normalized sense equal to unity. It follows that if $u_1(x)$ and $u_2(x)$ are any two solutions of equation (4.7), then $u_1(x + T)$ and $u_2(x + T)$ are also solutions of equation (4.7). Also, if $u_1(x)$ and $u_2(x)$ are linearly independent, then $u_1(x + T)$ and $u_2(x + T)$ must be linearly dependent on $u_1(x)$ and $u_2(x)$ because a second-order equation has only two linearly independent solutions. Therefore, there exist two constants for each solution that do not both vanish at the same time such that

$$\{u_i(x + T)\} = [A]\{u_i(x)\} , \tag{4.24}$$

where i = 1 and 2 and the matrix [A] contains the four constants

$$[A] = \begin{bmatrix} a_{11} & a_{12} \\ a_{21} & a_{22} \end{bmatrix} . \tag{4.25}$$

Applying the fundamental initial conditions from (4.22) and the normalized period to equation (4.24) and its derivative, we find the constants to be

$$\left.\begin{array}{llll} a_{11} = u_1(1) & a_{12} = \dot{u}_1(1) \\ a_{21} = u_2(1) & a_{22} = \dot{u}_2(1) \end{array}\right\} . \tag{4.26}$$

Once $u_1(x)$ and $u_2(x)$ are known the a_{ij} constants can be determined.

Since equations (4.7) and (4.11) are both a form of Hill's equation and have the same stability characteristics, the above process also holds true for a fundamental set of solutions, $z_1(x)$ and $z_2(x)$. In the actual numerical solution process it is the fundamental set of z_i solutions which are found, and they are transformed back into the u_1 form using equation (4.10). This is done for convenience, since the small oscillation and stability

results are more easily obtained from equation (4.11), as will be shown later. However, u_1 and u_2 will continue to be used in the development of the solution to avoid confusion.

It can also be stated that there exist fundamental sets of solutions having the property

$$v_i(x + T) = \lambda_i v_i(x) \ , i = 1, 2; \tag{4.27}$$

where λ_i are the eigenvalues of the matrix [A]. These eigenvalues may be complex. Equation (4.27) represents what are called Floquet normal solutions, and are related linearly to $u_i(x)$ by a 2 x 2 constant nonsingular matrix, [P], such that

$$\{u_i(x)\} = [P] \{v_i(x)\} \ . \tag{4.28}$$

The substitution of equation (4.28) into equation (4.24) yields

$$\{v_i(x + T)\} = [P]^{-1} [A] [P] \{v_i(x)\} \ , \tag{4.29}$$

or

$$\{v_i(x + T)\} = [B] \{v_i(x)\} \ . \tag{4.30}$$

The matrices [A] and [B] are said to be similar matrices because they have the same eigenvalues, that is

$$|[B] - \lambda_i [I]| = |[A] - \lambda_i [I]| = 0 \ , \ i = 1, 2. \tag{4.31}$$

The eigenvalues of matrix [A], which will also satisfy matrix [B], must now be found[1] . It follows from linear algebra that a nonsingular matrix [P] can be chosen so that [B] will have its simplest possible or Jordan canonical form. This form depends on the eigenvalues of [A] which are found by solving

$$|[A] - \lambda_i [I]| = 0 \ , \ i = 1, 2. \tag{4.32}$$

---

[1] It is hoped there will be no confusion between λ for the period parameter and λ_i for the eigenvalues.

This leads to the equation

$$\lambda_i^2 - 2\alpha\lambda_i + \Delta = 0 \ , \tag{4.33}$$

where

$$\alpha = \frac{1}{2}\left[u_1(1) + \dot{u}_2(1)\right] = \frac{1}{2}\left[a_{11} + a_{22}\right] \tag{4.34}$$

and

$$\Delta = u_1(1)\dot{u}_2(1) - \dot{u}_1(1)u_2(1) = a_{11}a_{22} - a_{12}a_{21}. \tag{4.35}$$

The quantity Δ represents the Wronskian determinant of $u_1(1)$ and $u_2(1)$ as defined by

$$\Delta = \begin{vmatrix} u_1(1) & \dot{u}_1(1) \\ u_2(1) & \dot{u}_2(1) \end{vmatrix} . \tag{4.36}$$

Since equations (4.7) and (4.11) have the same stability characteristics, the Wronskian of equation (4.11) can be analyzed to determine its value. From equation (4.11) for the two solutions z_1 and z_2, it follows that

$$\left.\begin{aligned} \ddot{z}_1(1) + p(x)z_1(1) &= 0 \\ \ddot{z}_2(1) + p(x)z_2(1) &= 0 \end{aligned}\right\} . \tag{4.37}$$

Subtracting z_2 times the first equation from z_1 times the second one gets

$$z_1(1)\ddot{z}_2(1) - \ddot{z}_1(1)z_2(1) = 0 \ , \tag{4.38}$$

which can be integrated to yield

$$\Delta(x) = z_1(x)\dot{z}_2(x) - \dot{z}_1(x)z_2(x) = \text{constant} \ . \tag{4.39}$$

Converting this back to the u_i solutions using equation (4.10), one finds that the expression is still equal to a constant. Evaluating this and using the initial conditions of (4.22) one gets

$$\Delta(x) \equiv 1 \ , \tag{4.40}$$

which is as it should be in the case of a Hill's equation [8]. This is an important result. It can be used later to indicate roughly the error in the numerical solutions for u_1 and u_2.

The stability parameter, α, is used to determine the value of the eigenvalues, λ_i, of [A]. With $\Delta = 1$, equation (4.33) yields

$$\lambda_{1,2} = \alpha \pm \sqrt{\alpha^2 - 1} \quad , \tag{4.41}$$

where the roots are related by

$$\lambda_1 \lambda_2 = 1 \quad . \tag{4.42}$$

If $\alpha = \pm |1|$, equation (4.41) yields only one eigenvalue, namely

$$\lambda = \alpha = \pm 1 \quad . \tag{4.43}$$

If $\alpha \neq 1$, equation (4.41) yields two distinct eigenvalues, and [B] takes on the diagonal form

$$[B] = \begin{bmatrix} \lambda_1 & 0 \\ 0 & \lambda_2 \end{bmatrix} . \tag{4.44}$$

It follows from equation (4.30) that

$$v_i(x + nT) = \lambda_i^n \, v_i(x) \quad , \tag{4.45}$$

where n is an integer and $i = 1$ and 2. Then as $x \rightarrow \infty$, $n \rightarrow \infty$ and

$$v_i(x) \rightarrow \begin{cases} 0 & \text{if} \quad |\lambda_i| < 1 \\ \infty & \text{if} \quad |\lambda_i| > 1 \end{cases} . \tag{4.46}$$

When $\lambda_i = 1$, v_i is periodic with period T. When $\lambda_i = -1$, v_i is periodic with period 2T. Thus the cases $\lambda_1 = \lambda_2 = \pm 1$ separate stable from unstable solutions for the fundamental set and are called transition values.

It remains to express equation (4.27) in normal Floquet form. First we multiply the respective equations by $\exp[-\gamma_i(x + T)]$, which yields

$$e^{-\gamma_i(x + T)} \, v_i(x + T) = e^{-\gamma_i x} \, v_i(x) \quad , \tag{4.47}$$

where

$$e^{-\gamma_i T} = \lambda_i \tag{4.48}$$

and

$$\gamma_i = \frac{1}{T} \ln \lambda_i \ . \tag{4.49}$$

The term γ_i in equation (4.49) is called the characteristic exponent. The right side of equation (4.47) is periodic with period T, and can be expressed as

$$e^{-\gamma_i x} v_i(x) = \phi_i(x) \ , \tag{4.50}$$

where $\phi_i(x + T) = \phi_i(x)$. Hence, $v_i(x)$ can be expressed in the normal form

$$v_i(x) = e^{\gamma_i x} \phi_i(x) \ . \tag{4.51}$$

For the case when $\lambda_i = \pm 1$, similar reasoning yields the same result for $v_1(x)$, but $v_2(x)$ will have the form

$$v_2(x) = e^{\gamma_2 x} \left[\phi_2(x) + \frac{x}{\lambda_2 T} \phi_1(x) \right] \tag{4.52}$$

due to the double root. These give expressions for the approximate normal Floquet solutions of equation (4.7) derived from the properties of the numerical solutions, $u_1(x)$ and $u_2(x)$. They are made up of well defined exponential functions multiplied by periodic functions, ϕ_i.

The stability of the fundamental set of solutions in Floquet form from equations (4.51) and (4.52) can be analyzed by calculating the value of α. When $|\alpha| > 1$, the absolute value of one of the λ_i is larger than one while that of the other is less than one, according to equation (4.42). This leads to γ_1 and γ_2 having equal magnitudes but opposite signs. Thus, one of the normal solutions is unbounded and the other is bounded as $x \rightarrow \infty$, as evidenced by equation (4.46). When $|\alpha| < 1$, the roots from equation (4.41) are complex conjugates having unit moduli. As stated before, the transition from stability to instability occurs for $|\alpha| = 1$, which corresponds to the repeated roots

$\lambda_1 = \lambda_2 = 1$ and $\lambda_1 = \lambda_2 = -1$ so that $\gamma_1 = \gamma_2 = 0$ or $i\pi$. The former case has a periodic normal solution with period T, while the latter case has a periodic normal solution of period 2T. The locus of transition values where $|\alpha| = 1$ is a very important outcome of this method and can be used to determine critical flow values that will produce neutrally stable solutions. The stability parameter, α, the eigenvalues, λ_i, and the characteristic exponents, γ_i, can be determined from equation (4.11) by numerically calculating the two linearly independent solutions, z_1 and z_2, during the first period of oscillation. With the help of these solutions and their first derivatives at $x = T$, one can calculate α and Δ from equations (4.34) and (4.35). Then the λ's and γs can be determined from equations (4.41) and (4.49) respectively.

The solutions u_1 and u_2 can be found by taking the numerical results for z_1 and z_2 from equation (4.11) and transforming them into u_1 and u_2 with the help of equation (4.10). But, due to numerical instabilities in the adaptive Runge-Kutta algorithm used here, errors will accumulate in the numerical process because the equation is stiff in cetain limited x intervals durring the integration over a period, [0,1]. The degree of stiffness increases as u_v departs more and more from unity.This aspect of the work will be discussed further below. Over the full range of the forcing function the solutions need to be extended over many periods in x, which will greatly reduce accuracy as the errors keep accumulating. To overcome this error accumulation the numerical solutions can be transformed into normal or Floquet solutions which in general have periodic factors as noted above. This would require numerical solutions of u_1 and u_2 for only one period of oscillation, thus minimizing the errors. This is also all that is required in the calculation of the previous stability parameters and characteristic exponents.

It then remains to find the components of the Floquet solutions in equation (4.51) in terms of the numerical u_i solutions. The γs have already been developed. Expressions for the periodic functions,ϕ_i, must then be found. This is begun by relating the u_i solutions to the v_i solutions using equation (4.28). To find the components of the matrix

[P] in (4.28), the eigenvectors corresponding to the eigenvalues of matrix [A] are found, such that

$$|\lambda [I] - [A]| [P] = 0 \ , \tag{4.53}$$

where, for cases i = 1 and 2

$$[P] = \begin{bmatrix} p_{1i} \\ p_{2i} \end{bmatrix} . \tag{4.54}$$

Expanding equation (4.53) for both values of i, four equations are obtained and can be expressed as

$$\left.\begin{aligned} a_{11}p_{1i} + a_{12}p_{2i} &= \lambda_i p_{1i} \\ a_{21}p_{1i} + a_{22}p_{2i} &= \lambda_i p_{2i} \end{aligned}\right\} . \tag{4.55}$$

From this set of equations, we find the ratio

$$\frac{p_{1i}}{p_{2i}} = \frac{a_{12}}{\lambda_i - a_{11}} = \frac{\lambda_i - a_{22}}{a_{21}} . \tag{4.56}$$

This leads to the modal matrix

$$[P] = \begin{bmatrix} a_{12} & a_{12} \\ \lambda_1 - a_{11} & \lambda_2 - a_{11} \end{bmatrix} = \begin{bmatrix} \lambda_1 - a_{22} & \lambda_2 - a_{22} \\ a_{21} & a_{21} \end{bmatrix} . \tag{4.57}$$

Either of these matrices can be used to transform between variables, or their average could be used to try and minimize errors in a computer code. Only the first form is used here.

From equation (4.28) it is seen that the inverse of [P] is needed to express the solutions in Floquet form. The inverse of [P] is

$$[P]^{-1} = \frac{1}{\Delta P}\begin{bmatrix} \lambda_2 - a_{11} & -a_{12} \\ -(\lambda_1 - a_{11}) & a_{12} \end{bmatrix} = \frac{1}{\Delta P}\begin{bmatrix} a_{21} & -(\lambda_2 - a_{22}) \\ -a_{21} & \lambda_1 - a_{22} \end{bmatrix} , \tag{4.58}$$

where

$$\Delta P = a_{12}(\lambda_2 - \lambda_1) = a_{21}(\lambda_1 - \lambda_2) \ . \tag{4.59}$$

For convenience, the first of these is chosen for use in the following development.

Applying equation (4.58) to equation (4.28), one finds that the Floquet normal solutions in terms of the numerical solutions are

$$v_1(x) = \frac{(\lambda_2 - a_{11})u_1(x) - a_{12}u_2(x)}{a_{12}(\lambda_2 - \lambda_1)} \tag{4.60}$$

$$v_2(x) = \frac{-(\lambda_1 - a_{11})u_1(x) + a_{12}u_2(x)}{a_{12}(\lambda_2 - \lambda_1)} \, . \tag{4.61}$$

Equation (4.51) can be solved for ϕ_i. It is found to be

$$\phi_i(x) = e^{-\gamma_i x} v_i(x) \, , \tag{4.62}$$

and its first derivative is

$$\frac{d\phi_i}{dx} = e^{-\gamma_i x}\left[\frac{dv_i}{dx} - \gamma_i v_i(x)\right] \, . \tag{4.63}$$

The normal Floquet solutions and their derivatives in terms of the numerical solutions from equations (4.60) and (4.61) can then be substituted into equations (4.62) and (4.63). Both ϕ_i and $\frac{d\phi_i}{dx}$ are periodic functions in x and we only need u_i numerical solutions over the first period to be continued indefinitely.

In summary, two linearly independent solutions to equation (4.7) can be found numerically, by starting with initial conditions for a fundamental set and integrating over one period of oscillation. The value of these solutions when x = T = 1 can be used to find the characteristic parameters of the solutions, namely: the stability parameter,α , the eigenvalues, λ_i, and the characteristic exponents, γ_i. These solutions can then be used to determine a periodic function which, along with the characteristic exponent, can be used to express an approximate normal Floquet form of the solutions which can be continued over many periods. It now remains to find the particular solution to the equation, to combine it with complementary function and to evaluate the constants of integration, A and B, in the complementary function in terms of the initial conditions.

4.3 The Particular Solution

To find the particular solution to the nonhomogeneous form of the first-order equation, one can use variation of parameters [12]. Ordinarily it is impossible to find a particular integral of a nonhomogeneous linear differential equation by inspection. But since a form of the homogeneous solution can be found by the Floquet theory, the general variation of parameters method enables one to replace the constants of integration in the complementary function with the functions a(x) and b(x). This is done by assuming a particular solution to the first-order equation of the form

$$u_p(x) = a(x)\,u_1(x) + b(x)\,u_2(x) \ , \tag{4.64}$$

where again $u_1(x)$ and $u_2(x)$ are the two fundamental solutions to the homogeneous solution, and a(x) and b(x) are functions of x that satisfy the additional condition

$$\frac{da}{dx}u_1 + \frac{db}{dx}u_2 = 0 \ . \tag{4.65}$$

Differentiating equation (4.64) with respect to x two times and applying the condition in equation (4.65) one gets

$$\frac{du_p}{dx} = a\frac{du_1}{dx} + b\frac{du_2}{dx} \tag{4.66}$$

and

$$\frac{d^2u_p}{dx^2} = a\frac{d^2u_1}{dx^2} + \frac{da}{dx}\frac{du_1}{dx} + b\frac{d^2u_2}{dx^2} + \frac{db}{dx}\frac{du_2}{dx} \ . \tag{4.67}$$

The particular solution must satisfy the original forced first-order equation. Substituting these results into equation (4.4) one has

$$a\left[\frac{d^2u_1}{dx^2} + p_1(x)\frac{du_1}{dx} + p_2(x)u_1\right] + b\left[\frac{d^2u_2}{dx^2} + p_1(x)\frac{du_2}{dx} + p_2(x)u_2\right]$$

$$+ \frac{da}{dx}\frac{du_1}{dx} + \frac{db}{dx}\frac{du_2}{dx} = \frac{\lambda^2}{u_0}F(\varepsilon,x) \ . \tag{4.68}$$

But both u_1 and u_2 are solutions of the homogeneous equation, so that the first two terms in equation (4.68) are zero according to equation (4.7). Therefore equation (4.68) is reduced to

$$\frac{da}{dx}\frac{du_1}{dx} + \frac{db}{dx}\frac{du_2}{dx} = \frac{\lambda^2}{u_0}F(\varepsilon,x) \quad . \tag{4.69}$$

Equations (4.65) and (4.69) yield two equations for the two unknowns, da/dx and db/dx. They can be written as

$$\begin{bmatrix} u_1 & u_2 \\ \dot{u}_1 & \dot{u}_2 \end{bmatrix}\begin{bmatrix} \dot{a} \\ \dot{b} \end{bmatrix} = \begin{bmatrix} 0 \\ \frac{\lambda^2}{u_0}F(\varepsilon,x) \end{bmatrix} . \tag{4.70}$$

The determinant of this system is

$$\Delta = u_1\dot{u}_2 - \dot{u}_1 u_2 \quad . \tag{4.71}$$

This is the Wronskian of the homogeneous equation from (4.39) and is equal to unity. Equation (4.70) yields two equations. Integrating them, one finds a(x) and b(x) to be

$$a(x) = -\lambda^2 \int_0^x \frac{u_2(\xi)}{u_0(\xi)} F(\varepsilon,\xi)\, d\xi$$

and

$$b(x) = \lambda^2 \int_0^x \frac{u_1(\xi)}{u_0(\xi)} F(\varepsilon,\xi)\, d\xi \quad , \tag{4.72}$$

where a(0) = b(0) = 0. Substituting these into equation (4.64) one gets the particular solution of

$$u_p(x) = \lambda^2\left[-u_1(x) \int_0^x \frac{u_2(\xi)}{u_0(\xi)} F(\varepsilon,\xi)\, d\xi + u_2(x) \int_0^x \frac{u_1(x)}{u_0(\xi)} F(\varepsilon,\xi)\, d\xi \right] . \tag{4.73}$$

When x = 0, both integrals in (4.73) vanish leaving

$$u_p(0) = 0 \ . \tag{4.74}$$

Differentiating equation (4.73) to obtain the particular growth rate, we find

$$\frac{du_p}{dx} = \lambda^2 \left[-\dot{u}_1(x) \int_0^x \frac{u_2(\xi)}{u_0(\xi)} F(\varepsilon,\xi)\, d\xi \ + \ \dot{u}_2(x) \int_0^x \frac{u_1(\xi)}{u_0(\xi)} F(\varepsilon,\xi)\, d\xi \right] . \tag{4.75}$$

Both of these integrals also vanish when x = 0, thus

$$\left.\frac{du_p}{dx}\right|_{x=0} = 0 \ . \tag{4.76}$$

Equations (4.73) and (4.75) represent the particular integral and its derivative for the normalized first-order equation. They can be combined with the complementaty function to obtain a complete integral of the differential equation and then the initial conditions can be used to solve for the constants of integration, A and B.

To be able to continue the particular solution numerically over many cycles we avail ourselves of the above normal or Floquet solution. Using it we can transform the particular solution into normal or Floquet form. To do this, we substitute u_1 , u_2 and their derivatives into the particular solution. The matrix [P] from equation (4.57) is used to get them in terms of the Floquet variables v_1 and v_2,. According to the relationship in equation (4.28),

$$u_1(x) = a_{12}[v_1(x) + v_2(x)] \tag{4.77}$$

$$u_2(x) = (\lambda_1 - a_{11})\, v_1(x) + (\lambda_2 - a_{11})\, v_2(x) \ . \tag{4.78}$$

Substituting these expressions back into equations (4.73) and (4.75), we find

$$u_p(x) = \lambda^2 a_{12}(\lambda_1 - \lambda_2)\left[v_1(x) \int_0^x \frac{v_2(\xi)}{u_0(\xi)} F(\varepsilon,\xi)\, d\xi - v_2(x) \int_0^x \frac{v_1(\xi)}{u_0(\xi)} F(\varepsilon,\xi)\, d\xi \right], \quad (4.79)$$

and its derivative

$$\frac{du_p}{dx} = \lambda^2 a_{12}(\lambda_1 - \lambda_2)\left[\dot{v}_1(x) \int_0^x \frac{v_2(\xi)}{u_0(\xi)} F(\varepsilon,\xi)\, d\xi - \dot{v}_2(x) \int_0^x \frac{v_1(\xi)}{u_0(\xi)} F(\varepsilon,\xi)\, d\xi \right]. \quad (4.80)$$

Equations (4.60) and (4.61) give v_1 and v_2 in terms of u_1 and u_2. Since the integrals in equations (4.79) and (4.80) both vanish when $x = 0$, initially one has

$$\left.\begin{aligned} u_p(0) &= 0 \\ \left.\frac{du_p}{dx}\right|_{x=0} &= 0 \end{aligned}\right\}. \quad (4.81)$$

Equations (4.79) through (4.81) represent the normal or Floquet form of the first-order particular solution, its particular growth rate, and the particular initial conditions. These can be combined with the Floquet form of the homogeneous solutions to write a complete integral for the first-order equation in normal Floquet form. At the upper limit of the integrals in equation (4.79) when $\xi = x$, the two exponential terms contained in the two Floquet variables when they are multiplied together become unity since γ_1 and γ_2 have the same magnitude but opposite signs for the case $\alpha > 1$. If the corresponding $\phi_i(x)$, $u_0(x)$ and $F(x,\varepsilon)$ are bounded in [0, x], then as $x \to \infty$, the first integral in (4.79) also approaches ∞ since $\gamma_1 > 0$ and the exponential part of v_1 dominates the solution. In the same regard, the second integral approaches a constant because $\gamma_2 < 0$ and the exponential part of v_2 vanishes. This means that for values of $\alpha > 1$, as is the case for this analysis, the first integral in equation (4.79) is unstable while the second integral is stable as $x \to \infty$. Exactly how unstable the first integral will become depends upon the magnitudes of the parameters such as γ_1.

4.4 First-Order Equation Solution

With the homogeneous solution and particular integral for the first-order equation found in both numerical and normal Floquet form, they can be combined to form the complete solution. One does this by multiplying the two linearly independent fundamental functions by arbitrary constants and adding these to the particular solution. Thus, the complete solution to the normalized first-order equation in (4.4) has the form,

$$u(x) = A\,u_1(x) + B\,u_2(x) + \lambda^2\left[-u_1(x) \int_0^x \frac{u_2(\xi)}{u_0(\xi)} F(\varepsilon,\xi)\, d\xi + u_2(x) \int_0^x \frac{u_1(\xi)}{u_0(\xi)} F(\varepsilon,\xi)\, d\xi \right], \qquad (4.82)$$

where A and B are the arbitrary constants that must be evaluated from the initial conditions. It is noted that although the variables to the left of the equality u_1 and u_2, they form the fundamental solution set for the first-order equation, they should not be confused with the notation in section 2.4 above for the two scale equations of the original Rayleigh-Plesset equation.

The initial conditions for the first-order equation were derived from the flaccid bubble analysis as in equation (2.45) giving the initial growth velocity. From equations (4.5) and (4.6) above we have

$$\left.\begin{aligned} u_1(0) &= 0 \\ \left.\frac{du_1}{dx}\right|_{x=0} &= \frac{1}{8} W_r (1+q)^{5/4} \sqrt{(1+K)} \left(-\frac{dC_p}{ds} \right)_{C_p=-K} \equiv C \end{aligned}\right\}. \qquad (4.83)$$

It was shown in the particular-solution analysis that both the particular solution and its derivative are equal to zero when x = 0. Applying this fact and equation (4.83) to equation (4.82) and its first derivative, one finds the equations,

$$A\,u_1(0) + B\,u_2(0) = 0, \qquad (4.84)$$

$$A\,\dot{u}_1(0) + B\,\dot{u}_2(0) = C. \qquad (4.85)$$

From the initial conditions of fundamental set of equations (4.22), we find that these two equations yield

$$A = 0, \tag{4.86}$$

$$B = C\ . \tag{4.87}$$

Substituting (4.86) and (4.87) into equation (4.82), one finds that the complete first-order solution looks like

$$u(x) = Cu_2(x) - \lambda^2\left[u_1(x) \int_0^x \frac{u_2(\xi)}{u_0(\xi)} F(\varepsilon,\xi)\, d\xi - u_2(x) \int_0^x \frac{u_1(\xi)}{u_0(\xi)} F(\varepsilon,\xi)\, d\xi \right], \tag{4.88}$$

where C is given by equation (4.83). Differentiating equation (4.88), one also finds that the complete first-order growth rate is

$$\frac{du}{dx} = C\dot{u}_2(x) - \lambda^2\left[\dot{u}_1(x) \int_0^x \frac{u_2(\xi)}{u_0(\xi)} F(\varepsilon,\xi)\, d\xi - \dot{u}_2(x) \int_0^x \frac{u_1(\xi)}{u_0(\xi)} F(\varepsilon,\xi)\, d\xi \right]. \tag{4.89}$$

To express the complete solution and its derivative in normal Floquet form, the u_i's must be expressed in terms of the Floquet variables. The substitution of equations (4.77) and (4.78) into (4.88) and (4.89) yields

$$u(x) = C\left[(\lambda_1 - a_{11})v_1(x) + (\lambda_2 - a_{11})v_2(x)\right]$$

$$+ \lambda^2 a_{12}(\lambda_1 - \lambda 2)\left[v_1(x) \int_0^x \frac{v_2(\xi)}{u_0(\xi)} F(\varepsilon,\xi)\, d\xi - v_2(x) \int_0^x \frac{v_1(\xi)}{u_0(\xi)} F(\varepsilon,\xi)\, d\xi \right], \tag{4.90}$$

and its derivative is

$$\frac{du}{dx} = C\left[(\lambda_1 - a_{11})\dot{v}_1(x) + (\lambda_2 - a_{11})\dot{v}_2(x)\right]$$

$$+ \lambda^2 a_{12}(\lambda_1 - \lambda_2)\left[\dot{v}_1(x)\int_0^x \frac{v_2(\xi)}{u_0(\xi)} F(\varepsilon,\xi)\, d\xi - \dot{v}_2(x)\int_0^x \frac{v_1(\xi)}{u_0(\xi)} F(\varepsilon,\xi)\, d\xi\right], \qquad (4.91)$$

where $v_1(x) = e^{\gamma_1 x}\,\phi_1(x)$ and $v_2(x) = e^{\gamma_2 x}\, f_2(x)$ as noted previously in equation (4.51). These are the complete first-order solution and its derivative in terms of the normal Floquet variables, v_i.

To study the complete first-order solution it is best to use the normal or Floquet form which can be continued from the first period for many periods in x. A computer code was developed which uses the zero-order solution and the forcing function in terms of the normalized bubble time x, along with values of u_v as input.

The first step needed is the numerical calculation of the homogeneous solutions, $u_1(x)$ and $u_2(x)$, for one period as $0 \le x \le 1$. As stated earlier, this was done by first finding z_1 and z_2 and converting them to u_i. It was noted that equation (4.11) becomes stiff as portions of p(x) become large with increasing values of u_v. For cases of large u_v, standard numerical techniques such as a Runge-Kutta method prove to be insufficient. But according to Gear [10], the fourth-order explicit Runge-Kutta method produces convergent and stable solutions for real values of the quantity h·p(x) between 0 and approximately 2.7. Here h is the step size in x and p(x) comes from equation (4.11). From equation (4.12) one sees that

$$p(0) = 2\lambda^2 \ge p(x)\ , \qquad (4.92)$$

so that

$$h{\cdot}p(x) \le 2h\lambda^2 < 2.7\ . \qquad (4.93)$$

If 200 steps are taken over the range $0 \leq x \leq 1$, equation (4.93) yields conservative values of $\lambda < 16.4$ which corresponds to a largest value of $u_v \approx 2.14$. If 100 steps are taken a value of $\lambda < 11.6$ is obtained, corresponding to a value of $u_v \approx 1.77$. Using a variable step size fourth-order Runge-Kutta method, one sees that the number of steps taken over the period of x for the entire range of u_v fell between 100 and 200. This then tells us that the numerical solutions obtained from this method are stable for values of u_v at least up to 1.77.

By looking at the curves of p(x) in figure 4.1 for higher values of u_v, for a number of steps between 100 and 200, we see that the value of p(x) only violates the inequality in equation (4.93) over very narrow strips near the values of $x = 0$ and $x = 1$. These regions of stiffness produce unstable solutions over very small intervals compared to the rest of the range of x where stable solutions are found. It was felt therefore, that the errors accumulated using this variable step size Runge-Kutta method might be acceptable. This is indeed the case, which will be verified later when the Wronskian of the system is calculated for a range of u_v values. Thus, we are quite fortunate in the fact that even though there exist regions of numerical instability over the range of x for the solutions to equation (4.11), these regions are small and a reliable proven numerical technique can be used to find the solutions with acceptable error.

The use of the WKB method was explored for this problem because the value of the parameter λ becomes large as u_v increases. It was found that although the equation is certainly stiff in such cases, many terms beyond the order of $1/\lambda^2$ must be obtained if one is to get a sufficiently accurate asymptotic expansion.

The variable step size fourth-order Runge-Kutta method was applied once for each solution, z_1 and z_2, and these were then converted back to u_i's using equation (4.10). These solutions and their derivatives, for one value of u_v, are shown in figures 4.3. Later on in the analysis the values of such solutions, along with $u_0(x)$, will need to be given in even increments of x for numerical integration purposes. To obtain evenly

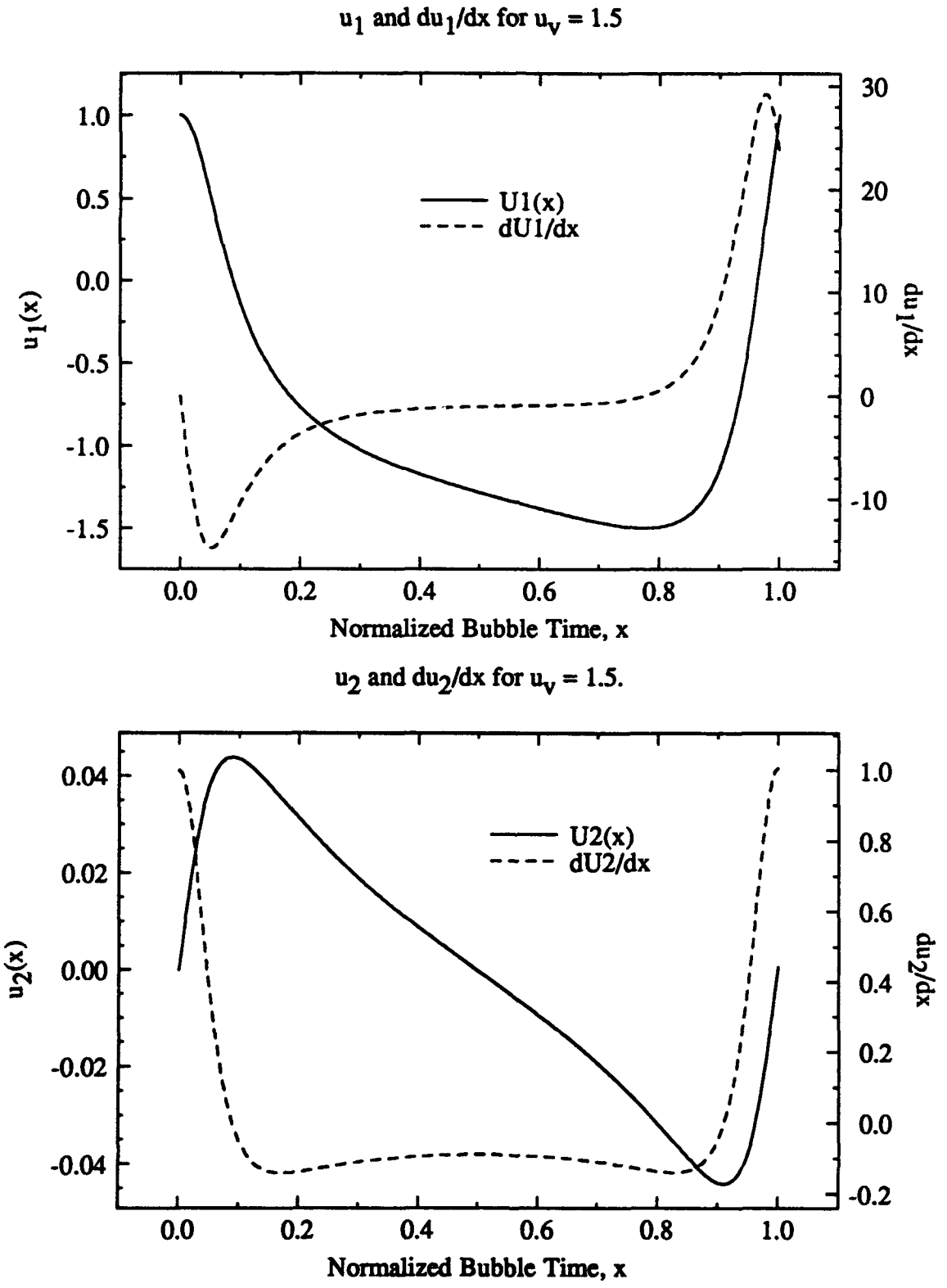

Figure 4.3 A Fundamental Set of Solutions of the Homogeneous First-Order Equation.

spaced values, a cubic interpolation scheme was used, which picked a target value of x and used the surrounding four known values of the solution to interpolate the corresponding value. The use of an interpolation scheme is also apt to add error to the solution. But since the solutions are well behaved and a third-order method [15] was used, these errors were felt to be insignificant. This same method was applied to get evenly spaced values of u_0 as input to the calculation of the first order solution.

The values of the fundamental solutions and their derivatives at x = 1 are next used to determine the constants in the matrix [A] from equation (4.26). From these values the Wronskian of the system can be determined using equation (4.35). This Wronskian is used to assess the accuracy of the numerical calculations of the fundamental solutions. As was shown for Hill's equation, the Wronskian should have a constant value of unity. By monitoring the value of the Wronskian for given values of u_v, the confidence that the solution is sufficiently accurate is measured. Figure 4.4 shows the scatter in values of the error (Δ - 1) over the range of u_v. It is seen that although the variations from $\Delta = 1$ increase with u_v, the difference is less than 10^{-5}, which is acceptable for this analysis. Closer inspection of this figure shows that great accuracy is obtained for values of u_v up to around 2, which verifies the numerical stability of the u_i solutions talked about earlier using the work of Gear [10]. As the value of u_v gets larger, the stiff regions of the equation produce some error in the solutions, but not enough to discredit the present use of the variable step size Runge-Kutta method.

The stability parameter, α, can also be determined from the values of matrix [A] using equation (4.34). The value of this parameter leads to dynamic stability assesment of the fundamental set of solutions used in the complete first-order solution. The fundamental set of solutions begins at a neutral stability point when $u_v = 1$, corresponding to a value of $\alpha = 1$, as shown in figure 4.5. This figure also shows that, exept for the special value of $u_v = 1$, α is greater than unity over the whole range of u_v values. Thus, for $1 > u_v > 1$, $\alpha > 1$ and the fundamental set of solutions has one bounded and one unbounded solution

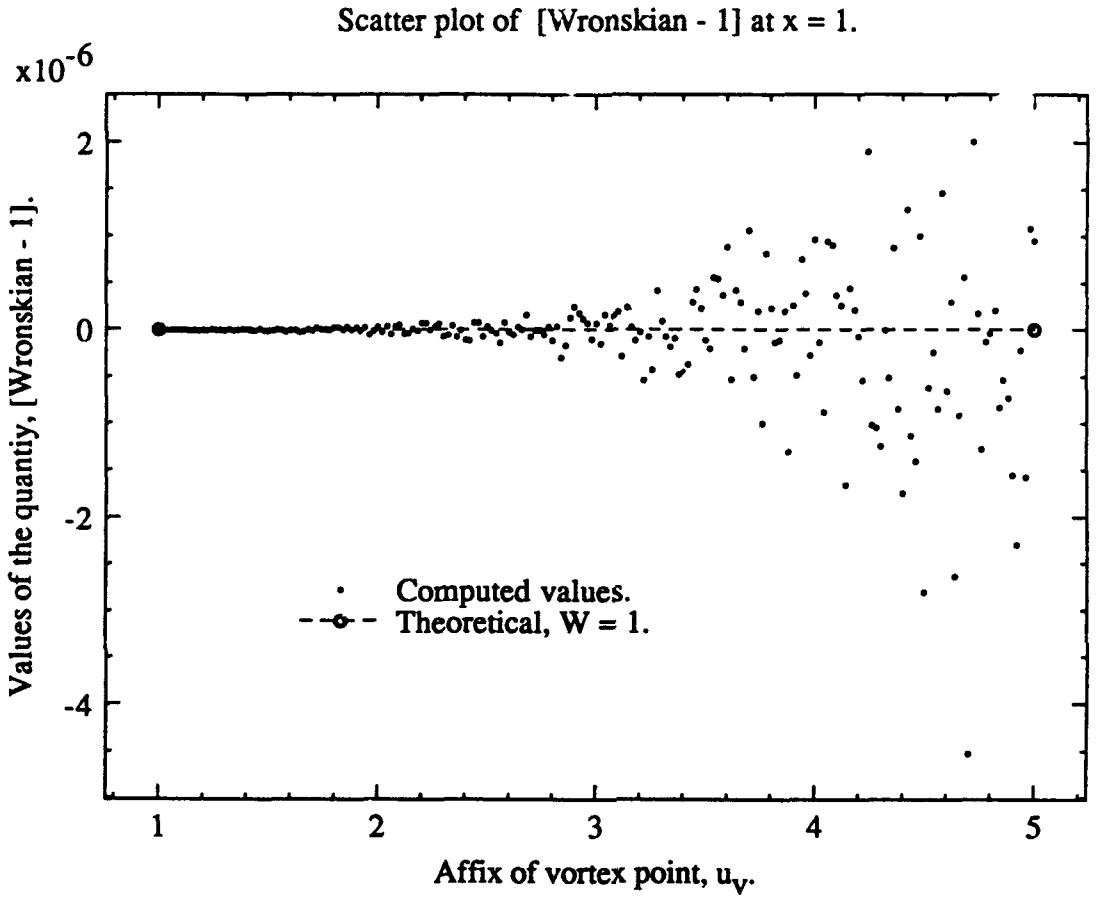

Figure 4.4 Scatter Plot Indicating the Numerical Errors in Calculations of the First-Order Solution.

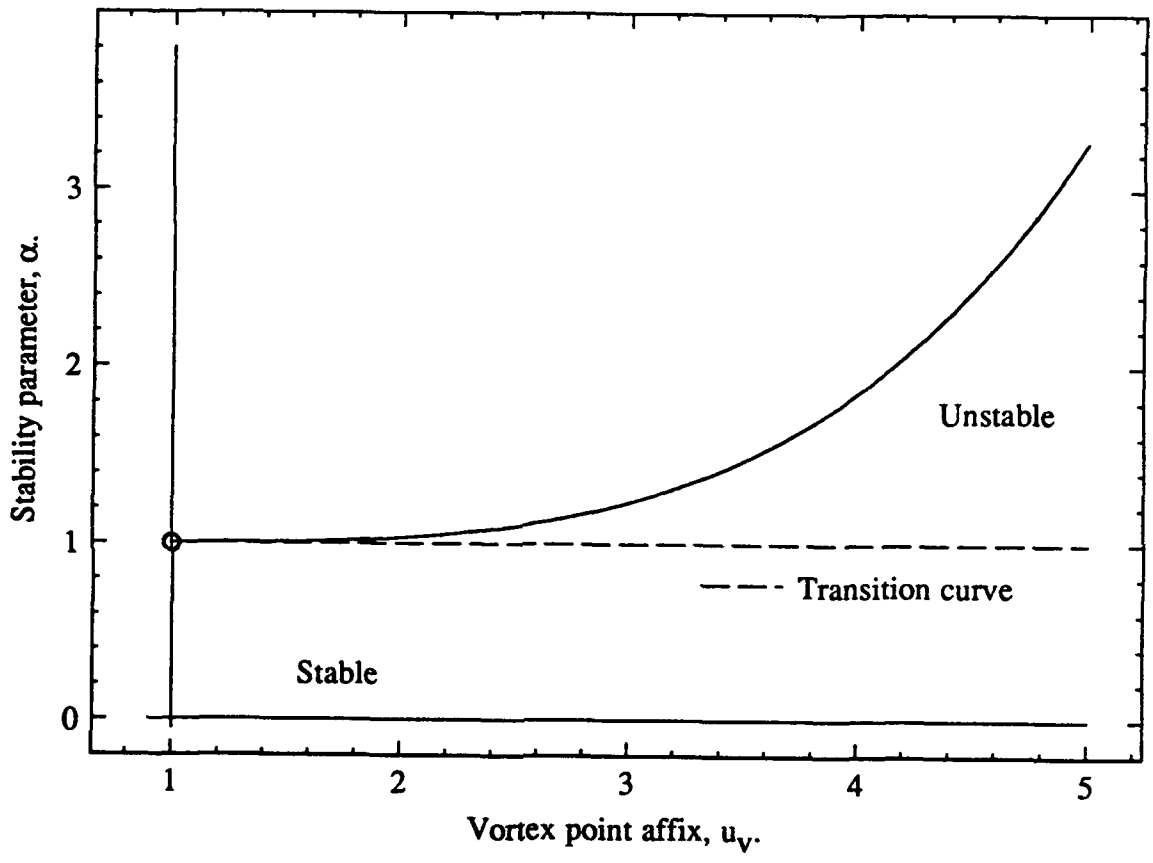

Figure 4.5 Stability of the First-Order Fundamental Set of Solutions for a Range of u_v.

as time increases, and excupt for, $u_v = 1$, no values of u_v do both of the the solutions become stable. For the case of $u_v = 1$, $\alpha = 1$ and $\lambda_1 = \lambda_2 = 1$, the fundamental set reduces to neutrally stable trigonometric solutions ofunit period and becomes unstable again with further decreases in u_v.

The next step is to determine the Floquet variables, $v_i(x)$ and $\dot{v}_i(x)$. For computational purposes, it is desired have them in the form of equation (4.51) which involves a well defined exponential function multiplied by a periodic function. From the α value, λ_1 and λ_2 can be determined from equation (4.41). From these, γ_1 and γ_2 can be determined from equation (4.41) with a unit period of T = 1. The known characteristic exponents take care of the exponential part of the Floquet variables.

Values of v_i for one period in x can be found using the fundamental set of solutions and equations (4.60) and (4.61). In the same fashion, $\dot{v}_i$ can be found. Then using equation (4.62) and its derivative with respect to x, the periodic ϕ_i and $\dot{\phi}_i$ can be determined. Figure 4.6 shows a plot of ϕ_i and $\dot{\phi}_i$ for several values of u_v. This then takes care of the periodic part of the Floquet variables. There now exists a form of $v_i(x)$ and $\dot{v}_i(x)$ that can be continued over many periods in x.

It remains now to determine the integrals involving the forcing function from the particular solution. This is simply done using Simpson's rule for evenly spaced values of $u_0(x)$, $v_i(x)$, and $F(\varepsilon,x)$. The same process is applied to the integrals in the first derivative equation. All these components are then combined as in equations (4.90) and (4.91). The constant C can be determined using the forcing function and equation (4.83).

The above steps are combined into a computer program contained in appendix A. Some of the input needed for the code is the pressure coefficient data for a circular cylinder and a cavitation number. For this example, a value of K = 2.3 was used along with a typical value of the free stream velocity of 40 fps. The initial nucleus radius size was taken to be 7 microns and a characteristic length for the circular cylinder was D = 2 in. Values of

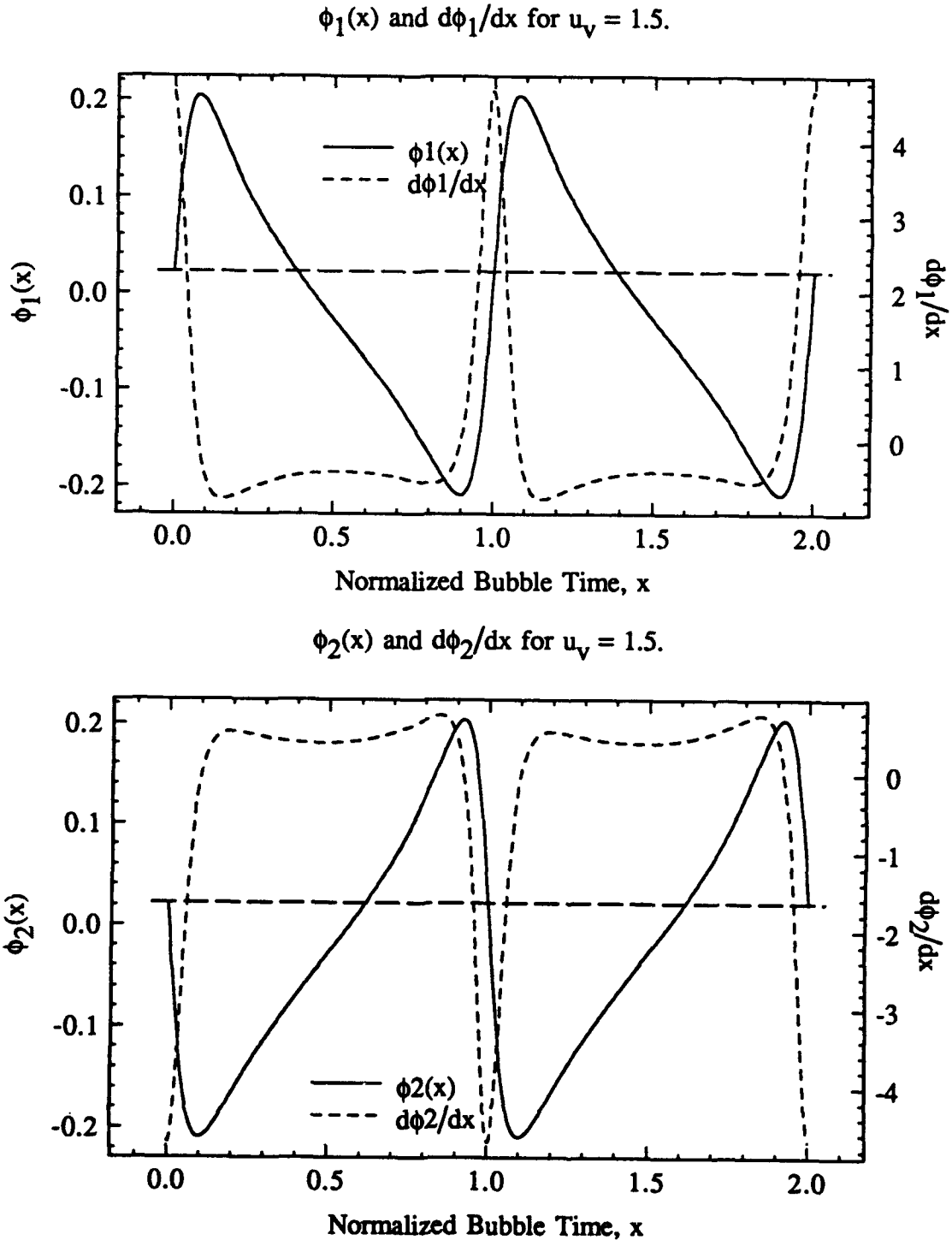

Figure 4.6 Periodic Parts of the Fundamental Set of Floquet Solutions Over Two Periods for $u_v = 1.5$.

the surface tension and density of water at 70 degrees were used and a dissolved air saturation pressure of 10 psia was also used. The computed value of u_v for these input parameters is $u_v = 0.5994$ and ε is 1.6×10^{-6}. But figures 4.7 and 4.8 show the complete first-order solution and its derivative over many periods in x for a value of $u_v = 1.5994$.

The reason for this change is that the calculated value of u_v from these input data fell below the critical value of unity for this investigation. The calculated value of u_v corresponds to small scale compressive air bubble oscillations which characterize the zero-order phase plane trajectories to the left of the $u_0(\tau) = 1$ point shown in figure 3.1. As was stated in chapter 3, the present numerical analysis deals only with vaporous growth trajectories to the right of this point. The extension of the code to smaller values of u_v could have been made, but it was not carried out; because the dynamic stability analyses for values of u_v to the left as well as to the right of the critical point show that, aside from the case of neutral stability at $u_v = 1$, all first order solutions are unstable as shown in figures 4.2 and 4.5. We concluded therefore that calculations carried out for $u_v = 1.5994$ can give a useful illustration of the consequences of the first-order instability.

It is seen from figure 4.7 that the total u_1 solution grows exponentially with x. For this case the value of α is greater than 1, thus producing exponential terms with positive exponents that will become unbounded as x increases. Figure 4.8 shows the derivative of this complete integral. Figures 4.9 and 4.10 show the homogeneous and particular parts of the first-order solution. From them we see that the large magnitude of the total u_1 solution comes from the homogeneous part. This is due the constant C multiplying the complementary function. C is of the order 10^3 for the given input values. Because this constant term is relatively large, it dominates the smaller oscillations from the particular part of the solution. The particular part of the solution grows at a slower rate than the homogeneous part due to the fact that the amplitude of the forcing function contained in the particular integrals grows rather slowly in terms of bubble time so that the modulated first order

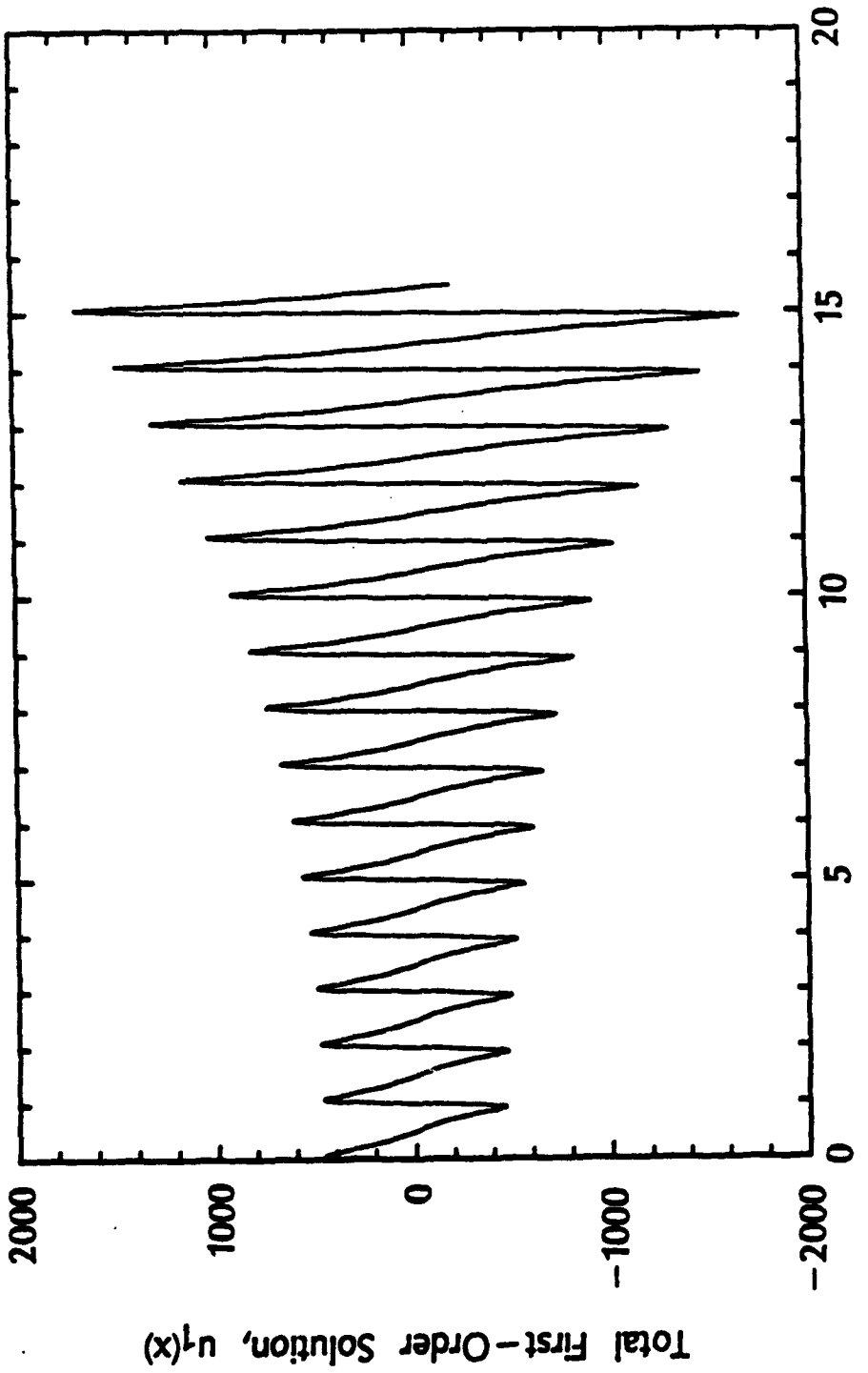

Figure 4.7 Complete First-Order Solution as a Function of Normalized Bubble Time Over Many Periods in x.

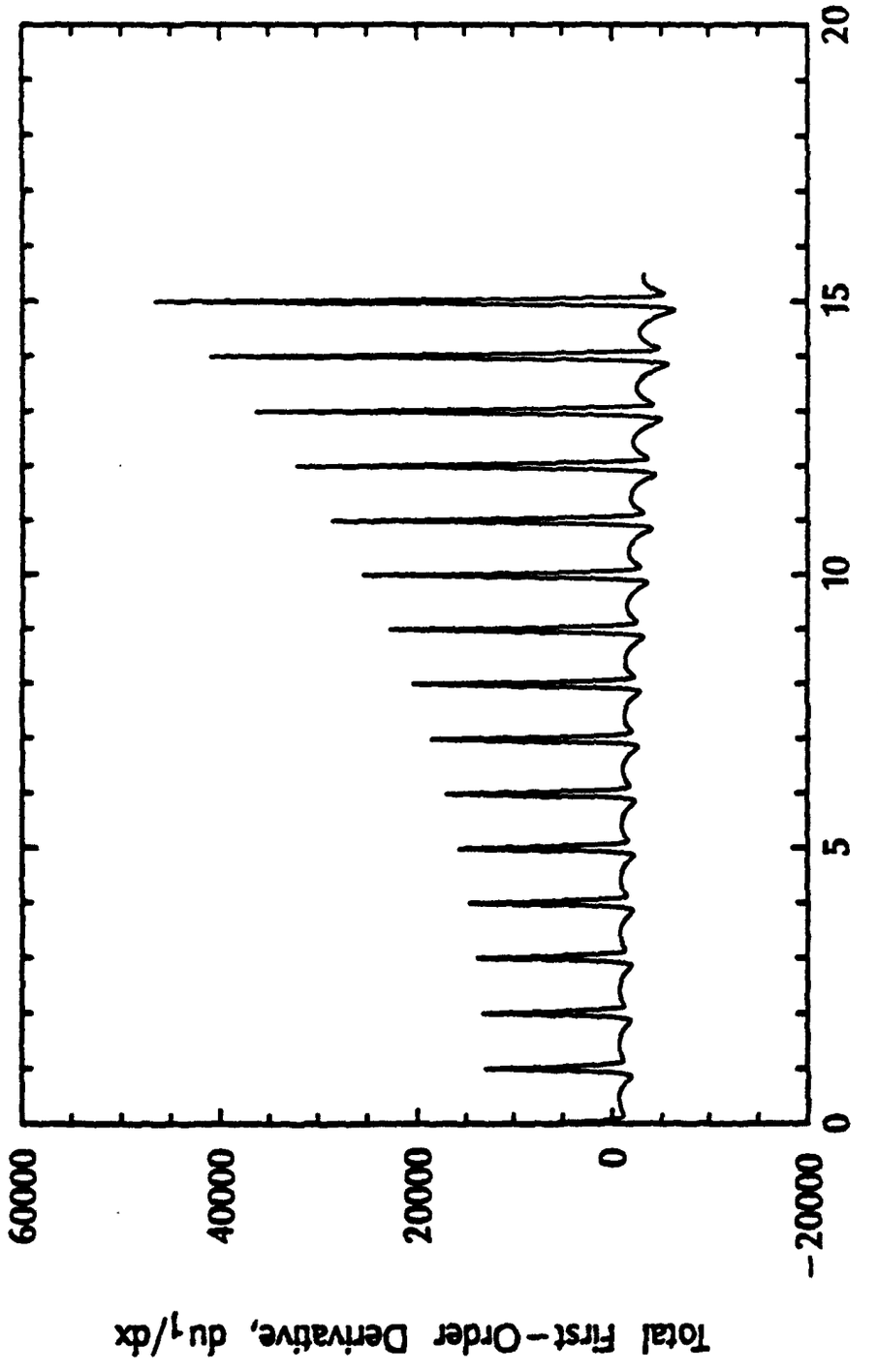

Figure 4.8 Derivative of the Complete First-Order Solution as a Function of Normalized Time Over Many Periods in x.

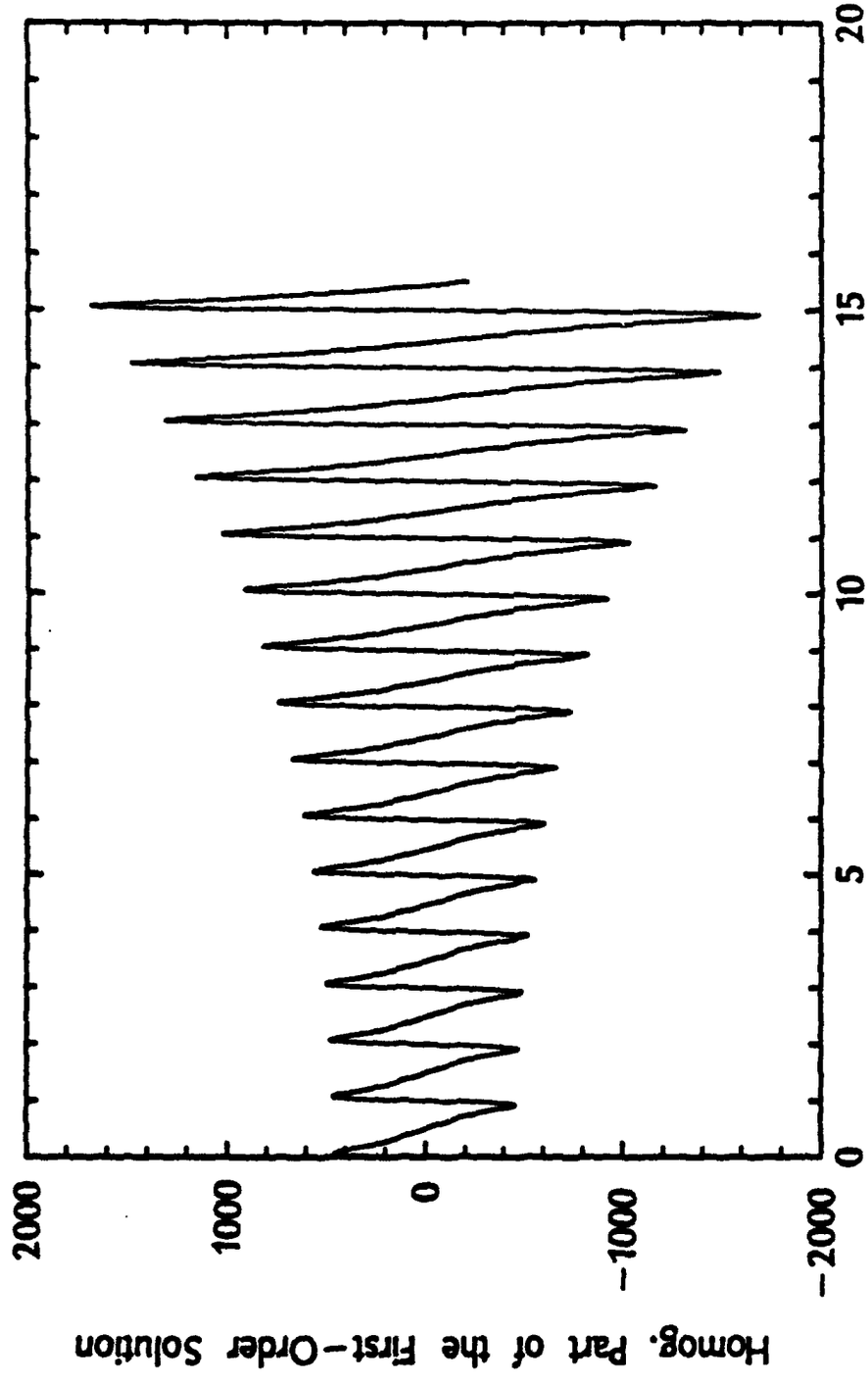

Figure 4.9 Homogeneous Part of the First Order Solution as a Function of Normalized Bubble Time

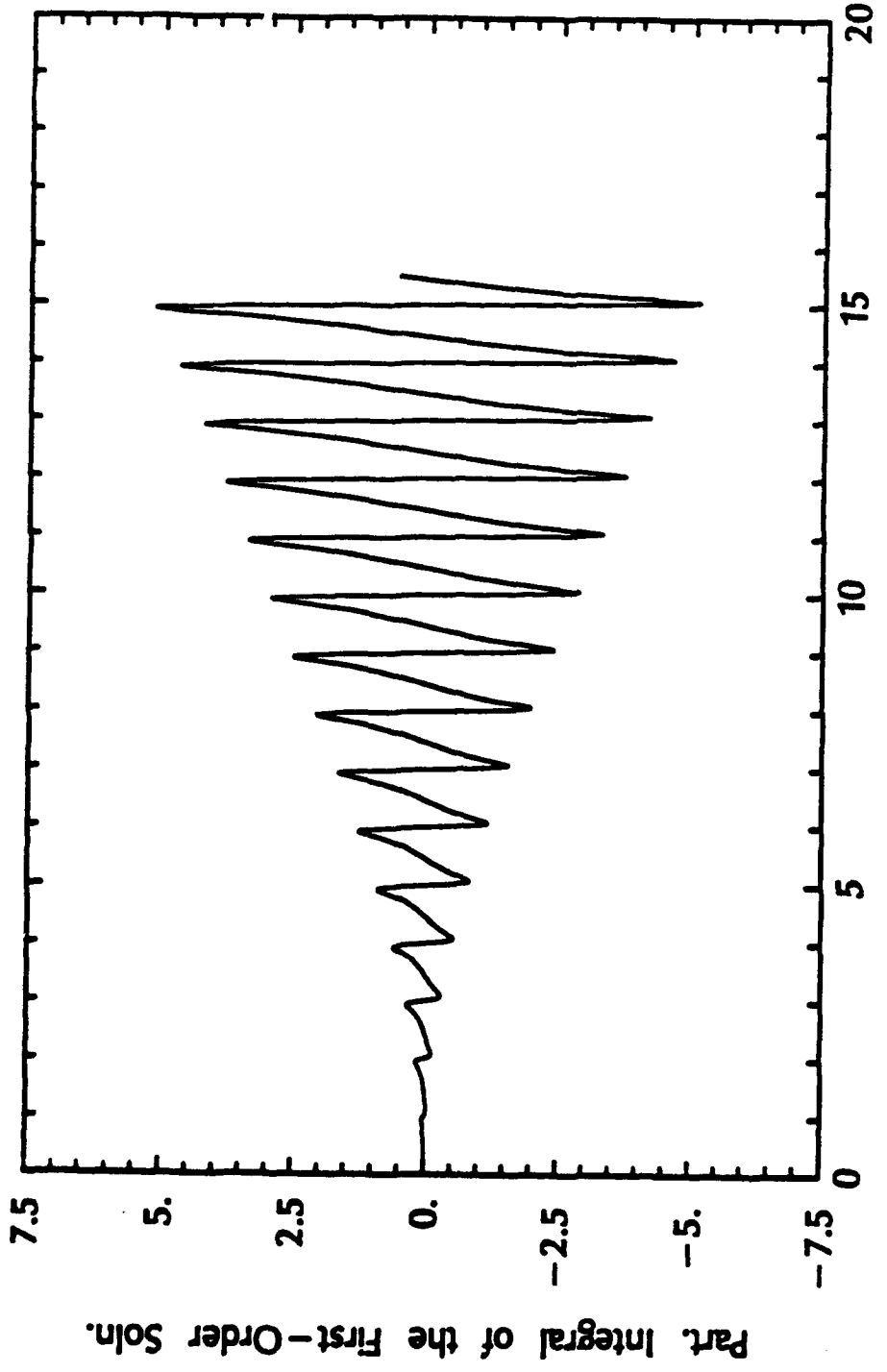

Figure 4.10 Particular Part of the First-Order Solution as a Function of Normalized Bubble Time

oscillations show a less rapid growth than does the complementary solution. But because ofthe presence of the complementary function in the particular solution, it is also basically unstable. It must be remembered also that since ε is of the order of 10^{-6}, the entire first order solution will be of the order of 10^{-3} compared to the zero-order solution. But it appears from their forms that the present zero and first order solutions can not lead to any useful inception criteria. It is necessary, therefore, that the suggestion developed at the end of section 3.53 above be seriously considered in a separate investigation. This is particularly important because it appears that the zero-order solution will frequently dominate the first order solution, at least in the initial phases of the forced bubble motions as examined here. Therefore, a more general reexamination of the zero-order solution centered around the integrability conditions is warranted.

The preceding results do not restrict the value of u_v and for that reason it has not been possible to give a closed form perturbation solution. On the other hand when $u_v = 1$ the solution is neutrally stable and there is a possibility that the forcing function can have more influence on the bubble growth than was found in the preceeding example. Therefore it is of interest to obtain a solution for this special case even though the condition $u_v = 1$ is too severe a restriction to make the result of practical value.

4.4.1 The Solution when $u_v = 1$

In Section 3.4.1 we found in the limit as $u_v \rightarrow 1$, that the zero-order oscillation parameter is $\lambda = \pi\sqrt{2}$ and according to Equation (2.20) the period is $T = (1+q)^{3/4}\lambda$. Therefore when $u_v = 1$, $1+q = \gamma$ and $T = \pi\gamma^{3/4}\sqrt{2}$. Moreover, the zero-order autonomous differential equation (3.1) and its initial conditions, (3.2) and (3.3), insure that at $u_v = 1$ the zero-order solution is simply $u_0(\tau) = 1$ for all values of the bubble time τ, as discussed in connection with Equation (3.14). Therefore we are free to consider the first order differential equation (4.4), for $u_1(\tau)$, and its initial conditions, equations (4.5) and (4.6). The fact that u_0 = constant in this case causes the derivatives of u_0 to vanish in

equation (4.4) and the limiting value of λ together with the unit value of u_0 permits one to simplify equation (4.4) to read

$$\frac{d^2u_1}{dx^2} + 4\pi^2 u_1 = 2\pi^2 F(t_s). \tag{4.92}$$

In equation (4.92) the forcing function argument has been transformed from real time, t, to dimensionless laboratory time $t_s = tD/V_0$, so that now

$$F(t_s) = \frac{1}{4} W_r [- C_p(t_s) - K] = \frac{1}{4} W_r F_1(t_s)$$

and in accordance with the discussion of Appendix B, the term $F_1(t_s)$ represents a closed form approximation to the numerical data used above. In shifted laboratory time F_1 is given by equation (B.3). Moreover, the normalized bubble time, x, is now a reduced form of equation (3.17) which becomes

$$x = \frac{\tau}{\pi \gamma^{3/4} \sqrt{2}} . \tag{4.93}$$

Since $t_s = \varepsilon\tau$, it follows that the laboratory time and the normalized bubble time are related by

$$t_s = \varepsilon x \pi \gamma^{3/4} \sqrt{2} . \tag{4.94}$$

Consequently when x is the independent variable the initial condition of equation (4.83) above becomes

$$\dot{u}_1(0) = C = \frac{1}{8} W_r \gamma^{5/4} \sqrt{1+K} \left[-\frac{dCp}{ds} \right]_{C_p = -K} , \tag{4.95}$$

while we have the condition $u_1(0) = 0$ as before.

The solution of Equation (4.92), subject to the prescribed initial conditions is well known:

$$u_1 = \frac{C}{2\pi} \sin 2\pi x + \frac{\pi}{4} W_r \int_0^x F_1(\varepsilon; \xi) \sin 2\pi(x-\xi)\, d\xi , \quad \text{for } x \le x_s, \tag{4.96a}$$

and if $x > x_s$,

$$u_1 = \frac{C}{2\pi}\sin 2\pi x + \frac{\pi}{4} W_r \left\{ \int_0^{x_s} F_1(\varepsilon;\xi)\sin 2\pi(x-\xi)\,d\xi \right.$$

$$\left. + (2.225 - K)\int_{x_s}^{x} \sin 2\pi(x-\xi)\,d\xi \right\}. \qquad (4.96b)$$

If we let $b = \pi\gamma^{3/4}\sqrt{2}$ we can write the approximate formula for $F_1(\varepsilon; x)$ for $t_s \le \hat{t}_s$ or for $x \le x_s$, as

$$F_1(\varepsilon; x) = a_1 - K + a_2 t_0(K) + a_2 \varepsilon b x + a_3 \sin[a_4 \varepsilon b x + a_4 t_0(K) + a_5]\,; \qquad (4.97)$$

and in the laminar separation zone when $x > x_s = (0.365 - t_0)/(\varepsilon b)$,

$$F_1(\varepsilon; x) = 2.225 - K, \qquad (4.98)$$

as already indicated in equation (4.96*b*). The quantity $t_0(K)$ is the origin of the forcing function and is given analytically in figure B4. The quantities $\hat{t}_s$ and x_s denote the separation point in shifted coordinates, $\hat{t} = t_s - t_0$.

Because of the form of equation (4.97), the integral in equation (4.96*a*) can be expressed as the sum, $I_1 + I_2 + I_3$, for $\hat{t} \le \hat{t}_s$ or $x \le x_s$. If x is greater than x_s there also will be a fourth integral, I_4, given by the second integral of (4.96*b*). Considering these integrals in order, one finds that

$$I_1 = \frac{a_1 - K + a_2 t_0(K)}{2\pi}(1 - \cos 2\pi x), \text{ if } x \le x_s \text{ or}$$

$$I_1 = \frac{a_1 - K + a_2 t_0(K)}{2\pi}\left[\cos 2\pi(x - x_s) - \cos 2\pi x_s\right], \text{ if } x > x_s.$$

$$I_2 = \frac{a_2 \varepsilon b}{2\pi}\left\{x - \frac{1}{2\pi}\sin 2\pi x\right\}, \text{ if } x \le x_s \text{ or}$$

$$I_2 = \frac{a_2 \varepsilon b}{2\pi}\left\{x_s \cos 2\pi(x - x_s) + \frac{1}{2\pi}[\sin 2\pi(x - x_s) - \sin 2\pi x]\right\}, \text{ if } x > x_s.$$

Using the trigonometrical addition formulæ and integrating, one can write I_3 as

$$I_3 = \frac{a_3}{2}\left\{\frac{1}{2\pi + a_4\varepsilon b}\left[\sin(a_4\varepsilon b x + \phi) + \sin(2\pi x - \phi)\right] + \frac{1}{2\pi - a_4\varepsilon b}\left[\sin(a_4\varepsilon b x + \phi) - \sin(2\pi x + \phi)\right]\right\},$$

where $\phi = a_4 t_0(K) + a_5$ and $0 \le x \le x_s$. For the case in which $x \ge x_s$ we have,

$$I_3 = \frac{a_3}{2}\left\{\frac{1}{2\pi + a_4\varepsilon b}\left[\sin\{a_4\varepsilon b x + \phi - 2\pi(x - x_s)\} + \sin(2\pi x - \phi)\right] + \frac{1}{2\pi - a_4\varepsilon b}\left[\sin\{a_4\varepsilon b x + \phi + 2\pi(x - x_s)\} - \sin(2\pi x + \phi)\right]\right\}.$$

Continuing with the case $x > x_s$, we evaluate the last integral, I_4 in equation (4.96*b*), in order to account for the constant pressure in the separation bubble. This last result is

$$I_4 = \frac{2.225 - K}{2\pi}[1 - \cos 2\pi(x - x_s)].$$

Then the complete closed-form solution to order ε can be written as

$$u(x) = u_0 + \varepsilon u_1 = 1 + \varepsilon\left\{\frac{C}{2\pi}\sin 2\pi x + \frac{\pi}{4}W_r[I_1 + I_2 + I_3 + I_4]\right\}, \qquad (4.99)$$

where $I_4 = 0$ if $x \le x_s$. Because of the approximations representing $F_1(\varepsilon,x)$ from Appendix B and the stability of the solution in this case, one can examine the influence of the forcing function on the solution given in equation (4.99). As already found in the general case, the term from the initial condition simply provides a steady oscillation of amplitude $\frac{\varepsilon C}{2\pi}$ at the natural frequency of the bubble.

The interesting part of the solution is found in the sum of the integrals. We shall use the artificial example of $\varepsilon = 0.001$, $K = 2.3$, $\gamma = 12.9$ and $b = 30.3$. From these data and with the help of equation (4.94) and figure B5 one sees that $x_s = 10$. We also find that $t_0 = 0.06$ from figure B4. Then since we have γ, K and u_v, the Weber number can be found from figure 3.2, and it is $W_r = 24$. These parameters and the coefficients, a1, ..., a5, from figure B3 are all that one needs in order to evaluate the term, $\frac{\pi}{4}W_r[I_1 + I_2 + I_3 + I_4]$, in equation (4.99). The result of this calculation is shown in figure 4.11, below. The figure

shows that the fundamental vibration of the bubble is modulated by the forcing function as one expects. The bubble grows and starts to collapse but when the bubble reaches the laminar separation zone its collapse is arrested and the bubble simply vibrates in place. The growth shown by this example is modest, compared to the initial condition which contributes the term, 43.35 $\sin 2\pi x$. Consequently, even though this initial term provides no growth its effect will obscure the forcing function response. It also evident that the condition $u_v = 1$ is too restrictive. No inception calculations can be carried out if u_v is so constrained even if the growth were greater. As this example shows, however, the first order solution does respond to the forcing function as expected.

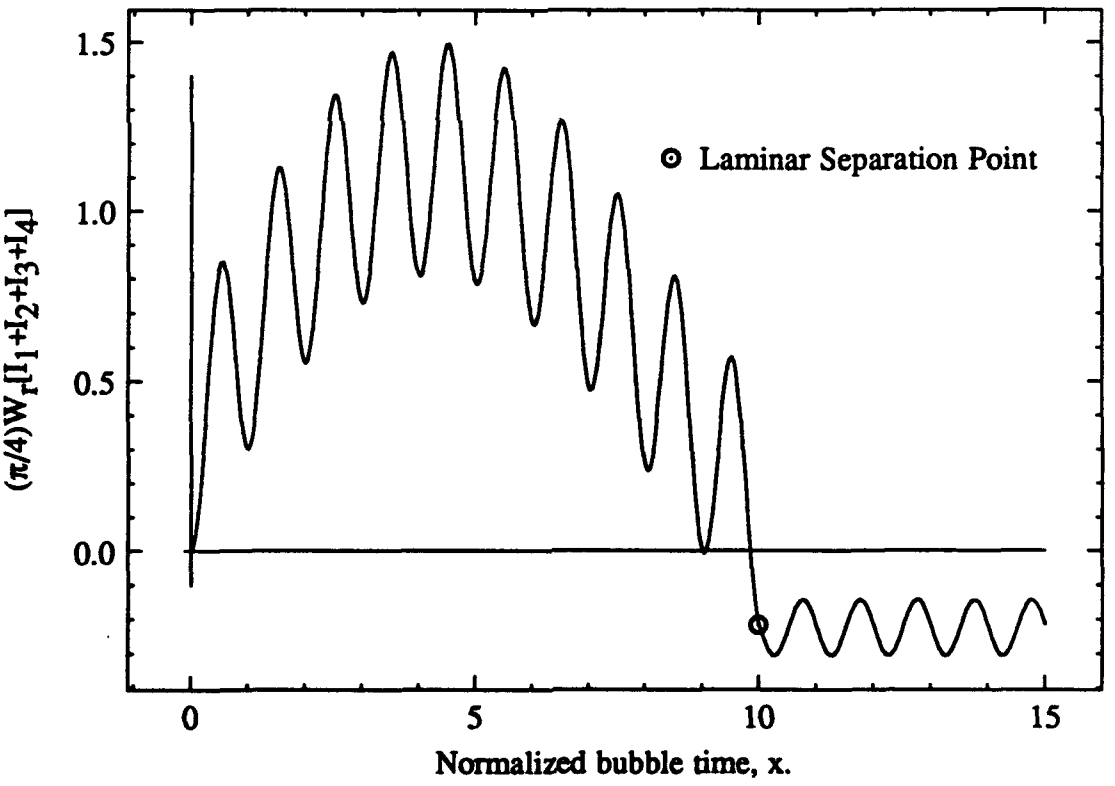

Figure 4.11 Particular First-Order Solution for $u_v = 1$ as Calculated from the Convolution Integrals of Equations (4.96*a*) and (4.96*b*).

CHAPTER 5

SUMMARY AND CONCLUSIONS

This investigation has sought to solve the forced Rayleigh-Plesset equation for the dynamics of forced vaporous growth of a cavitation bubble in an inviscid incompressible flow about submerged bodies using a two-scale perturbation expansion. Of course, the introduction of a viscous term into the equation could well introduce a third time scale. Experience with straight forward numerical integrations of the forced Rayleigh-Plesset equation with and without viscosity has shown the viscous term to have negligible effect for relatively long pulse forcing functions of interest here. Other simplifying assumptions were that the isothermal bubbles are spherical and that they do not interact with each other or with the surface of the submerged body. For further simplification we suppose that the pressure distribution on the body supplies the excitation for the bubble dynamical equation and that the boundary layer slows the progress of the bubble along the surface in a very rudimentary way. The bubble growth is not coupled to the shear layer. The two time scales arise firstly, from the natural period of a microbubble itself and secondly, from the time required for the growing vapor bubble to move through the low pressure region on the body. The first of these dimensionless times is the fast "bubble time" and the second is the slow "laboratory time". The ratio of slow to fast times is the perturbation parameter, ϵ.

The first part of this investigation dealt with the forcing function that drives the growth of the bubble. Baker [2] used pressure coefficient data from a hemispherical headform having a short laminar bubble followed by turbulent reattachment. The present analysis considers a new possibility for a forcing function, namely the supercritical flow about a circular cylinder, because this flow exhibits a laminar separation bubble just upstream of the turbulent separation point. It presents an instance of cavitation inception

not previously studied in this context, and may help to determine if this type of analysis can be applied to any body which has a boundary layer with a short laminar separation bubble. Using pressure coefficient data for a circular cylinder and employing a very simple bubble convection model , we converted these data into a forcing function dependent on the slow laboratory time.

Next, the kinematics of a bubble as it travels through the high pressure region on the body were considered because this region lies directly upstream of the vaporous growth region. These results were used to derive initial conditions at the start of vaporous growth. Using the two time scales of the present problem, the dynamical equations and their initial conditions were derived to the third order of the small parameter, ε. A few errors were found and corrected in similar equations derived by Baker.

The relationships between the measurable flow, body and bubble parameters were then considered in order to indicate their effect on the range ε. It was found useful to express these several parameters as dimensionless quantities and to relate them to practical experimental ranges of the variables to cover likely applications of this analysis. As Baker showed from his zero-order phase plane study, there is a single parameter, u_v, the affix of the vortex point in the zero order phase plane, that relates the bubble dynamics to key flow parameters such as the cavitation number, Weber number and dissolved air content. This then is the single parameter which characterizes each member of the family of solutions.

A solution of the zero-order equation was next obtained. For small values of u_v in the neighborhood of unity, the zero-order solution is nearly sinusoidal. Thus a simple closed form approximate solution for small oscillations in u_v was found using trigonometric functions which correctly displayed the periods and amplitudes of the u_0 solution. Although Baker's zero-order solution in the form, $\tau = f(u_0)$, showed good results, it can not be inverted, The solution of the first-order equation requires the zero order solution to have the form $u_0(\tau)$. Therefore, a numerical u_0 solutions were found for

one period in x that are accurate over the range of u_v values. The solution for one period can be reused over large ranges in x due to its periodicity.

Considerable study centered upon the first-order integrability condition and it suggests that the zero-order solution should be independent of the slow laboratory time. The integrability condition is a second order partial differential equation for u_0 consisting of those terms having mixed partial derivatives in the first order equation that must be set equal to zero. The above independence will be true only if the arbitrary functions of the slow time, which result from partial integrations with respect to the fast time, are in fact completely independent functions. This is the situation ordinarily encountered and it is a fundamental precondition in thpresent investigation. That the zero order solution is then independent of t_s was shown explicitly for the small oscillation approximation to the zero order solution. Next the integrability condition itself was examined from the viewpoint of the theory of charactersitics. In addition the most general functional form of u_0 was found in terms of the two time scales by direct integration. These considerations verified that the zero order solution should not depend on independent arbitrary functions of the slow time. The importance of this comes in the fact that all terms involving derivative of u_0 with respect to t_s in the higher order equations vanish, presumably suppressing secular terms in the solutions. It also allows both the zero and higher order order equations to be written as ordinary differential equations instead of partial differential equations.

Finally, the first-order equation was solved. This turned out to be a nonhomogeneous linear second-order differential equation with periodic coefficients which are functions u_0. It was found that the homogeneous form of this equation could be transformed into a special form of Hill's equation. For small oscillations in u_v, the first order solution can be approximated in terms of Mathieu functions. This fact was used to investigate the departure of the solution from a neutrally stable state, involving only simple harmonic oscillations, to unstable states as the oscillation amplitude increases with increasing u_v.

The linearity of the first-order equation enabled the superposition of the complimentary solution and the particular integral in order to arrive at the complete integral for the first-order problem. The solution to the homogeneous form of the first-order equation can be found using Floquet theory. This solution in normal Floquet form was found numerically for one period in x, then extended over more periods using the periodicity of the Floquet variables. Variation of parameters was then used to derive the particular integral and the initial conditions were used in conjunction with the complete solution to evaluate the constants of integration. Again it was found that these constants are independent of laboratory time, and that only the bubble time appears explicitly in the solution.

Normally the u_1 solution would be multiplied by the first-order of ε and be added to the u_0 solution to obtain an approximate result to the governing Rayleigh-Plesset equation. But in this investigation, only the nature of the complete first-order solution was obtained. This is because the actual value of u_v which is consistent with the other flow parameters for the test case is $u_v = 0.5994$. This value defines a zero order phase plane trajectory to the left of $u_v = 1.0$, denoting compressive oscillations of u_0. The present study has been limited to cases for which the zero-order trajectories lie to the right of $u_v = 1.0$, corresponding to oscillations of expansion which would naturally seem to lead to further vaporous growth under the influence of a forcing function. The present example shows that this may not always be true. Nevertheless a specific example for $u_v = 1.5994$ has been worked out in order to indicate important features of the present solution.

New things that have emerged from this work include the small oscillation theory which showed that trigonometric functions can be used to derive approximate results to both the zero and first-order solutions for values of u_v close to unity. To the authors' knowledge, this is the first application of the Floquet theory to bubble dynamics. This approach makes it possible to investigate the dynamic stability of the solutions and we found that aside from the small oscillation case at $u_v = 1$, all other solutions are unstable. It

was also useful because numerical work was only needed over the first period of the first order complementary complementary function, u_1, thereby minimizing error accumulation since the complete solution is extended over many periods. The forcing function for the circular cylinder was used to show one example of the solution. It is presented to demonstrate that a numerical solution can be found using different but appropriate bodies. The chief practical physical interpretation to be obtained from these calculations is that the lack of stable solutions prevents their use for the inception problem.

Finally we note that our our decision to satisfy the first order integrability condition by taking the zero order solution to be independent of the slow laboratory time, t_s, has had a profound effect on the outcome of this research. This choice was based upon the fact that in the absence of additional conditions on the problem, constants or functions of integration are arbitrary independent functions of the slow time. Perhaps the most important effect of this requirement may be the dynamic instability found in the first order solution. Consequently it appears that if one abandons his insistence that that the functions of integration in the zero order solution be independent arbitrary functions of the slow time, then further progress might be possible and a physically acceptable solution might be the outcome. Whether or not a generalized approach to the problem as suggested in section 3.5.3 above can succeed in changing the present unsatisfactory state of affairs remains to be investigated.

REFERENCES

[1] Parkin, B. R., "The Onset of Bubble-Ring Cavitation on Hemispherical Headforms," *Journal of Fluids Engineering*, Vol. 104, pp. 115-122 (March 1982).

[2] Baker, Brian B., "A Multiple-Scales Partial Solution of the Pulse-Forced Rayleigh-Plesset Equation of Cavitation Bubble Dynamics," M.S. Thesis, Department of Aerospace Engineering, The Pennsylvania State University (December 1987), also Parkin, B. R. and Brian B. Baker, "Bubble Dynamics and Cavitation Inception Theory," *Journal of Ship Research*, Vol. 32, No. 3, pp. 155-167 (September 1988).

[3] Ihara, A. and Murai, H., "Cavitation Inception on a Circular Cylinder at Critical and Supercritical Flow Range,"in Blaine R. Parkin and William B. Morgan, (Eds.) *International Symposium on Cavitation Inception - 1984*, FED-Vol. 16, The American Society of Mechanical Engineers, United Engineering Center, 345 E. 47th Street, New York N.Y. 10017 pp. 121-126. (December 1984).

[4] Gowen, F. E. and E. W. Perkins, "Drag of Circular Cylinders for a Wide Range of Reynolds Numbers and Mach Numbers," NACA TN 2960, Washington D.C. (1953).

[5] Moran, Jack, *An Introduction to Theoretical and Computational Aerodynamics*, John Wiley & Sons, New York, New York (1984).

[6] Schlichting, H., *Boundary Layer Theory*, McGraw-Hill Book Company, New York, New York (1968).

[7] Goldstein, S., *Modern Developments in Fluid Dynamics*, Volume 1, Oxford University Press, Amen House, London (1938).

[8] Nayfeh, Ali H. and Dean T. Mook, *Nonlinear Oscillations*, John Wiley & Sons, New York, New York (1979).

[9] Abramowitz, M. and I. A. Stegun (Eds.), *Handbook of Mathematical Functions*, pp. 721-750, National Bureau of Standards, Applied Mathematics Series, Superintendent of Ducuments, Goverment Printing Office, Washington D.C. (1964).

[10] Gear, C. William, *Numerical Initial Value Problems In Ordinary Differential Equations*, Prentice-Hall, Inc., Englewood Cliffs, New Jersey (1971).

[11] Simmonds, James G. and James E. Mann, Jr., *A First Look at Perturbation Theory*, Robert E. Krieger Publishing Company, Malabar, Florida (1986).

[12] Wylie, C. Ray and Louis C. Barrett, *Advanced Engineering Mathematics*, Fifth Edition, McGraw-Hill Book Company, New York, New York (1982).

[13] Parkin, B. R., "A Possible Criterion for Cavitation Inception on Hemispherical Headforms," *Journal of Fluids Engineering*, Vol. 103, (December 1981), pp. 577-582.

[14] Smith, J. M., *Mathematical Modeling and Digital Simulation for Engineers and Scientists*, 2nd Edition, John Wiley & Sons, New York, New York (1987), pp. 49-50.

[15] Press, W. H., B. P. Flannery, S. A. Tenkolsky and W. T. Vetterling, *Numerical Recipes, The Art of Scientific Computing*, Cambridge University Press, Cambridge, U.K. (1986).

[16] Plesset, M.S., "The Dynamics of Cavitation Bubbles," *Trans. ASME, Jounal of Applied Mechanics*, Vol 16 (1949) pp. 228-231.

APPENDIX A

FORTRAN CODE LISTING

This is a listing of the computer code used to do all the calculations. This includes calculating the forcing function, zero-order solution and first-order solution. Since phases of the code were developed at different times throughout the analysis and pieced together into this final code, its working order is by no means the most efficient. The important result is that it works.

The code is written in standard FORTRAN 77, and was run on both a MACINTOSH PC and a VAX 11-780 system. Many of the numerical subroutines have been adapted from *Numerical Recipes* by Press et al. [15] which made much of the programming easier and more efficient.

The inputs needed for the code are provided from three different files. The first file corresponding to unit 10 contains initial values to perform the first-order integration. These include the initial and final values of x for one period, X1 and X2, an estimated step size to be used in the Runge-Kutta routine, H, the required accuracy used in the integration, EPS, the minimum step size allowed, HMIN, and the number of first-order equations to be solved, N, which is two for this problem. The code then reads the initial values of the fundamental set of solutions into the 2 dimensional array Z0.

The next input file corresponding to unit 11 contains the basic parameters of the flow. These include the cavitation number, XKVAL, the free stream velocity in ft/s, VNOT, the initial free stream nucleus radius in μm, RNOT_MIC, the characteristic body length in in., DIAM_INCH, the density of the liquid in slugs/ft^3, RHO, the surface tension of the liquid in lb/ft, SIGMA, and the dissolved air pressure in psia, PA_INCH. Unit 12 corresponds to the input file containing the pressure coefficient

versus dimensionless arc length data. It is read by first inputing the total number of data points, NUM_PTS, and then reading the table for S and CP.

These parameters are input with their given physical dimensional units. The code automatically converts each parameter into consistent units and eventually into the proper nondimensional form. It then converts the input into a corresponding value of u_v and forcing function, then it solves the zero-order and first-order equations. The output of the program includes the total first-order solution into unit 40, the first-order stability parameters into units 15 and 16, and a summary of the inputed and calculated flow parameters into unit 45. Simple modifications can be made to the code in order to output any of the intermediate variables.

```
      PROGRAM U1TOTAL
C++++ +++ +++++++++ +++++++++ +++++++++ +++++++++ +++++++++ +++++++++
C THIS PROGRAM CLACULATES BOTH THE ZERO-ORDER AND FIRST-ORDER
C SOLUTIONS TO THE FORCED RAYLEIGH-PLESSET EQUATION. IT FIRST
C READS IN THE INITIAL DATA, AND THEN CALCULATES A FORCING
C FUNCTION FOR THE PROBLEM. THE ZERO-ORDER SOLUTION IS THEN FOUND
C NUMERICALLY, AND IT IS USED TO OBTAIN THE FIRST-ORDER SOLUTION
C FROM FLOQUET THEORY. THE RESULTS ARE OUTPUTED IN THE FILE
C UTOT.DAT.
C++++ +++ +++++++++ +++++++++ +++++++++ +++++++++ +++++++++ +++++++++
      IMPLICIT REAL*8(A-H, O-Z)
      DIMENSION Z0(2,2),S(50),CP(50),A(2,2),
     1          XE(201),U0E(201),U0EP(201),
     2          U1E(201),U1EP(201),U2E(201),U2EP(201),
     3          PHI1(201),PHI1P(201),PHI2(201),PHI2P(201),
     4          XTIME(10000),UTOT(10000),UTOTP(10000),
     5          FF(10000)
    1 FORMAT(5X,'i',8X,'Uv',10X,'Alpha',9X,'Wronskian',4X,'Scatter',
     1       4x,'Ave.Error')
    2 FORMAT(5F10.5, I5)
    3 FORMAT(I5, 2F10.5)
    4 FORMAT(2X,I4,3F12.8,2E12.4)
    5 FORMAT(5X,'i',8X,'Uv',10X,'Lamda',' Steps',6x,'Lam1',8x,'Lam2',
     2       8x,'Gam1',8x,'Gam2')
    6 FORMAT(2X,I4,F12.8,F13.8,I6,4F12.8)
    7 FORMAT(2X,I4)
    8 FORMAT(2X,I4,5(2X,F14.8))
    9 FORMAT(45X,F14.8)
   10 FORMAT(2X,I8)
   11 FORMAT(2(2X,F11.8))
   12 FORMAT(2X,A,F14.8)
   13 FORMAT(/,'FOR Uv = ',F7.4,',',' LAMBDA = ',
     1       F13.8,/,5X,'i',13X,'X',18X,'UTOT',14X,'UTOTP',
     2       14X,'HOMOG',15X,'PART')
      OPEN(UNIT = 10, FILE ='SOLVE.dat', STATUS ='OLD')
      OPEN(UNIT = 11, FILE ='INPUT.DAT', STATUS ='OLD')
      OPEN(UNIT = 12, FILE='CPSMOOTH.DAT',STATUS ='OLD')
      OPEN(UNIT = 15, FILE='Alpha-Uv.dat',STATUS ='NEW')
      OPEN(UNIT = 16, FILE='LAM-GAM.DAT',STATUS ='NEW')
      OPEN(UNIT = 40, FILE='UTOT.DAT',STATUS ='NEW')
      OPEN(UNIT = 45, FILE='VARIABLE.OUT',STATUS ='NEW')
C---- READING IN INITIAL DATA
        READ(10,2) X1,X2,H,EPS,HMIN,N
        READ(10,3) (K, Z0(L,1), Z0(L,2), L = 1,2)
      IP = 0
      IBIN = 0
C---- READING IN GIVEN FLOW PARAMETERS
        READ(11,9) XKVAL
        READ(11,9) VNOT
        READ(11,9) RNOT_MIC
        READ(11,9) DIAM_INCH
        READ(11,9) RHO
        READ(11,9) SIGMA
        READ(11,9) PA_INCH
        READ(12,10) NUM_PTS
        READ(12,11) (S(I),CP(I),I=1,NUM_PTS)
C---- CONVERT TO SIMILAR UNITS
      RNOT = RNOT_MIC*1.0D-04/3.048D+01
      PA = PA_INCH*1.44D+02
      DIAM = DIAM_INCH/1.2D+01
C---- CALCULATE INITIAL PARAMETERS
      GAMMA = PA*RNOT/(2.0D+00*SIGMA)
      WEB = VNOT*VNOT*RHO*RNOT/SIGMA
      Q = WEB*XKVAL/4.0D+00
      EPSIL = RNOT*DSQRT(WEB/2.0D+00)/DIAM
      UV = DSQRT(GAMMA/(1.0D+00+Q))
      WRITE(15,1)
      WRITE(16,5)
      I = 1
      ONE = 1.0D+00
      HUV=0.2D-01
      PI = 4.0D+00*DATAN(ONE)
C---- SPECIAL CASE FOR Uv = 1
      IF(UV.GT.ONE) GO TO 20
        ALPHA = 1.0D+00
        W = 1.0D+00
        AMDA = PI*DSQRT(2.0D+00)
        ALP1 = 0.0D+00
        UV1 = UV
        SCAT = 0.0D+00
        AVER = SCAT
        GO TO 30
C---- CALCULATE STABILITY PARAMETERS, Uo, AND U1
   20 CALL ZED(ALPHA,W,SCAT,AVER,AMDA,Z0,UV,X1,X2,H,EPS,
     1         HMIN,N,PI,JE,AM1,AM2,GAM1,GAM2,A,
     2         XE,U0E,U0EP,U1E,U1EP,U2E,U2EP)
C---- SPECIAL CASE FOR Uv = 1
   30 IF(UV.EQ.ONE) THEN
        JE = 0
        AM1 = ONE
        AM2 = ONE
        GAM1 = 0.0D+00
        GAM2 = GAM1
      END IF
C---- CALCULATE THE FORCING FUNCTION
      CALL FORCE(NUM_PTS,S,CP,XKVAL,UV,Q,EPSIL,AMDA,
     1           NEPTS,XTIME,FF,SLOPE)
C---- WRITE OUT THE PARAMETERS
      WRITE(45,12) 'CAVITATION NUMBER,              K = ',XKVAL
      WRITE(45,12) 'FREE STREAM VELOCITY,          Vo = ',VNOT
      WRITE(45,12) 'INITIAL NUCLEUS RADIUS,        Ro = ',RNOT
      WRITE(45,12) 'HEADFORM DIAMETER,              D = ',DIAM
      WRITE(45,12) 'DENSITY @ T = 70,             RHO = ',RHO
      WRITE(45,12) 'SURFACE TENSION,            SIGMA = ',SIGMA
      WRITE(45,12) 'DISSOLVED AIR PRESSURE,        Pa = ',PA
      WRITE(45,12) 'AIR CONTENT,                GAMMA = ',GAMMA
      WRITE(45,12) 'WEBER NUMBER,                  Wr = ',WEB
      WRITE(45,12) 'Q,                              Q = ',Q
```

```
      WRITE(45,12) 'EPSILON,                    EPSILON = ',EPSIL
      WRITE(45,12) 'SLOPE,                      SLOPE = ',SLOPE
      WRITE(15,4) I,UV,ALPHA,W,SCAT,AVER
      WRITE(16,6) I,UV,AMDA,JE,AM1,AM2,GAM1,GAM2
      WRITE( 6,4) I,UV,ALPHA,W,SCAT,AVER
C---- CALCULATE THE INITIAL CONDITION CONSTANT
      C = AMDA*WEB*(1.0D+00+Q)**2.5D+00*DSQRT(1.0D+00+K)
     1       *SLOPE/8.0D+00
C---- CALCUALTE THE PERIODIC PHI1 VALUES
      CALL ALPHAGT1(UV,ALPHA,A,AM1,AM2,GAM1,GAM2,XE,U1E,U1EP,
     1              U2E,U2EP,PHI1,PHI1P,PHI2,PHI2P)
      WRITE(40,13) UV,AMDA
      NPHASE = 0
C-------------------------------------------------------------
C CALCULATING BOTH HOMOGENEOUS AND PARTICULAR PARTS OF THE U1
C SOLUTION. IN THIS CASE, I IS THE GLOBAL COUNTER THAT RUNS THE
C LENGTH OF THE SOLUTION FOR PARAMETERS SUCH AS XTIME AND THE
C FORCING FUNCTION. NPHASE KEEPS TRACK OF WHICH PERIOD XTIME IS
C IN. NP IS THEN THE PERIOD COUNTERTHAT RUNS FROM 1 TO 201 FOR
C PARAMETERS SUCH AS PHI AND Uo. THIS SAME SETUP IS USED IN THE
C LOOP THAT CALCULATES THE INTEGRALS. IT USES J AS THE GLOBAL
C COUNTER, NIPHASE AS THE PERIOD TRACKER, AND NIP AS THE PERIOD
C COUNTER.
C-------------------------------------------------------------
      DO 60 I = 1, 10000, 2
         NP = I - NPHASE*200
         IF(I.GE.NEPTS) GO TO 70
C---- CALCULATING HOMOGENEOUS SOLUTION ----
         HOMOG = C*((AM1-A(1,1))*PHI1(NP)*DEXP(GAM1*XTIME(I))
     1            + (AM2-A(1,1))*PHI2(NP)*DEXP(GAM2*XTIME(I)))
         HOMOGP = C*((AM1-A(1,1))*(AM1*PHI1(NP)+PHI1P(NP))
     1              *DEXP(GAM1*XTIME(I)) + (AM2-A(1,1))*
     2              (AM2*PHI2(NP)+PHI2P(NP))*DEXP(GAM2*XTIME(I)))
         X3 = 0.0D+00
         SUM1 = 0.0D+00
         SUM2 = 0.0D+00
         IF((NPHASE.EQ.0).AND.(I.EQ.1)) THEN
            PART = 0.0D+00
            GO TO 55
         END IF
         H = XTIME(I)/(I-1)
         NIPHASE = 0
C---- CALCULATING PARTICULAR SOLUTION USING SIMPSON'S RULE ON INTEGRALS --
         DO 50 J = 3, I, 2
            NIP = J - NIPHASE*200
            X1 = X3
            X2 = X1 + H
            X3 = X2 + H
            SIMP1 = PFUN1(XTIME(I),X1,GAM1,GAM2,PHI1(NIP-2),
     1                    U0E(NIP-2),FF(J-2))
            SIMP2 = PFUN1(XTIME(I),X2,GAM1,GAM2,PHI1(NIP-1),
     1                    U0E(NIP-1),FF(J-1))
            SIMP3 = PFUN1(XTIME(I),X3,GAM1,GAM2,PHI1(NIP),
     1                    U0E(NIP),FF(J))
            SUM1 = SUM1 + H*(SIMP1+4.0D+00*SIMP2+SIMP3)/3.0D+00
            SIMP1 = PFUN2(XTIME(I),X1,GAM1,GAM2,PHI2(NIP-2),
     1                    U0E(NIP-2),FF(J-2))
            SIMP2 = PFUN2(XTIME(I),X2,GAM1,GAM2,PHI2(NIP-1),
     1                    U0E(NIP-1),FF(J-1))
            SIMP3 = PFUN2(XTIME(I),X3,GAM1,GAM2,PHI2(NIP),
     1                    U0E(NIP),FF(J))
            SUM2 = SUM2 + H*(SIMP1+4.0D+00*SIMP2+SIMP3)/3.0D+00
            IF(J.GE.(NIPHASE+1)*200) NIPHASE = NIPHASE + 1
   50    CONTINUE
         PART = AMDA*AMDA*A(1,2)*(AM2-AM1)*(PHI2(NP)*SUM1-
     1          PHI1(NP)*SUM2)
         PARTP = AMDA*AMDA*A(1,2)*(AM2-AM1)*((AM2*PHI2(NP)+
     1           PHI2P(NP))*SUM1 - (AM1*PHI1(NP)+PHI1P(NP))*SUM2)
C---- SUMMING UP BOTH PARTS OF THE SOLUTION
   55    UTOT(I) = HOMOG + PART
         UTOTP(I) = HOMOGP + PARTP
         WRITE(40,8) I,XTIME(I),UTOT(I),UTOTP(I),HOMOG,PART
         IF(I.GE.(NPHASE+1)*200) NPHASE = NPHASE + 1
   60    CONTINUE
   70    STOP
         END
      SUBROUTINE ZED(ALPHA,W,SCAT,AVER,AMDA,Z0,UV,X1,X2,H,EPS,
     1               HMIN,N,PI,JE,AM1,AM2,GAM1,GAM2,A,
     1               XE,U0E,U0EP,U1E,U1EP,U2E,U2EP)
C++++ +++ +++++++++ +++++++++ Sun Apr 22, 1990 18:21:54 +++ +++++++++
C Adaptive-steps program for solving ordinary differential equations
C of order n.
C N = no. of 1st order equations = n.   |    Y(n) = Dependent variable
array.
C DYDX(n) = 1st derivatives of Y(n).    |    X = independent variable
C H = Estimated step size.              |    X1 = Initial value of X.
C NMAX = 10, max no. of 1st order DE's. |    X2 = Maximum value of X.
C N, H, UV, & initial X & Y(1) values are entered by programmer in an
C input file.  Functions DYDX are coded by programmer in subroutine
C DERIVS below.
C++++ +++ +++++++++ +++++++++ +++++++++ +++++++++ +++++++++ +++++++++
      IMPLICIT REAL*8(A-H, O-Z)
      COMMON/Z122/ KMAX, DXSAV, XP(201), YP(10,201)
      DIMENSION YSTART(10),Z0(2,2),A(2,2),U0(300),XX(300),
     1          XE(201),U0E(201),U0EP(201),
     2          Z1E(201),Z1EP(201),Z2E(201),Z2EP(201),
     3          U1E(201),U1EP(201),U2E(201),U2EP(201)
      ONE =1.0D+00
      ZERO=0.0D+00
      TEST = ZERO
      HA = 0.5D-02
C---- FIND Umax, LAMBDA, AND THE PERIOD INTEGRAL, I
      CALL UMAX(UM, TI, AMDA, UV, PI)
      ER = ZERO
      JE = 0
C---- FIND THE ZERO-ORDER SOLUTION
      CALL U2ERO(XX,U0,UM, AMDA, UV, PI)
      L = 1
```

```
C---- STORE EVENLY-SPACED VALUEA OF U0(X) AND dU0/dX IN ARRAYS
XE,UOE,&UOEP
      CALL UOEVEN(XX,U0,UV,UM,AMDA,XE,UOE,UOEP)
C---- SETTING INITIAL VALUES OF Z1 FOR INTEGRATION
   20 YSTART(1) = Z0(L,1)
      YSTART(2) = Z0(L,2)
C---- INTEGRATION OF Z1 AND Z2
      CALL ODEINT(YSTART, N, X1, X2, EPS, H, HMIN, MOK, NBAD, KOUNT,
     1            U, QA, XX, U0, UV, AMDA, PI, ER, JE, KAS)
      IF(L .EQ. 1) THEN
C---- SETTING A MATRIX VALUES
         A(L,1) = YP(1,KOUNT)
         A(L,2) = YP(2,KOUNT)
C---- GETTING EVEN SPACE VALUES OF Z1 AND dZ1/dX
         CALL ZEVEN(KOUNT,XE,Z1E,Z1EP)
         Z1E(1) = ONE
         Z1EP(1) = ZERO
      ELSE
C---- SETTING A MATRIX VALUES
         A(L,1) = YP(1,KOUNT)
         A(L,2) = YP(2,KOUNT)
C---- GETTING EVEN SPACE VALUES OF Z2 AND dZ2/dX
         CALL ZEVEN(KOUNT,XE,Z2E,Z2EP)
         Z2E(1) = ZERO
         Z2EP(1) = ONE
C---- CALCULATING ALPHA
         ALPHA = (A(1,1) + A(2,2))/2.0D+00
         AVER = ER/JE
C---- CALCUALTING THE WRONSKIAN
         W = A(1,1)*A(2,2) - A(1,2)*A(2,1)
         SCAT = W - 1.0D+00
         SQ = DSQRT(DABS(ALPHA*ALPHA - ONE))
C---- CALCULATING FLOQUET PARAMETERS, LAMBDA1 AND LAMBDA2
         AM1 = ALPHA + SQ
         AM2 = ALPHA - SQ
C---- CALCULATING FLOQUET CHARACTERISTIC EXPONENTS, GAMMA1 AND GAMMA2
         GAM1 = DLOG(AM1)
         GAM2 = DLOG(AM2)
         GO TO 30
      END IF
      L = L + 1
      GO TO 20
C---- DETERMINE FUNDAMENTAL SOLUTIONS U1E AND U2E FROM Z1E AND Z2E ------
   30 DO 40 J = 1,201
         U1E(J)  = Z1E(J)/UOE(J)**1.5D+00
         U2E(J)  = Z2E(J)/UOE(J)**1.5D+00
         U1EP(J) = (Z1EP(J)*UOE(J)**1.5D+00 - 1.5D+00*Z1E(J)
     1              *DSQRT(UOE(J))*UOEP(J))/(UOE(J)*UOE(J)*UOE(J))
         U2EP(J) = (Z2EP(J)*UOE(J)**1.5D+00 - 1.5D+00*Z2E(J)
     1              *DSQRT(UOE(J))*UOEP(J))/(UOE(J)*UOE(J)*UOE(J))
   40 CONTINUE
    8 FORMAT(2X,I4,5(2X,F13.8))
   11 FORMAT(/,2X,'FOR Uv= ',F7.4,',',' Umax = ',F13.8,',',' LAMBDA =',
     1       F13.8,/,5X,'I',10X,'X',13X,'UTOT',14X,'UTOTP')
      RETURN
      END
      SUBROUTINE ALPHAGT1(UV,ALPHA,A,AM1,AM2,GAM1,GAM2,XE,
     1                    U1E,U1EP,U2E,U2EP,PHI1,PHI1P,PHI2,PHI2P)
C++++ +++ +++++++++ +++++++++ +++++++++ +++++++++ +++++++++ +++++++++
C SUBROUTINE CALCULATING V AND PHI FOR THE CASE WHEN ALPHA > 1,
C IN WHICH CASE BOTH LAMBDAS AND GAMMAS ARE REAL.  ALPHA, UV, A11'S,
C X, U1 AND U2 AND THEIR DERIVATIVES ARE INPUTED INTO THE SUBROUTINE.
C++++ +++ +++++++++ +++++++++ +++++++++ +++++++++ +++++++++ +++++++++
      IMPLICIT REAL*8(A-H, O-Z)
      DIMENSION A(2,2),XE(201),U1E(201),U1EP(201),U2E(201),U2EP(201),
     1          PHI1(201),PHI1P(201),PHI2(201),PHI2P(201)
C---- CALCULATING P INVERSE MATRIX ----
      DET  = A(1,2)*(AM2-AM1)
      PI11 = (AM2-A(1,1))/DET
      PI12 = -A(1,2)/DET
      PI21 = -(AM1-A(1,1))/DET
      PI22 = A(1,2)/DET
C---- CALCUALTING V'S AND PHI'S ----
      DO 20 I = 1, 201
         V1  = PI11*U1E(I) + PI12*U2E(I)
         V2  = PI21*U1E(I) + PI22*U2E(I)
         V1P = PI11*U1EP(I) + PI12*U2EP(I)
         V2P = PI21*U1EP(I) + PI22*U2EP(I)
         PHI1(I)  = DEXP(-GAM1*XE(I))*V1
         PHI2(I)  = DEXP(-GAM2*XE(I))*V2
         PHI1P(I)  = DEXP(-GAM1*XE(I))*(V1P-GAM1*V1)
         PHI2P(I)  = DEXP(-GAM2*XE(I))*(V2P-GAM2*V2)
   20 CONTINUE
      RETURN
      END
      SUBROUTINE UOEVEN(XX,U0,UV,UM,AMDA,XE,UOE,UOEP)
C++++ +++ +++++++++ +++++++++ +++++++++ +++++++++ +++++++++ +++++++++
C STORE EVENLY-SPACED VALUES OF U0(X) AND dU0/dX IN ARRAYS XE, UOE, &UOEP.
C++++ +++ +++++++++ +++++++++ +++++++++ +++++++++ +++++++++ +++++++++
      IMPLICIT REAL*8(A-H, O-Z)
      DIMENSION XA(4),YA(4),XX(300),U0(300),
     1          XE(201),UOE(201),UOEP(201)
      ONE = 1.0D+00
      ZERO = 0.0D+00
      AE = ZERO
      HA = 0.5D-02
      M = 201
      DO 20 I = 2, 101
        IF(AE.EQ.ZERO) THEN
          K = 1
          KAS = K
          XE(1) = AE
          UOE(1) = ONE
          UOEP(1) = ZERO
          UOE(201) = ONE
          UOEP(201) = ZERO
          XE(201) = ONE
          AE = HA
```

```
          END IF
C---- FIND THE VALUE OF K ALLOWING FOR PERIODICITY OF U0
          CALL HUNT(XX,M+97,AE,K)
          KAS = K
          IF(K.LT.2) THEN
           XA(1) = -XX(2)
           XA(2) = XX(K)
           XA(3) = XX(K+1)
           XA(4) = XX(K+2)
           YA(1) = U0(M+3)
           YA(2) = U0(K)
           YA(3) = U0(K+1)
           YA(4) = U0(K+2)
          ELSE
           XA(1) = XX(K-1)
           XA(2) = XX(K)
           XA(3) = XX(K+1)
           XA(4) = XX(K+2)
           YA(1) = U0(K-1)
           YA(2) = U0(K)
           YA(3) = U0(K+1)
           YA(4) = U0(K+2)
          END IF
C---- USE CUBIC INTERPOLATION FOR U0(X)
          CALL POLINT(XA,YA,4,AE,Y,DY)
          XE(I) = AE
          U0E(I) = Y
          ER = ER + DY
          EPSI = ONE - Y/UM
          IF(I.EQ.101) THEN
            U0E(I) = UM
            U0EP(I) = ZERO
          ELSE IF(EPSI.LT.1.5D-04) THEN
            U0EP(I) = AMDA*DSQRT(2.0D+00*(UM+UV)*(UM-UV)*EPSI/Y)/Y
            J = 202-I
            U0E(J) = U0E(I)
            U0EP(J) = -U0EP(I)
            XE(J) = ONE-XE(I)
          ELSE
            U0EP(I) = AMDA*DSQRT((2.0D+00*UV*UV*DLOG(Y)-Y*Y+ONE)/Y)/Y
            J = 202 - I
            U0E(J) = U0E(I)
            U0EP(J) = -U0EP(I)
            XE(J) = ONE-XE(I)
          END IF
          AE = AE + HA
          K = KAS
   20    CONTINUE
         RETURN
         END
         SUBROUTINE ZEVEN(KOUNT,XE,ZE,ZEP)
C++++ +++ +++++++++ +++++++++ +++++++++ +++++++++ +++++++++ +++++++++
C STORE EVENLY-SPACED VALUES OF Z1(X) AND dZ1/dX IN ARRAYS XE, Z1E, &Z1EP.
C++++ +++ +++++++++ +++++++++ +++++++++ +++++++++ +++++++++ +++++++++
      IMPLICIT REAL*8(A-H, O-Z)
      COMMON/Z122/ KMAX, DXSAV, XP(201), YP(10,201)
      DIMENSION XA(4),YA(4),YAP(4),
     1          XE(201),ZE(201),ZEP(201)
      ONE = 1.0D+00
      ZERO = 0.0D+00
      HA = 0.5D-02
      AE = HA
      XE(1) = ZERO
      XE(201) = ONE
      ZE(1) = YP(1,1)
      ZE(201) = YP(1,KOUNT)
      ZEP(1) = YP(2,1)
      ZEP(201) = YP(2,KOUNT)
      K = 1
      DO 40 I = 2, 200
         CALL HUNT(XP,KOUNT,AE,K)
         KAS = K
         IF(K.LT.2) THEN
           K = 2
         ELSE IF(K.GT.KOUNT-2) THEN
           K = KOUNT - 2
         ELSE
           K = K
         END IF
         XA(1) = XP(K-1)
         XA(2) = XP(K)
         XA(3) = XP(K+1)
         XA(4) = XP(K+2)
         YA(1) = YP(1,K-1)
         YA(2) = YP(1,K)
         YA(3) = YP(1,K+1)
         YA(4) = YP(1,K+2)
         CALL POLINT(XA,YA,4,AE,Y,DY)
         XE(I) = AE
         ZE(I) = Y
         ER = ER + DY
         XA(1) = XP(K-1)
         XA(2) = XP(K)
         XA(3) = XP(K+1)
         XA(4) = XP(K+2)
         YAP(1) = YP(2,K-1)
         YAP(2) = YP(2,K)
         YAP(3) = YP(2,K+1)
         YAP(4) = YP(2,K+2)
         CALL POLINT(XA,YAP,4,AE,Y,DY)
         ZEP(I) = Y
         ER = ER + DY
         AE = AE + HA
         K = KAS
   40    CONTINUE
         RETURN
      END
      SUBROUTINE UMAX(UM, TIUV, AMDA, UV, PI)
```

```
C++++ +++ +++++++++ +++++++++ +++++++++ +++++++++ +++++++++ +++++++++
C Bisection routine finds the root of f(Uv,Umax) = 0 for any value of
C Uv.Then an integration from u = 1 to Umax gives the integral I(Uv).
C This subroutine returns the corresponding values of Umax = UM,
C I(Uv) = TIUV and Lamda = 2I(Uv).
C++++ +++ +++++++++ ++++.++++ +++++++++ +++++++++ +++++++++ +++++++++
      IMPLICIT REAL*8(A-H, O-Z)
      TDOTF(XV, X) = DSQRT(X*X*X/(2.0D+00*XV*XV*DLOG(X)+1.0D+00-X*X))
      EPSI = 5.0D-09
      RT2 = DSQRT(2.0D+00)
      M = 201
      C = UV
C++++ +++ +++++ Special routine for Uv=1 & very near 1.++++ +++++++++
      IF(UV .EQ. 1.0D+00) THEN
         UM = 1.0D+00
         TIUV = PI/DSQRT(2.0D+00)
         AMDA = TIUV + TIUV
         RETURN
      END IF
      IF(C .LE. 1.03D+00) THEN
         AC = 0.75D+00*(C*C + 1.0D+00)/(C*C)
         AA = 1.0D+00/AC
         BC = 3.0D+00*(C*C - 1.0D+00)/(C*C)
         Z = C*C - 1.0D+00
         G = PI*(1.0D+00 - Z*(1.0D+00 - Z*(3.0D+00
     1     - 5.0D+00*Z/4.0D+00)/8.0D+00)/4.0D+00)/RT2
         IF(C .LE. 1.001D+00) THEN
            YM = BC*(1.0D+00 + BC*(1.0D+00 + BC/(2.0D+00*AC*AC))
     1        / (4.0D+00*AC*AC))/(2.0D+00*AC)
         ELSE
            YM = AC - DSQRT(AC*AC - BC)
         END IF
         R = 2.0D+00*AC - YM
         RR = 1.0D+00/R
         UM = YM + 1.0D+00
         TIUV = G*(1.0D+00 + (3.0D+00 + AA + RR + (3.0D+00 + (1.0D+00
     1        + 1.5D+00*AA)*AA + RR + 9.0D+00*(1.0D+00 + (2.0D+00
     2        + RR)*RR)/4.0D+00)*YM/4.0D+00)*YM/4.0D+00)
         AMDA = TIUV + TIUV
         RETURN
      END IF
C++++ +++ +++++ For Uv>1.03, search for sign change in f(Uv,Umax).+++
      S = (UV - 1.0D+00)/100.0D+00
      U1 = UV + S
      U2 = U1+S
      F1 = 2.0D+00*UV*UV*DLOG(U1) + 1.0D+00 - U1*U1
      F2 = 2.0D+00*UV*UV*DLOG(U2) + 1.0D+00 - U2*U2
      IF(ABS(F1) .LT. EPSI) THEN
         UM = U1
         RETURN
      ELSE IF(ABS(F2) .LT. EPSI) THEN
         UM = U2
         RETURN
      END IF
   10 IF(F1*F2 .GT. 0.0D+00) THEN
         U1 = U2
         U2 = U2 + S*U1/UV
         F1 = F2
         F2 = 2.0D+00*UV*UV*DLOG(U2)+1.0D+00-U2*U2
         GO TO 10
      ELSE
C++++ +++ +++++++++ Bisection finds root, Umax(Uv).++++++++ +++++++++
   20    IF(ABS(U2 - U1) .LE. EPSI) GO TO 30
         U3 = (U1 + U2)/2.0D+00
         F3 = 2.0D+00*UV*UV*DLOG(U3)+1.0D+00-U3*U3
         IF(F3 .EQ. 0.0D+00) GO TO 30
         IF(F3*F2 .GT. 0.0D+00) THEN
            U2 = U3
            F2 = F3
            GO TO 20
         ELSE
               U1 = U3
               F1 = F3
               GO TO 20
         END IF
      END IF
   30 UM = (U1 + U2)/2.0D+00
C++++ +++ Simpson's rule for half-period integral, I(Uv).++ +++++++++
      H = (UM - 1.0D+00)/(M-1)
      X0 = 1.0D+00 + H
      X1 = X0 + H
      F0 = TDOTF(UV, X0)
      F1 = TDOTF(UV, X1)
      SING = 2.0D+00*H*F0
      K = 1
      X3 = 1.0D+00
      SUM = SING + (F0 + F1)*H/2.0D+00
      DO 40 J = 3, M-4, 2
         X2 = X1 + H
         X3 = X2 + H
         K = (J+3)/2
         SUM = SUM + H*(TDOTF(UV,X1) + 4.0D+00*TDOTF(UV,X2)
     1       + TDOTF(UV, X3))/3.0D+00
         X1 = X3
   40 CONTINUE
      SONG = 2.0D+00*H*TDOTF(UV,UM-H)
      TIUV = SUM + (TDOTF(UV,X1) + TDOTF(UV, UM-H))*H/2.0D+00 + SONG
      AMDA = TIUV + TIUV
      RETURN
      END
      SUBROUTINE UZERO(X,U,UM, AMDA, UV, PI)
C++++ +++ +++++++++ +++++++++ +++++++++ +++++++++ +++++++++ +++++++++
C This code returns a numerical inversion of the bubble dynamical
C zero-order solution for Uo(x) = U(i). The array, X = x(i), is the
C normalized bubble time. The output arrays, U and X have 300 elements.
C The x(i) are not evenly spaced. Input values of Uv, Uo|max and Lamda
C are required. Uv is the phase-plane affix of the vortex point of the
C zero-order dynamical equation.
```

```
C++++ +++ +++++++++ +++++++++ +++++++++ +++++++++ +++++++++ +++++++++
      IMPLICIT REAL*8(A-H, O-Z)
      DIMENSION X(300),U(300)
      TDOTF(XV,X) = DSQRT(X*X*X/(2.0D+00*XV*XV*DLOG(X)+1.0D+00-X*X))
      RT2 = DSQRT(2.0D+00)
      M = 201
      LL = M-4
      H = (UM - 1.0D+00)/(M - 1)
      C = UV
C++++ +++ +++++ Special routine for Uv=1 & very near 1.++++ +++++++++
      IF(C .EQ. 1.0D+00) THEN
         HK = 1.0D+00/2.04D+02
         X0 = 0.0D+00
         TI = PI/RT2
         DO 17 K = 1,204
            X(K) = X0
            U(K) = 1.0D+00
            X0 = X0 + HK
17       CONTINUE
         X(205) = 1.0D+00
         RETURN
      END IF
C++++ Simpson's rule on upper half of phase-plane trajectory gives Uo(x).
      X(1) = 0.0D+00
      U(1) = 1.0D+00
      X2 = 1.0D+00 + H
      X3 = X2 + H
      F2 = TDOTF(C, X2)
      F3 = TDOTF(C, X3)
      SING = 2.0D+00*H*F2
      SUM = SING
      SONG = 2.0D+00*H*TDOTF(C, UM-H)
      X(2) = SUM/AMDA
      U(2) = X2
      SUM = SUM + (F2 + F3)*H/2.0D+00
      X(3) = SUM/AMDA
      U(3) = X3
      X1 = X3
      DO 50 J = 3, LL, 2
         X2 = X1 + H
         X3 = X2 + H
         K = 1 + (J+3)/2
         SUM = SUM + H*(TDOTF(C,X1) + 4.0D+00*TDOTF(C,X2)
     1         + TDOTF(C, X3))/3.0D+00
         X(K) = SUM/AMDA
         U(K) = X3
         X1 = X3
50    CONTINUE
      K = K + 1
      F1 = TDOTF(C,X1)
      F2 = TDOTF(C,UM-H)
      SUM = SUM + (F1 + F2)*H/2.0D+00
      X(K) = SUM/AMDA
      U(K) = UM - H
      K = K + 1
      SUM = SUM + SONG
      X(K) = SUM/AMDA
      U(K) = UM
      K = K + 1
C+++ Use symmetry of Uo instead of integration on lower phase-plane
trajectory.+
      DO 60 I = 1,102
         J = 103 + I
         K = 103 - I
         X(J) = 1.0D+00 - X(K)
         U(J) = U(K)
60    CONTINUE
C++++ +++ +++++++++ Extend Uo and x arrays to 300 points for
interpolation.
      DO 70 I = 2,96
         J = 204 + I
         X(J) = 1.0D+00 + X(I)
         U(J) = U(I)
70    CONTINUE
      RETURN
      END
      SUBROUTINE DERIVS(X,Y,DYDX,N,U,QA,XX,U0,UV,AMDA,PI,ER,JE,KAS)
C++++ +++ +++++++++ +++++++++ +++++++++ +++++++++ +++++++++ +++++++++
C Computes the derivatives on the right hand sides of all N first order
C D.E's. Y(1) = z, Y(2) = z' = DYDX(1) and z"= DYDX(2).
C++++ +++ +++++++++ +++++++++ +++++++++ +++++++++ +++++++++ +++++++++
      IMPLICIT REAL*8(A-H, O-Z)
      DIMENSION Y(N), DYDX(N),XX(300),U0(300)
      CALL GETQ(U,QA,XX,U0,UV,AMDA,X,PI,ER,JE,KAS)
      DYDX(1) = Y(2)
      DYDX(2) = - AMDA*AMDA*QA*Y(1)
      RETURN
      END
      SUBROUTINE GETQ(U,QA,XX,U0,UV,AMDA,A,PI,ER,JE,KAS)
C++++ +++ +++++++++ +++++++++ +++++++++ +++++++++ +++++++++ +++++++++
C A driver for Subroutine QX. GETQ returns values of Uo(x), Uo'(x),
C q(x) & q'(x) at any value of x. QX generates tabular data for the
C arrays U0, U0P, Q, & QP. GETQ uses table look up and interpolation
C on U0 to get U at the prescribed x in [0,1] and Uv. The other quantities
C are then calculated directly from Uo. The array q(x) is the variable
C coefficient in the standard-form first-order equation,
C z"+ (Lamda**2)q(x)z(x) = 0, where u(x) = z/(Uo(x))**1.5.
C++++ +++ +++++++++ +++++++++ +++++++++ +++++++++ +++++++++ +++++++++
      IMPLICIT REAL*8(A-H, O-Z)
      DIMENSION XA(4),YA(4),Y1(4),Y2(4),Y3(4),
     1          XX(300),U0(300)
      EPSI = 5.0D-09
      M = 201
      ONE = 1.0D+00
      IF(A .EQ. 0.0D+00) THEN
        KAS = 1
        GO TO 10
      END IF
```

```
          K = KAS
        IF(A .EQ. ONE) THEN
   10     U = ONE
          QA = (5.0D+00*UV*UV - ONE)/2.0D+00
          RETURN
        END IF
C++++ +++ +++++ Find the value of K allowing for periodicity of Uo.
        CALL HUNT(XX, M+97, A, K)
        KAS = K
        IF(K .LT. 2) THEN
           XA(1)=-XX(2)
           XA(2)=XX(K)
           XA(3)=XX(K+1)
           XA(4)=XX(K+2)
           YA(1)=U0(M+2)
           YA(2)=U0(K)
           YA(3)=U0(K+1)
           YA(4)=U0(K+2)
        ELSE
           XA(1)=XX(K-1)
           XA(2)=XX(K)
           XA(3)=XX(K+1)
           XA(4)=XX(K+2)
           YA(1)=U0(K-1)
           YA(2)=U0(K)
           YA(3)=U0(K+1)
           YA(4)=U0(K+2)
        END IF
C++++ +++ +++++ use cubic interpolation for Uo(x).
        CALL POLINT(XA, YA, 4, A, Y, DY)
        U = Y
        ER = ER + DY
        JE = JE + 1
C++++ +++ +++++ Calculate QA at x = A.
        QA = (5.0D+00*UV*UV/(Y*Y) - ONE)/(2.0D+00*Y*Y*Y)
        RETURN
        END
        SUBROUTINE HUNT(XX,N,X,JLO)
C++++ +++ +++++++++ +++++++++ +++++++++ +++++++++ +++++++++ +++++++++
C GIVEN XX(N) AND A TARGET VALUE, X, THIS SEARCH & BISECTION CODE RETURNS
C A VALUE JLO SUCH THAT XX(JLO) <= X <= XX(JLO+1).  XX(N) MUST BE
C MONOTONIC, EITHER INCREASING OR DECREASING.  IF JLO = 0 OR JLO = N + 1
C IS RETURNED, THEN X IS OUT OF RANGE.  INPUT JLO IS TAKEN AS THE INITIAL
C GUESS FOR JLO ON OUTPUT.
C++++ +++ +++++++++ +++++++++ +++++++++ +++++++++ +++++++++ +++++++++
        IMPLICIT REAL*8(A-H, O-Z)
        DIMENSION XX(N)
        LOGICAL ASCND
        ASCND = XX(N).GT.XX(1)
        IF(JLO.LE.0.OR.JLO.GT.N) THEN
          JLO = 0
          JHI = N + 1
          GO TO 3
        END IF
        INC = 1
        IF(X.GE.XX(JLO).EQV.ASCND) THEN
 1        JHI = JLO + INC
          IF(JHI.GT.N) THEN
            JHI = N + 1
          ELSE IF(X.GE.XX(JHI).EQV.ASCND) THEN
            JLO = JHI
            INC = INC + INC
            GO TO 1
          END IF
        ELSE
          JHI = JLO
 2        JLO = JHI - INC
          IF(JLO.LT.1) THEN
            JLO = 0
          ELSE IF(X.LT.XX(JLO).EQV.ASCND) THEN
            JHI = JLO
            INC = INC + INC
            GO TO 2
          END IF
        END IF
 3      IF(JHI-JLO.EQ.1) RETURN
        JM = (JHI + JLO)/2
        IF(X.GT.XX(JM).EQV.ASCND) THEN
          JLO = JM
        ELSE
          JHI = JM
        END IF
        GO TO 3
        END
        SUBROUTINE ODEINT(YSTART, NVAR, X1, X2, EPS, H1, HMIN, NOK,
     1          NBAD, KOUNT, U, QA, XX,U0,UV, AMDA, PI,ER,JE,KAS)
C++++ +++ +++++++++ +++++++++ +++++++++ +++++++++ +++++++++ +++++++++
C RUNGE-KUTTA driver with adaptive stepsize control. Integrates the
C NVAR starting values YSTART from X1 to X2 with accuracy EPS, storing
C intermediate results in the common block /Z1Z2/. H1 should be set as
C a guessed first step size, HMIN as the minimum allowed stepsize
C (can be zero). On output NOK and NBAD are the number of good and bad
C (but retired and fixed) steps taken, and YSTART is replaced by values
C at the end of the integration interval. Derivs is the user supplied
C subroutine for calculating the right hand side derivative, while RKQC
C is the name of the stepper routine to be used. PATH contains its own
C information about how often an intermediate value is to be stored.
C++++ +++ +++++++++ +++++++++ +++++++++ +++++++++ +++++++++ +++++++++
        IMPLICIT REAL*8(A-H, O-Z)
        COMMON/Z1Z2/ KMAX, DXSAV, XP(201), YP(10,201)
        DIMENSION YSTART(10),YSCAL(10),Y(10),DYDX(10),
     1            XX(300),U0(300)
        MAXSTP = 1000
        NMAX = 10
        TWO = 2.0D+00
        ZERO = 0.0D+00
        TINY = 1.0D-30
        X=X1
```

```
      H = SIGN(H1, X2-X1)
      NOK = 0
      NBAD = 0
      KOUNT = 0
C++++ +++ User storage for intermediate results. Preset DXSAV and KMAX.+
      KMAX = 300
      DXSAV = 9.5D-03
      DO 11 I = 1,NVAR
         Y(I) = YSTART(I)
   11 CONTINUE
C++++ +++ +++++++++ Assures storage of first step.+++++++++ +++++++++
      IF(KMAX .GT. ZERO) XSAV = X - DXSAV*TWO
C++++ +++ +++++++++ Take at most MAXSTP steps.+++ +++++++++ +++++++++
      DO 16 NSTP = 1, MAXSTP
         CALL DERIVS(X,Y,DYDX,NVAR,U,QA,XX,UO,UV,AMDA,PI,ER,JE,KAS)
         DO 12 I=1,NVAR
C Scaling used to monitor accuracy. This general purpose choice can be
C modified if need be.++++++++ +++++++ +++++++++ +++++++++ +++++++++
            YSCAL(I) = ABS(Y(I)) + ABS(H*DYDX(I)) + TINY
   12    CONTINUE
         IF(KMAX .GT. ZERO) THEN
            IF(ABS(X-XSAV) .GT. ABS(DXSAV)) THEN
C++++ +++ +++++++++ Store intermediate results.++ +++++++++ +++++++++
               IF(KOUNT .LT. KMAX-1) THEN
                  KOUNT = KOUNT + 1
                  XP(KOUNT) = X
                  DO 13 I = 1,NVAR
                     YP(I,KOUNT) = Y(I)
   13                CONTINUE
                  XSAV = X
               END IF
            END IF
         END IF
C++++ +++ +++++If step can overshoot end, cutdown step size.+++++++++
         IF((X+H-X2)*(X+H-X1) .GT. ZERO) H = X2 - X
         CALL RKQC(Y, DYDX, NVAR, X, H, EPS, YSCAL, HDID, HNEXT,
     1              U, QA, XX,UO,UV, AMDA, PI, ER, JE, KAS)
         IF(HDID .EQ. H) THEN
            NOK =  NOK + 1
         ELSE
            NBAD = NBAD + 1
         END IF
C++++ +++ +++++++++ +++++++++ Are we done? ++++++ +++++++++ +++++++++
         IF((X-X2)*(X2-X1) .GE. ZERO) THEN
            DO 14 I = 1,NVAR
               YSTART(I) = Y(I)
   14       CONTINUE
            IF(KMAX .NE. ZERO) THEN
               KOUNT = KOUNT + 1
C++++ +++ +++++++++ +++++++++ Save final step.+++ +++++++++ +++++++++
               XP(KOUNT) = X
               DO 15 I = 1,NVAR
                  YP(I,KOUNT) = Y(I)
   15          CONTINUE
            END IF
C++++ +++ +++++++++ +++++++++ Normal exit.+++++++ +++++++++ +++++++++
            RETURN
         END IF
         IF(ABS(HNEXT) .LT. HMIN) THEN
            PAUSE'Stepsize smaller than minimum'
            STOP
         ELSE
            H = HNEXT
         END IF
   16 CONTINUE
      PAUSE 'Too many steps'
      RETURN
      END
      SUBROUTINE RKQC(Y, DYDX, N, X, HTRY, EPS, YSCAL, HDID, HNEXT,
     1                U, QA, XX,UO,UV, AMDA, PI, ER, JE, KAS)
C++++ +++ +++++++++ +++++++++ +++++++++ +++++++++ +++++++++ +++++++++
C Fith-order Runge-Kutta step with monitoring of local truncation error
C to insure accuracy and adjust stepsize. Inputs are the dependent
C variable vector Y of length N and its derivative DYDX at the starting
C value of the independent variable X. Also input are the stepsize to be
C attempted HTRY, the required accuracy EPS, and the vector YSCAL against
C which the error is scaled. On output, Y and X are replaced by their
C new values. HDID is the stepsize actually accomplished, and HNEXT is
C the estimated next stepsize. DERIVS is the user-supplied subroutine
C that computes the right-hand side derivatives.
C++++ +++ +++++++++ +++++++++ +++++++++ +++++++++ +++++++++ +++++++++
      IMPLICIT REAL*8(A-H, O-Z)
      DIMENSION Y(N),DYDX(N),YSCAL(N),YTEMP(10),YSAV(10),
     1          DYSAV(10),XX(300),UO(300)
      NMAX = 10
      PGROW = -2.0D-01
      PSHRINK = -2.5D-01
      FCOR =1.0D+00/1.5D+01
C++++ +++  The value of ERRCON = (4/SAFETY)**(1/PGROW), see use below.++
      ONE = 1.0D+00
      SAFETY = 9.0D-01
      ERRCON = 5.7665D-04
C++++ +++ +++++++++ +++++++++ Save initial values.+++++++++ +++++++++
      XSAV = X
      DO 11 I = 1,N
         YSAV(I) = Y(I)
         DYSAV(I) = DYDX(I)
   11 CONTINUE
C++++ +++ Set step size to its initial trial value & take two half steps.
      H = HTRY
    1 HH = 0.5D+00*H
      CALL RK4(YSAV,DYSAV,N,XSAV,HH,YTEMP,U,QA,XX,UO,
     1         UV,AMDA,PI,ER,JE,KAS)
      X = XSAV +HH
      CALL DERIVS(X,YTEMP,DYDX,N,U,QA,XX,UO,
     1            UV,AMDA,PI,ER,JE,KAS)
      CALL RK4(YTEMP,DYDX,N,X,HH,Y,U,QA,XX,UO,
     1         UV,AMDA,PI,ER,JE,KAS)
```

```
        X = XSAV + H
        IF(X .EQ. XSAV) THEN
           PAUSE 'Step size not significant in RKQC.'
           STOP
        ELSE
C++++ +++ +++++++++ +++++++ Take one large step.+ +++++++++ +++++++++
           CALL RK4(YSAV,DYSAV,N,XSAV,H,YTEMP,U,QA,XX,U0,
     1              UV,AMDA,PI,ER,JE,KAS)
        END IF
C++++ +++ +++++++++ +++++++++ Evaluate accuracy.+ +++++++++ +++++++++
        ERRMAX = 0.0D+00
        DO 12 I = 1,N
           YTEMP(I) = Y(I) - YTEMP(I)
           ERRMAX = MAX(ERRMAX, ABS(YTEMP(I)/YSCAL(I)))
   12   CONTINUE
C++++ +++ +++++++++ Scale relative to required tollerance.+ +++++++++
        ERRMAX = ERRMAX/EPS
C++++ +++ +++++++++ Truncation error too large; reduce stepsize.+++++
        IF(ERRMAX .GT. ONE) THEN
           H = SAFETY*H*(ERRMAX**PSHRINK)
C++++ +++ +++++++++ +++++++++ Try again.+++++++++ +++++++++ +++++++++
           GO TO 1
        ELSE
C++++ +++ +++++++++ ++Step succeeded. Compute size of next step.+++++
           HDID = H
           IF(ERRMAX .GT. ERRCON) THEN
              HNEXT = SAFETY*H*(ERRMAX**PGROW)
           ELSE
              HNEXT = 4.0D+00*H
           END IF
        END IF
C++++ +++ +++++++++ Mop up fifth-order truncation error.+++ +++++++++
        DO 13 I=1,N
           Y(I) = Y(I) + YTEMP(I)*FCOR
   13   CONTINUE
        RETURN
        END
        SUBROUTINE RK4(Y,DYDX,N,X,H,YOUT,U,QA,XX,U0,
     1                 UV,AMDA,PI,ER,JE,KAS)
C++++ +++ +++++++++ +++++++++ +++++++++ +++++++++ +++++++++ +++++++++
C Given values of N variables Y and their derivatives DYDX, known at X,
C use the fourth-order Runge-Kutta method to advance the solution over
C an interval H and return the incremented variables as YOUT, which need
C  not be a distinct array from Y. The user supplies the subroutine
C DERIVS(X,Y,DYDX,...) which returns derivatives DYDX at X. Up to 10
C functions ,Y(I) , can be handled.
C++++ +++ +++++++++ +++++++++ +++++++++ +++++++++ +++++++++ +++++++++
        IMPLICIT REAL*8(A-H, O-Z)
        DIMENSION Y(N), DYDX(N), YOUT(N), YT(10), DYT(10),
     1            DYM(10),XX(300),U0(300)
        HH = H*0.5D+00
        H6 = H/6.0D+00
        XH = X + HH
        DO 11, I = 1,N
           YT(I) = Y(I) + HH*DYDX(I)
   11   CONTINUE
        CALL DERIVS(XH,YT,DYT,N,U,QA,XX,U0,
     1              UV,AMDA,PI,ER,JE,KAS)
        DO 12 I = 1,N
           YT(I) = Y(I) + HH*DYT(I)
   12   CONTINUE
        CALL DERIVS(XH,YT,DYM,N,U,QA,XX,U0,
     1              UV,AMDA,PI,ER,JE,KAS)
        DO 13 I = 1,N
           YT(I) = Y(I) + H*DYM(I)
           DYM(I) = DYT(I) + DYM(I)
   13   CONTINUE
        CALL DERIVS(X+H,YT,DYT,N,U,QA,XX,U0,
     1              UV,AMDA,PI,ER,JE,KAS)
        DO 14 I = 1,N
           YOUT(I) = Y(I) + H6*(DYDX(I) + DYT(I) + 2.0D+00*DYM(I))
   14   CONTINUE
        RETURN
        END
        SUBROUTINE POLINT(XA, YA, N, X, Y, DY)
C++++ +++ +++++++++ +++++++++ +++++++++ +++++++++ +++++++++ +++++++++
C Given arrays XA and YA, each of length N, and given a value X, this
C routine returns a value Y and an error estimate DY. If P(x) is the
C polynomial of degree N-1 such that P(XAj) = YAj, j = 1,...,N, then
C the returned value Y = P(X)
C++++ +++ +++++++++ +++++++++ +++++++++ +++++++++ +++++++++ +++++++++
        IMPLICIT REAL*8(A-H, O-Z)
        DIMENSION XA(N), YA(N), C(10), D(10)
        NS = 1
        DIF = ABS(X-XA(1))
        DO 11 I = 1,N
           DIFT = ABS(X-XA(I))
           IF(DIFT .LT. DIF) THEN
              NS = I
              DIF = DIFT
           END IF
        C(I) = YA(I)
        D(I) = YA(I)
   11   CONTINUE
        Y = YA(NS)
        NS = NS - 1
        DO 13 M = 1,N-1
           DO 12 I = 1,N-M
              HO = XA(I) - X
              HP = XA(I+M) - X
              W = C(I+1) - D(I)
              DEN = HO - HP
              IF(DEN .EQ. 0.0D+00) THEN
                 PAUSE '2 Identical XA input values'
                 STOP
              END IF
              DEN = W/DEN
              D(I) = HP*DEN
```

```
            C(I) = HO*DEN
   12       CONTINUE
            IF(2.0D+00*NS .LT. N-M) THEN
               DY = C(NS+1)
            ELSE
               DY = D(NS)
               NS = NS-1
            END IF
            Y = Y + DY
   13    CONTINUE
         RETURN
         END
      SUBROUTINE FORCE(NUM_PTS,S,CP,XKVAL,UV,Q,EPSIL,AMDA,
     1                 NEPTS,ETIME,EFORCEF,SLOPE)
C +++++++++++++++++++++++++++++++++++++++++++++++++++++++++++++++
C ++++++       INTEGRATION SUBROUTINE TO FIND THE FORCING
C ++++++       FUNCTION FOR GIVEN INPUTS OF CP AND S.
C +++++++++++++++++++++++++++++++++++++++++++++++++++++++++++++++
      IMPLICIT REAL*8 (A-H, O-Z)
      DIMENSION S(50),CP(50),SE(201),CPE(201),XTIME(201),
     1          TIME(201),FORCEF(201),TSHIFT(201),FSHIFT(201),
     2          ETIME(10000),EFORCEF(10000)
      EXTERNAL FEVEN,CPEVEN,SIMPSON,SHIFT,HUNT, POLINT
C---- GET THE SLOPE AT CP = -K FOR THE INITIAL CONDITION
        DO 10 I = 1, NUM_PTS
          IF(CP(I).GE.-XKVAL) GO TO 10
          SLOPE = -(CP(I)-CP(I-1))/(S(I)-S(I-1))
          GO TO 15
   10   CONTINUE
   15   CALL CPEVEN(NUM_PTS,S,CP,SE,CPE,H)
        CALL SIMPSON(SE,CPE,4,200,H,XKVAL,TIME,FORCEF)
        CALL SHIFT(TIME,FORCEF,200,NSHIFT,TSHIFT,FSHIFT)
        WRITE(6,*) 'GOT SHIFTED FORCE(ts)'
C---- MUST NOW CONVERT BUBBLE TIME INTO NORMALIZED X TIME
        DO 20 I = 1, NSHIFT
          XTIME(I) = TSHIFT(I)/(EPSIL*AMDA*(1.0D+00+Q)**0.75D+00)
   20   CONTINUE
        WRITE(6,101) 'LAST X VALUE IS = ',XTIME(NSHIFT)
  101   FORMAT(2X,A,F8.5)
C---- GET MATCHING 201 POINTS FOR EACH PERIOD OF THE FORCING FUNCTION
        CALL FEVEN(NSHIFT,XTIME,FSHIFT,XKVAL,NEPTS,ETIME,EFORCEF)
      RETURN
      END
      SUBROUTINE FEVEN(NPTS,TIME,FORCEF,XKVAL,
     1                 NEPTS,ETIME,EFORCEF)
C+++++++++++++++++++++++++++++++++++++++++++++++++++++++++++++++
C CALCULATES VALUES OF THE FORCING FUNCTION FOR EVENLY SPACED VALUES
C OF THE LAB TIME, ts. NPTS IS THE NUMBER OF F vs t POINTS INPUTED,
C BEGINNING WITH ts = 0 BUT ONLY GOING UP TO A VALUE CORESSPONDING
C TO s LENGTHS JUST PAST SEPARATION. (NOT NECESSARILY UP TO ts = 1)
C+++++++++++++++++++++++++++++++++++++++++++++++++++++++++++++++
      IMPLICIT REAL*8 (A-H, O-Z)
      DIMENSION TIME(201),FORCEF(201),ETIME(10000),
     1          EFORCEF(10000),XA(4),YA(4)
      ZERO = 0.0D+00
      HA = 0.5D-02
      AE = HA
      M = NPTS
      ETIME(1) = ZERO
      ETIME(10000) = TIME(NPTS)
      EFORCEF(1) = ZERO
      EFORCEF(10000) = FORCEF(NPTS)
      K = 1
      NEPTS = 1
      DO 40 I = 2, 10000
        CALL HUNT(TIME,M,AE,K)
        KAS = K
        IF(K.LT.2) THEN
          K = 2
          GO TO 30
        ELSE IF(K.LT.NPTS-2) THEN
          GO TO 30
        ELSE
          K = NPTS-2
        END IF
   30   XA(1) = TIME(K-1)
        XA(2) = TIME(K)
        XA(3) = TIME(K+1)
        XA(4) = TIME(K+2)
        YA(1) = FORCEF(K-1)
        YA(2) = FORCEF(K)
        YA(3) = FORCEF(K+1)
        YA(4) = FORCEF(K+2)
        CALL POLINT(XA,YA,4,AE,Y,DY)
        ETIME(I) = AE
        EFORCEF(I) = Y
        ER = ER + DY
        AE = AE + HA
        NEPTS = NEPTS + 1
        IF(AE.GE.TIME(NPTS)) GO TO 50
   40   CONTINUE
   50   RETURN
        END
      SUBROUTINE SIMPSON(X,Y,M,N,H,XKVAL,TIME,FORCEF)
C +++++++++++++++++++++++++++++++++++++++++++++++++++++++++++++++
C              SUBROUTINE USING SIMPSONS RULE
C              TO INTEGRATE THE DATA POINTS
C +++++++++++++++++++++++++++++++++++++++++++++++++++++++++++++++
      IMPLICIT REAL*8 (A-H, O-Z)
      DIMENSION X(201),Y(201),TIME(201),FORCEF(201)
C---- THE FUNCTION BEING INTEGRATED
      TFUN(CC) = 1.0D+00/DSQRT(1.0D+00 - CC)
C---- STARTING VALUE TO TAKE CARE OF SINGULARITY
      START = 2.0D+00*X(3)/DSQRT(1.0D+00 - Y(3))
C---- CONVERTING ARCLENGTH DATA INTO LABORATORY TIME
      TIME(2) = START
      TIMEL = START
        DO 50 J = M, N, 2
```

```
          T1 = TFUN(Y(J-1))
          T2 = TFUN(Y(J))
          T3 = TFUN(Y(J+1))
          SIMP = (T1 + 4.0*T2 + T3)*H/3.0D+00
          TIME(J) = TIMEL + SIMP
          TIMEL = TIME(J)
  50      CONTINUE
C---- CALCULATING FORCING FUNCTION FOR GIVEN CAVITATION NUMBER
          DO 60 J = 2, N, 2
          FORCEF(J) = -(Y(J)+XKVAL)
  60      CONTINUE
      RETURN
      END
      SUBROUTINE SHIFT(TIME,FORCEF,N,NPTS,TSHIFT,FSHIFT)
C +++++++++++++++++++++++++++++++++++++++++++++++++++++++++++++++
C AXIS SHIFT SUBROUTINE CONVERTING THE INITIAL POINT OF
C VAPOROUS GROWTH TO THE POINT ts = 0.
C +++++++++++++++++++++++++++++++++++++++++++++++++++++++++++++++
      IMPLICIT REAL*8 (A-H, O-Z)
      DIMENSION TSHIFT(201),XA(4),YA(4)
      DIMENSION TIME(201),FORCEF(201),FSHIFT(251)
      EXTERNAL POLINT
          DO 10 L = 4, N, 2
             IF(FORCEF(L).LE.0.0D+00) GO TO 10
             XA(1) = TIME(L-4)
             XA(2) = TIME(L-2)
             XA(3) = TIME(L)
             XA(4) = TIME(L+2)
             YA(1) = FORCEF(L-4)
             YA(2) = FORCEF(L-2)
             YA(3) = FORCEF(L)
             YA(4) = FORCEF(L+2)
             CALL POLINT(YA,XA,4,0.0D+00,Y,DY)
             TNOT = Y
             LCOUNT = L
             GO TO 20
  10      CONTINUE
  20    NPTS = (N - LCOUNT + 4)/2
        FSHIFT(1) = 0.0D+00
        TSHIFT(1) = 0.0D+00
        K = 2
          DO 30 L = LCOUNT, N, 2
             FSHIFT(K) = FORCEF(L)
             TSHIFT(K) = TIME(L) - TNOT
             K = K + 1
  30      CONTINUE
      RETURN
      END
        SUBROUTINE CPEVEN(NPTS,S,CP,SE,CPE,HA)
C++++ +++ +++++++++ +++++++++ +++++++++ +++++++++ +++++++++ +++++++++
C STORE EVENLY SPACED VALUES OF CP(S) IN ARRAY CPE
C++++ +++ +++++++++ +++++++++ +++++++++ +++++++++ +++++++++ +++++++++
        IMPLICIT REAL*8(A-H, O-Z)
        DIMENSION S(201),CP(201),SE(201),CPE(201),XA(4),YA(4)
        EXTERNAL HUNT,POLINT
        HA = (S(NPTS)-S(1))/200
        AE = HA
        SE(1) = S(1)
        SE(201) = S(NPTS)
        CPE(1) = CP(1)
        CPE(201) = CP(NPTS)
        K = 1
        DO 40 I = 2, 200
           CALL HUNT(S,NPTS,AE,K)
           KAS = K
           IF(K.LT.2) THEN
             K = 2
           ELSE IF(K.GT.NPTS-2) THEN
             K = NPTS - 2
           ELSE
             K = K
           END IF
             XA(1) = S(K-1)
             XA(2) = S(K)
             XA(3) = S(K+1)
             XA(4) = S(K+2)
             YA(1) = CP(K-1)
             YA(2) = CP(K)
             YA(3) = CP(K+1)
             YA(4) = CP(K+2)
           CALL POLINT(XA,YA,4,AE,Y,DY)
           SE(I) = AE
           CPE(I) = Y
           ER = ER + DY
           AE = AE + HA
           K = KAS
  40       CONTINUE
        RETURN
        END
C++++++++++++++++++++++++++++++++++++++++++++++++++++++++++++++
C INTEGRAL FUNCTIONS FOR THE PARTICULAR SOLUTION
C++++++++++++++++++++++++++++++++++++++++++++++++++++++++++++++
        REAL*8 FUNCTION PFUN1(X,XH,G1,G2,XP,U,F)
        IMPLICIT REAL*8 (A-H,O-Z)
            PFUN1 = DEXP(G2*X+G1*XH)*XP*F/U
        RETURN
        END
        REAL*8 FUNCTION PFUN2(X,XH,G1,G2,XP,U,F)
        IMPLICIT REAL*8 (A-H,O-Z)
            PFUN2 = DEXP(G1*X+G2*XH)*XP*F/U
        RETURN
        END
```

APPENDIX B

PRESSURE DATA TABULATION AND FORCING FUNCTION CALCULATION

B 1. Data Tabulation

This appendix tabulates two sets of pressure coefficient, C_p, versus dimensionless arc length, s, for a circular cylinder at supercritical Reynolds numbers. Table B.1 contains the original data as read from a graph given by Gowen and Perkins [4]. Since these data, as read, did not produce a smooth curve, Lagrangian interpolation was used to produce evenly spaced points over the interesting range of s. These points were then smoothed. They are given in in Table B.2 and they are the input $C_p(s)$ data used in the Fortran code.

Table B.1 Original Data

No.	s	Cp
1	0.0000	1.0000
2	0.0403	0.9600
3	0.0873	0.9200
4	0.3491	0.5000
5	0.6981	-0.5750
6	1.0472	-1.8313
7	1.2217	-2.2531
8	1.2654	-2.3063
9	1.3090	-2.3813
10	1.3526	-2.4563
11	1.3963	-2.5000
12	1.4399	-2.5531
13	1.4835	-2.5688
14	1.5272	-2.5667
15	1.5708	-2.5583
16	1.6144	-2.5000
17	1.6581	-2.4406
18	1.7017	-2.3500
19	1.7453	-2.2750
20	1.8326	-2.2438
21	1.9200	-2.1625

Table B.2 Smoothed Data

No.	s	Cp
1	0.000	1.00000000
2	0.064	0.93858008
3	0.128	0.87090363
4	0.192	0.78682947
5	0.256	0.68326172
6	0.320	0.55809864
7	0.384	0.41404022
8	0.448	0.25018646
9	0.512	0.06653735
10	0.576	-0.13690708
11	0.640	-0.36078890
12	0.704	-0.60684652
13	0.768	-0.86596418
14	0.832	-1.11726326
15	0.896	-1.35007730
16	0.960	-1.56440630
17	1.024	-1.76025025
18	1.088	-1.93760915
19	1.152	-2.09648302
20	1.216	-2.22826666
21	1.280	-2.33585874
22	1.344	-2.43371901
23	1.408	-2.51203038
24	1.472	-2.55500333
25	1.536	-2.55466889
26	1.600	-2.50791555
27	1.664	-2.41927707
28	1.728	-2.32443463
29	1.792	-2.26472235
30	1.856	-2.22700000
31	1.920	-2.22500000
32	1.984	-2.22500000
33	2.048	-2.22500000
34	2.112	-2.22500000
35	2.176	-2.22500000
36	2.240	-2.22500000
37	2.304	-2.22500000

B 2. Pressure Distribution and Forcing Function on the Cylinder

As noted in Chapter 2 we have used the data as read from curves presented in Reference 4 for low speed but supercritical Reynolds numbers as a basic set for this investigation. In this section we discus an alternative approach to the numerical approach employed in the Fortan program of Appendix A, which may not necessarily be as precise as that of the code, but which can be advantageous for engineering applications. The data as read and smoothed data are given above. Some of the points as read are plotted in figure B.1 . A curve has been fitted to these data in order to give them an approximate analytical representation over the limited range of importance for inception in order that the analytical approximation can be a reasonably close approximation. The region of constant pressure indicates roughly the position of the laminar separation bubble on the cylinder which is followed by boundary layer separation and a turbulent free shear layer bounding the wake behind the cylinder. Figure B.1 appears to span the range of arc lengths of interest for possible vaporous cavitation bubble growth.

The derivation of a forcing function requires that the pressure distribution be converted from the dimensionless arc length on the body to the dimensionless laboratory time t_s, as seen by a typical bubble moving with the vortex sheet which approximates the boundary layer in this study. We can write the laboratory time as in Equation (2.15):

$$t_s = \int_{1.15}^{s} \frac{d\zeta}{\sqrt{1 - C_p(s)}} \quad , \tag{B.1}$$

were the lower limit denotes the first abscissa of the seventeen points in Figure B.1. The upper limit refers to each successive point. Rather than use the curve fit for the pressure distribution, we have used the data as shown by the points in Figure B1 and the trapezoidal rule in order to correlate all plotted points with t_s. The seventeen points are shown in the plot of figure B2 in which t_s is the abscissa. This correlation was fitted by a polynomial as also shown in the figure. From these correlated (s,t_s) points, each $C_p(s)$ point was assigned

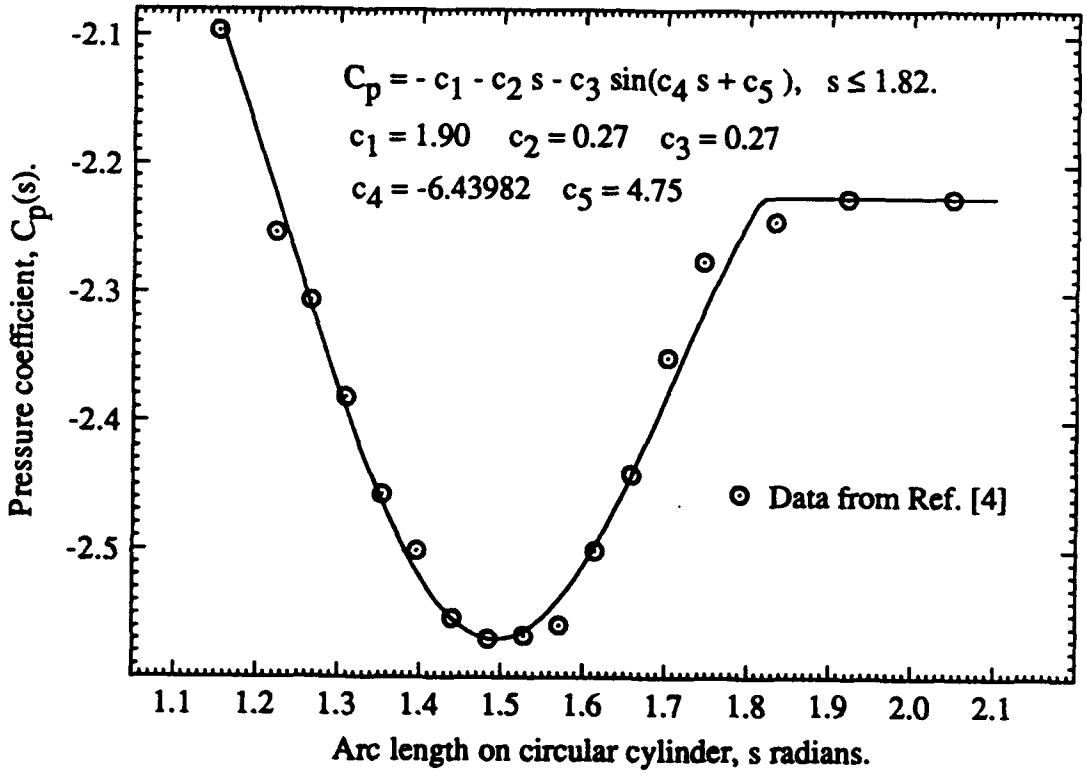

Figure B1 Pressure Distribution Data and Approximating Curve Fit for a Circular Cylinder at Supercritical Reynolds Number.

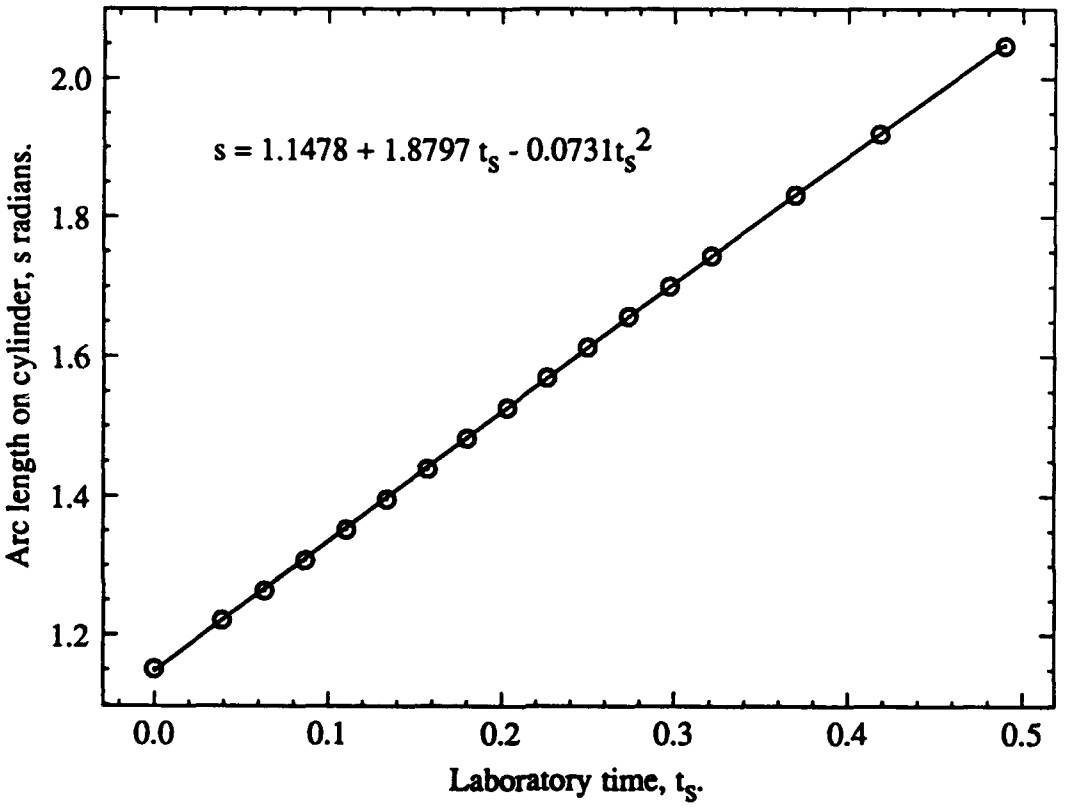

Figure B2 Correlation of Arc Length to Dimensionless Laboratory Time for a Circular Cylinder.

a value of t_s in order to construct a $C_p(t_s)$ plot as shown in figure B3 . Again, an approximating curve fit was found for these points in order to permit an analytical representation for the forcing function,

$$F(t_s) = \frac{1}{4} W_r [- C_p(t_s) - K].$$

As explained in Section 2.2, when one traces the pressure distribution starting at the stagnation point, the forcing function has its origin at the first zero of the quantity $[C_p(t_s) - K]$. The laboratory time for this point will be called t_0 and it can be found from a trial and error solution of the equation,

$$F_1(t_s) = a_1 + a_2 t_0 + a_3 \sin(a_4 t_0 + a_5) - K = 0, \qquad (B.2)$$

in which the notation, $F_1(t_s)$, indicates a radial Weber number of $\frac{1}{4}$, or more simply, the quantity, $- C_p - K$. The solution of (B.2) was found for the five successive K values of 2.1, 2.2, 2.3, 2.4 and 2.5, as illustrated in Figure B4. A cubic fitting curve for $t_0(K)$ is also shown in the figure. Then we can put $t_s = t_0(K) + \hat{t}$ in Equation (B.2) in order to write the forcing function for various $\hat{t}$ as

$$F_1(\hat{t}) = a_1 + a_2(t_0 + \hat{t}) + a_3 \sin(a_4 \hat{t} + a_4 t_0 + a_5) - K . \qquad (B.3)$$

A short Fortran program was written to find the values of t_0 and evaluate $F_1(\hat{t})$ for the five K values. Figure B5 shows the function $F_1(\hat{t})$ although the abscissa is labeled as t_s in order to emphasize the fact that the forcing function is measured in units of laboratory time. Figure B.5 also shows the start of laminar separation at the junction of the curves from equation (B.3) and the straight segments, having ordinates at 2.225 - K. At any K this ordinate is constant because once a nucleus finds itself in the laminar separation bubble it will grow in place by air diffusion until it becomes large enough to be swept into the turbulent free shear layer downstream of the cylinder. This approximate laminar separation point is defined in terms of the shifted laboratory time by

$$\hat{t}_s = 0.365 - t_0(K). \qquad (B.4)$$

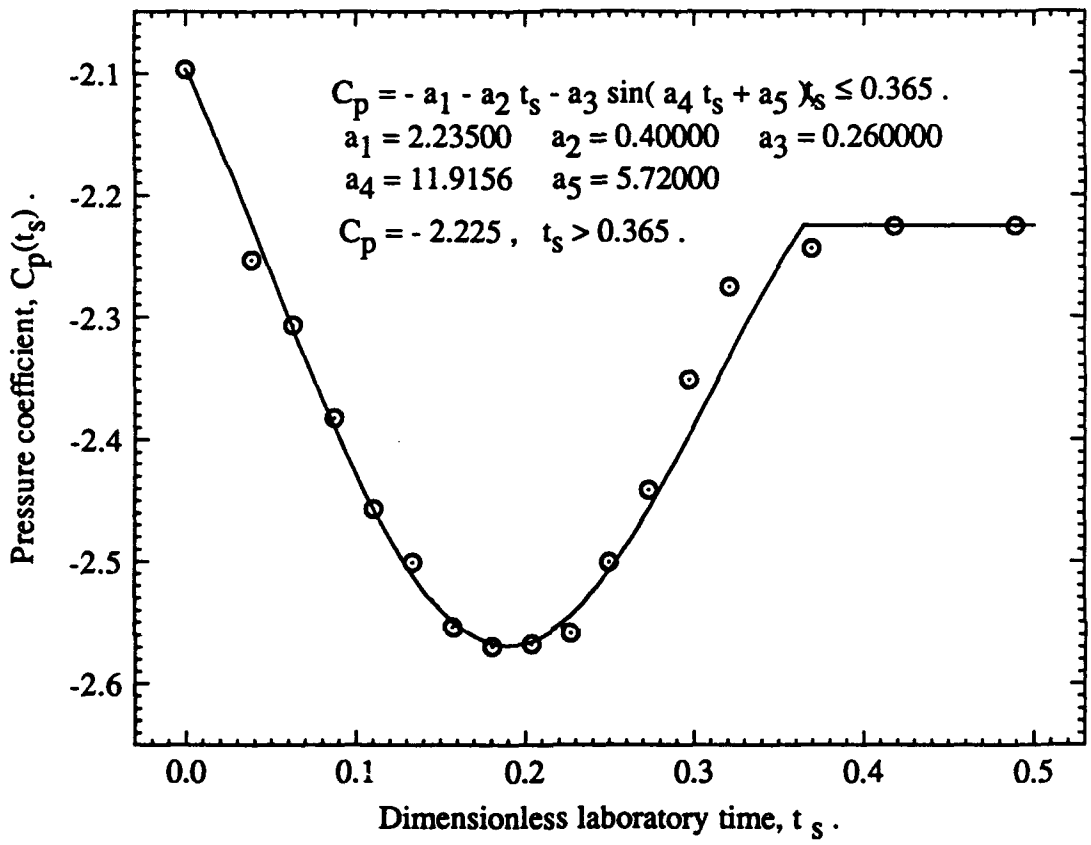

Figure B3 Pressure Distribution on the Cylinder in Terms of Dimensionless Laboratory Time.

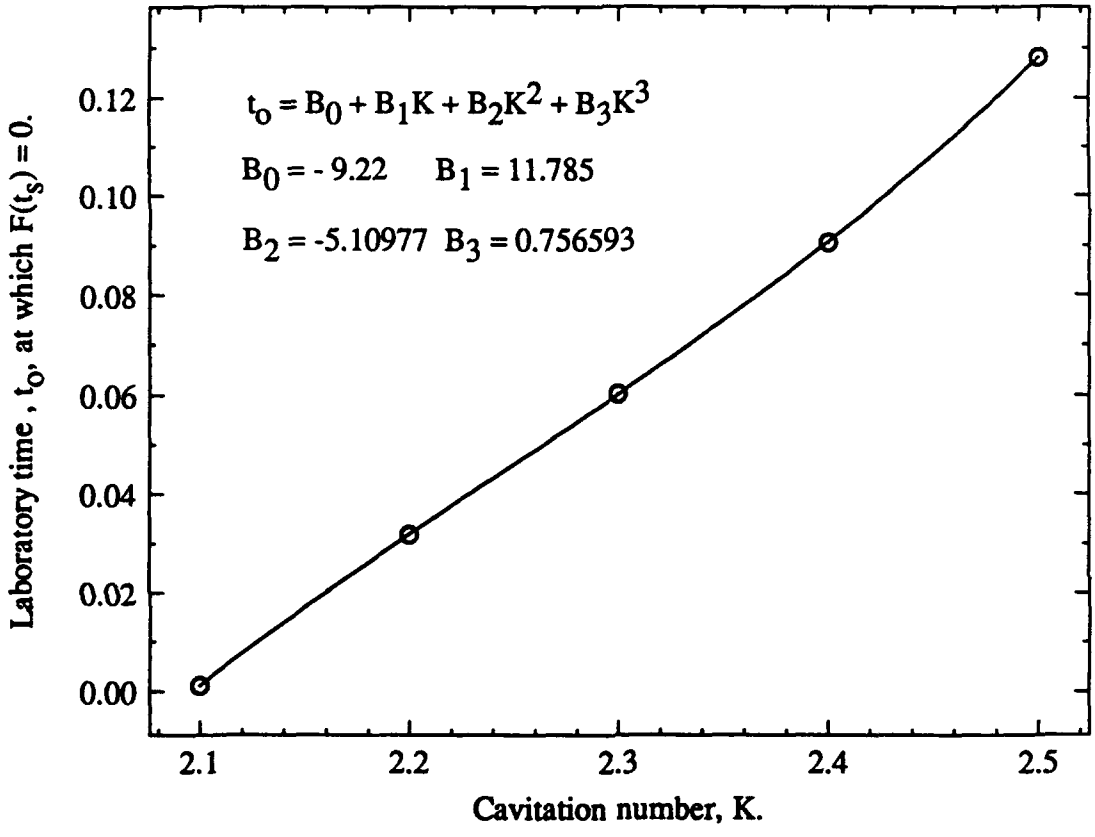

Figure B4 Abscissa of Forcing Function Origin in Laboratory Time for a Range of Cavitation Numbers.

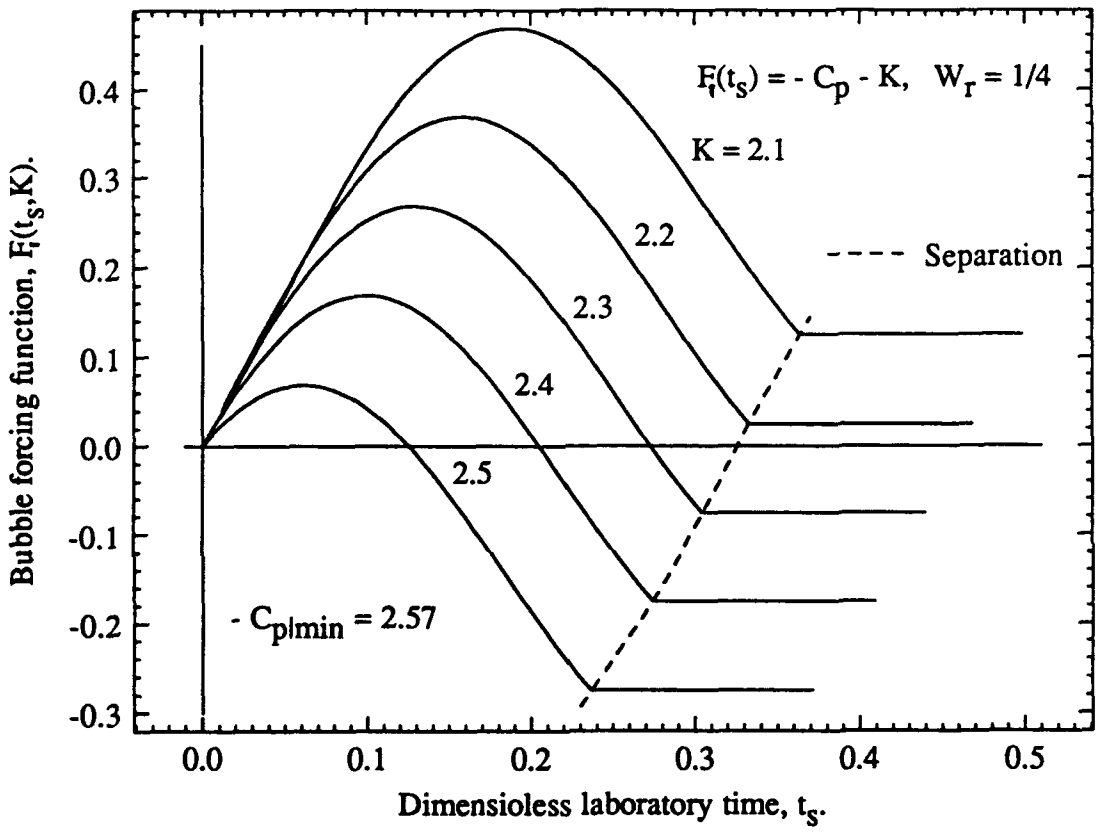

Figure B5. The Bubble Forcing Function for Various Cavitation Numbers.

A further calculation is required in order to evaluate the initial condition $\dot{u}_1(0) = C$ in shifted time coordinates in accordance with equation (2.46). The evaluation depends upon the derivative dC_p/ds at the point $s_0 = s_0[t_0(K)]$. The calculation is facilitated by use of the additional fitting function,

$$s_0(t_0) = 1.478 + 1.8797t_0 - 0.0731t_0^2. \tag{B.5}$$

For then at any value of K the derivative dC_p/ds can be evaluated from the curve fit of Figure B.1 at the correct value of s_0.

In the special case when $u_v = 1$, we have $1+ q = \gamma$ and Equation (2.46) can be written as

$$\dot{u}_1(0) = C = \frac{1}{8} W_r \sqrt{\gamma(1+ K)} \left[-\frac{dCp}{ds} \right]_{C_p = -K}. \tag{B.6}$$

Equation (B.6) pertains to $\frac{du_1}{dt_s}$ evaluated at $t_s \approx t_0$ (or $\hat{t} = 0$ in shifted coordinates.) When $u_v = 1$ these results can be used to obtain a closed–form approximate solution for bubble growth in this special case.

Or more generally, equations (B.3), (B.4) and (B.5) can be used to replace some of the purely numerical parts of a code such as that discussed in Appendix A. In such a procedure, we recall that since F_1 holds for a Weber number such that $(\frac{1}{4}W_r) = 1$ the forcing function is calculated from

$$F(t_s) = \frac{1}{4} W_r F_1(t_s). \tag{B.7}$$

Morover, although the present example supposes that a laminar separation bubble is present, there appears to be no reason to restrict the preceding approach to shuch flows. The method should apply to unseparated boundary layer flows also.

APPENDIX C

LIMITING VALUE OF THE OSCILLATION–PERIOD PARAMETER $\lambda(u_v)$

A convenient starting point for the present analysis is equation (3.20) which defines the oscillation period parameter as

$$\lambda(u_v) \equiv \frac{T(u_v)}{(1+q)^{3/4}} = 2I(u_v), \tag{3.20}$$

where the half–period integral, $I(u_v)$, is defined by equation (3.15) as

$$I(u_v) = \int_1^{u_m} \sqrt{\frac{\zeta^3}{2u_v^2 \ln(\zeta) - \zeta^2 + 1}}\, d\zeta. \tag{3.15}$$

We seek the limit of $I(u_v)$ as $u_v \to 1$. Consequently, as we have seen, $u_m = 1 + y_m$ and $\zeta = 1 + y$, where u_m is the amplitude of oscillation and $0 \le y \le y_m < 1$ because the amplitudes are small when u_v is in the neighborhood of unity. Therefore we can rewrite equation (3.15) as

$$I = \int_0^{y_m} \sqrt{\frac{(1+y)^3}{(2/3)u_v^2 y[y^2 - \kappa y + \mu]}}\, dy, \tag{C.1}$$

where the denominator of the radicand has been expanded to $O(y^3)$ and factored to account for the root at $y = 0$. The coefficients of the quadratic are $\kappa = \frac{3}{2}\frac{u_v^2 + 1}{u_v^2}$ and $\mu = 3\frac{u_v^2 - 1}{u_v^2}$. We also know that y_{max} is a zero of the denominator. It is the smaller root of the quadratic at $y_m = \frac{\kappa}{2} - \sqrt{(\frac{\kappa}{2})^2 - \mu}$. The larger root is given by

$b_0 = \frac{\kappa}{2} + \sqrt{(\frac{\kappa}{2})^2 - \mu}$. Therefore, in ascending order, the three roots are $0, < y_m, < b$.

Next we can put $y = y_m \xi$ in order to write (C.1) as

$$I = \int_0^1 \sqrt{\frac{(1 + y_m \xi)^3}{(2/3)\, u_v^2 b_0 \xi (1-\xi)[1 - (y_m \xi / b_0)]}}\, d\xi. \qquad (C.2)$$

Now we expand the factor,

$$\frac{(1 + y_m \xi)^{3/2}}{[1 - (y_m \xi / b_0)]^{1/2}} = 1 + \frac{1}{2}(3 + \frac{1}{b_0}) y_m \xi + \frac{3}{8}(1 + \frac{2}{b_0} + \frac{1}{b_0^2}) y_m^2 \xi^2 + \dots ,$$

which enables us to decompose (C.2) into three integrals. These become

$$I = \frac{1}{\sqrt{(2/3)\, u_v^2 b_0}} \left\{ I_1 + \frac{1}{2}(3 + \frac{1}{b_0}) y_m I_2 + \frac{3}{8}(1 + \frac{2}{b_0} + \frac{1}{b_0^2}) y_m^2 I_3 \right\}, \qquad (C.3)$$

in which

$$I_1 = \int_0^1 \frac{d\xi}{\sqrt{\xi(1-\xi)}}, \quad I_2 = \int_0^1 \frac{\xi\, d\xi}{\sqrt{\xi(1-\xi)}}, \quad \text{and} \quad I_3 = \int_0^1 \frac{\xi^2 d\xi}{\sqrt{\xi(1-\xi)}}.$$

Clearly, $I_1 = \pi$ and $I_2 = \frac{\pi}{2}$. The third integral, I_3, can be dealt with if the radicand in its integrand is written as $\frac{1}{4} - (\xi - \frac{1}{2})^2$. Then the numerator becomes

$$(\xi - \tfrac{1}{2})^2 + (\xi - \tfrac{1}{2}) + \tfrac{1}{4} .$$

Therefore I_3 can be expressed as the sum of three integrals, which upon integration give

$$I_3 = \frac{1}{8}(\frac{\pi}{2} + \frac{\pi}{2}) + \frac{\pi}{4} = \frac{3\pi}{8} .$$

These values of I_1, I_2 and I_3 can now be put into equation (C.3). The result is

$$I = \frac{\pi}{\sqrt{(2/3)\, u_v^2 b_0}} \left\{ 1 + \frac{1}{4}(3 + \frac{1}{b_0}) y_m + \frac{9}{64}(1 + \frac{2}{b_0} + \frac{1}{b_0^2}) y_m^2 \right\} \qquad (C.4)$$

As $u_v \to 1$, $\kappa \to 3$, $\mu \to 0$, $y_m \to 0$ and $b_0 \to 3$. Therefore $I \to \frac{\pi}{\sqrt{2}}$. From this result and equation (3.20) it follows that

$$\lambda(1) = \pi\sqrt{2} = 2.2214415 . \qquad (C.5)$$

Next we repeat the analysis using a different method. Therefore we return to the integral I and write it as

$$I = \frac{1}{u_v}\sqrt{\frac{3}{2}}\int_0^{y_m}(1+y)\sqrt{\frac{(1+y)}{y(y_m-y)(b_0-y)}}\,dy = \frac{1}{u_v}\sqrt{\frac{3}{2}}\,(I_1+I_2), \qquad (C.6)$$

where

$$I_1 = \int_0^{y_m}\sqrt{\frac{(1+y)}{y(y_m-y)(b_0-y)}}\,dy \quad \text{and} \quad I_2 = \int_0^{y_m}\sqrt{\frac{y(1+y)}{(y_m-y)(b_0-y)}}\,dy$$

are complete elliptic integrals. The properties of such integrals are discussed in detail by Byrd and Friedman[1]. In terms of the roots displayed by the factors in the integrands we can write

$$k^2 = \frac{y_m(b_0+1)}{b_0(y_m+1)}\,,\ g = \frac{2}{\sqrt{b_0(y_m+1)}},\ \alpha^2 = \frac{y_m}{b_0} \quad \text{and} \quad \phi = \sin^{-1}\sqrt{\frac{b_0(y_m-y)}{y_m(b_0-y)}}\,.$$

For complete integrals the lower limit of integration is $y = 0$ and $\phi = \frac{\pi}{2}$ but if $y = y_m$, $\phi = 0$. Then we have $I_1 = 2\sqrt{\frac{(y_m+1)}{b_0}}\left(F(\frac{\pi}{2}, k) + \frac{(y_m - b_0)}{(y_m+1)}\prod(\frac{\pi}{2}, \alpha^2, k)\right)$, where $F(\frac{\pi}{2}, k)$ is the complete elliptic integral of the first kind and where $\prod(\frac{\pi}{2}, \alpha^2, k)$ is the complete elliptic integral of the third kind. Then we take the limit as $u_v \to 1$, $y_m \to 0$, $k \to 0$, and $\alpha \to 0$. Hence $F(\frac{\pi}{2}, 0) = \frac{\pi}{2}$ and $\prod(\frac{\pi}{2}, 0, 0) = F(\frac{\pi}{2}, 0) = \frac{\pi}{2}$.

Recalling that $b_0 = 3$ in the limit, we see that

---

[1]Paul F. Byrd and Morris D. Friedman, *Handbook of Elliptic Integrals for Engineers and Physicists*, Springer Verlag, Berlin, 1954. See p. 116, #255.20 and #255.11.

$$I_1 = \frac{2}{\sqrt{3}} \frac{\pi}{2} (1 - 3) = -\frac{2\pi}{\sqrt{3}} .$$

From Byrd and Friedman we find that I_2 can be expressed in terms of elliptic integrals of the first, second and third kinds. After some manipulation they can be written in the form of complete integrals as

$$I_2 = 2\sqrt{(y_m + 1)b_0}\left\{-E(\frac{\pi}{2},k) + (1 + \frac{b_0 + 1}{y_m + 1})F(\frac{\pi}{2},k) + (1 - \frac{b_0 + 1}{y_m + 1})\Pi(\frac{\pi}{2}, \alpha^2, k)\right\}.$$

In view of the limiting values of the several parameters one finds that

$$I_2 = 2\sqrt{3}\left(-\frac{\pi}{2} + \frac{5\pi}{2} - \frac{3\pi}{2}\right) = \pi\sqrt{3}$$

Then from equation (C.6) with $u_v = 1$ we find that

$$I = \sqrt{\frac{3}{2}}\left(-\frac{2\pi}{\sqrt{3}} + \pi\sqrt{3}\right) = \frac{\pi}{\sqrt{2}} ,$$

in agreement with the value of I given above. Therefore the value of I given in equation (C.5) is confirmed.

APPENDIX D

BACKGROUND NOTES

D 1 Basic Bubble Dynamics

The well known Rayleigh-Plesset differential equation governs the growth or collapse of a spherical vapor bubble in a perfect fluid when the static pressure surrounding the bubble varies with the time, t, [16]. In the present investigation we shall consider the vaporous growth of such bubbles in a flow in which the the bubble, in moving along the surface of a submerged body, is influenced by its pressure distribution. The bubble will contain air and water vapor so that the dynamic force balance is

$$\rho\left(R\ddot{R} + \frac{3}{2}\dot{R}^2\right) = p_i - \frac{2\sigma}{R} - p(t). \qquad \text{(D 1)}$$

In this equation R(t) is the bubble radius, ρ is the liquid density, σ is the surface tension and p(t) is the static pressure distribution on the body as seen by the moving bubble. The pressure inside the bubble is p_i and if the bubble is isothermal , $p_i = p_v + p_a (R_0/R)^3$. Here p_v is the vapor pressure and p_a is the air pressure in the bubble at radius R_0 in the free stream. The radius R_0 is the size of a typical microscopic cavitation nucleus and p_a is related to the dissolved air content in the water. Therefore the basic equation of present interest is

$$\rho\left(R\ddot{R} + \frac{3}{2}\dot{R}^2\right) = p_v + p_a (R_0/R)^3 - 2\sigma/R - p(t). \qquad \text{(D 2)}$$

Next we shall introduce dimensionless variables. We start by letting $R = r R_0$ and observe that

$p(t) = p_0 - \frac{1}{2}\rho V_0^2 C_p$ and that $p_v = p_0 + \frac{1}{2}\rho V_0^2 K$, where C_p is the pressure coefficient on the submerged body and K is the cavitation number. Therefore we have $p_v - p(t) = -\frac{1}{2}\rho V_0^2 (C_p + K)$. Substitution of these definitions into the differential equation leads to

$$\frac{\rho R_0^2}{2\sigma/R_0}(r\ddot{r} + \frac{3}{2}\dot{r}^2) = (\frac{p_a}{2\sigma/R_0})\frac{1}{r^3} - \frac{1}{r} + \frac{1}{4}W_r(-C_p - K), \qquad (D\ 3)$$

where the definition of W_r is $W_r = \frac{\rho V_0^2}{\sigma/R_0}$, the radial Weber number. We shall define the air content parameter by $\gamma = \frac{p_a}{2\sigma/R_0}$ and also observe that the factor $\frac{\rho R_0^2}{2\sigma/R_0}$ has the dimension of [Time]^2. Therefore we shall define a new dimensionless time τ by $\tau = t\sqrt{(2\sigma)/(\rho R_0^2)}$. Consequently we can write the dimensionless equation of motion as

$$r\frac{dr^2}{d\tau^2} + \frac{3}{2}(\frac{dr}{d\tau})^2 = \frac{\gamma}{r^3} - \frac{1}{r} + F(t), \qquad (D\ 4)$$

where the forcing function is defined by

$$F(t) = \frac{1}{4}W_r[-C_p(t) - K]. \qquad (D\ 5)$$

D 2 Laminar Separation and Cavitation on Circular Cylinders

Cavitation inception observations on circular cylinders have been reported by Ihara and Murai [3]. Their experiments were designed to see whether or not laminar separation plays a role in the onset of cavitation on smooth cylinders in critical and supercritical flow ranges and on cylinders having a boundary layer trip. They observed inception resembling bubble-ring cavitation in the reattachment region when a laminar bubble was present at Reynolds as high as 3.27×10^5 on a smooth cylinder. They called this cavitation "bubble-line"cavitation. Ordinarily, supercritial flow is encountered at Reynolds numbers of 3×10^5 or greater. No tunnel wall effect corrections are noted in the paper. Such effects must have been present because the tunnel height was 5.42 cylinder diameters, and at a Reynolds number of 3.3×10^5 a minimum pressure coefficient of -2.9 is reported. This C_p magnitude is somewhat larger that those ordinarily observed in the absence of wall effects. This fact is of

minor importance because these authors' measurements do establish the role of laminar separation on smooth circular cylinders in this Reynolds number range; but it suggests to us that we should use the pressure measurements of Gowen and Perkins [3] which appear to be free of wall effects.